AD-A075 541 MATERIALS RESEARCH LAB INC GLENWOOD ILL F/G 13/5
FRACTURING CHARACTERISTICS OF ADHESIVE JOINTS.(U)
SEP 78 S MOSTOVOY , E J RIPLING N00019-77-C-0256

UNCLASSIFIED NL

1 OF 2
AD-
A075541

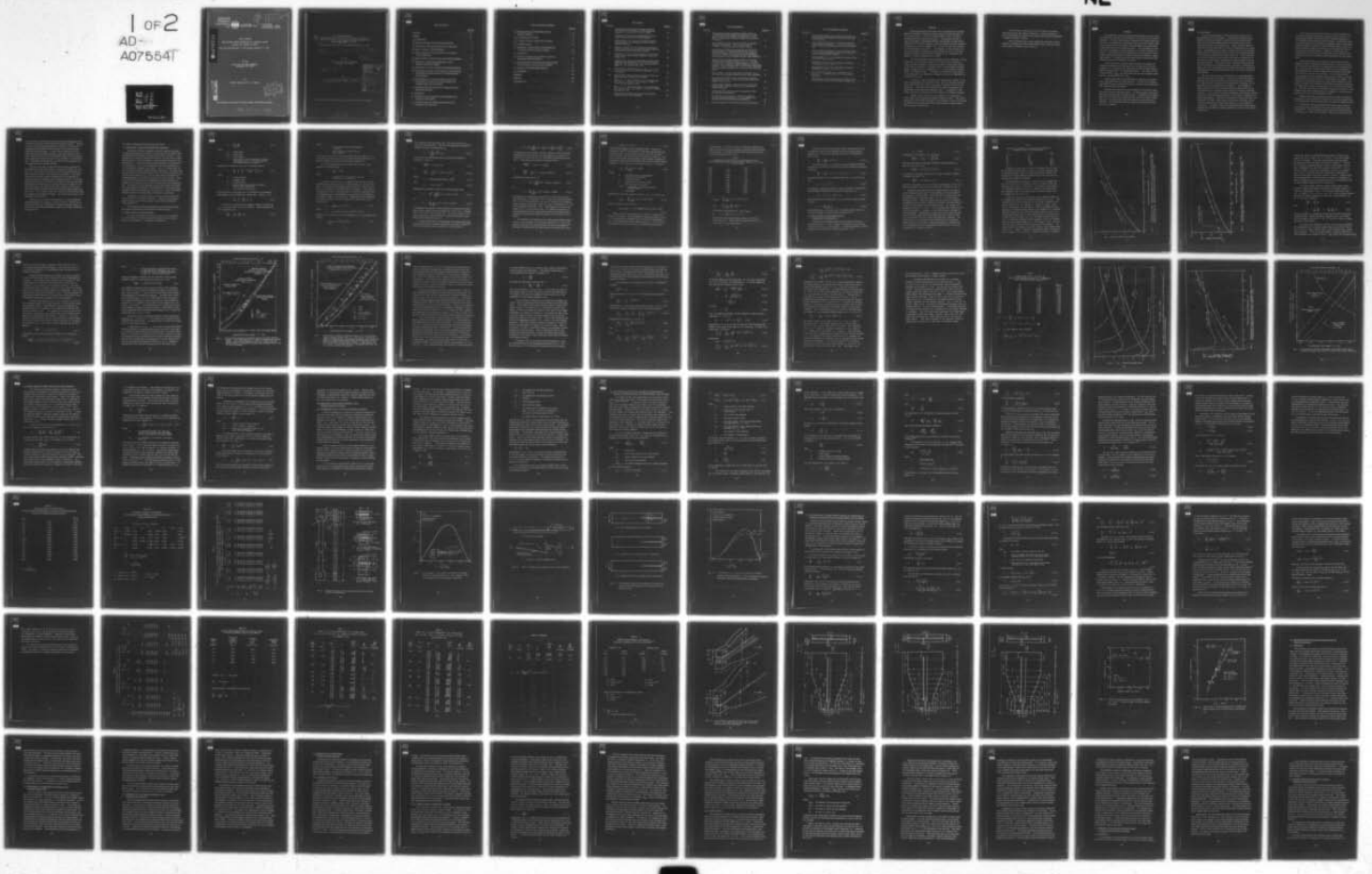

Materials Research Laboratory, Inc.

One Science Road
Glenwood, Illinois 60425

♦ Area Code 312
♦ Local telephone 755-8760
♦ Chicago telephone 785-4020

LEVEL

AD A075541

FINAL REPORT

FRACTURING CHARACTERISTICS OF ADHESIVE JOINTS

Contract No. N00019-77-C-0256

For the period February 1, 1977 through September 15, 1978

For the

NAVAL AIR SYSTEMS COMMAND
Washington, DC 20360

By

Sheldon Mostovoy and E. J. Ripling

DDC FILE COPY

DDC
RECEIVED
OCT 25 1979
A

This document is approved for public release; distribution unlimited.

79 10 25 021

FINAL REPORT

FRACTURING CHARACTERISTICS OF ADHESIVE JOINTS

Contract No. N00019-77-C-0256

For the period February 1, 1977 through September 15, 1978

Final rept. 1 Feb 77 – 15 Sep 78,

124

For the

NAVAL AIR SYSTEMS COMMAND
Washington, DC 20360

15 Sep 78

Accession For
NTIS GRA&I
DDC TAB
Unannounced
Justification
By
Distribution/
Availability Codes
Dist | Avail and/or special
A

By

Sheldon Mostovoy and E. J. Ripling

This document is approved for public release; distribution unlimited.

403973

JUB

Table of Contents

Table of Contents, Continued

List of Tables

List of Illustrations

List of Illustrations, Continued

Foreword

This report describes the work done on determining the Fracture Mechanics Parameters of Adhesive Joints during the period February 2, 1977 through July 31, 1978, the concluding period in what has been a continuing effort for more than ten years. Consequently several sections of the report, including the Section I Introduction, contain review material from the current program, as well as material from other programs, particularly an Air Force program (e.g., see Ref. 8) that bears directly on results obtained in this work. For example, the test techniques sections include those developed during this program, as well as from other programs designed to model service conditions, so that quantitative predictions of service performance can be made.

The test techniques described include those for evaluation of mode-I (Section 2) and for combined modes I and II and I and III (Section 3). These tests were designed to determine the effect of mixed-mode loading on the fracture properties of adhesive bonds for monotonically increasing loading, steady loads in an environment, i.e., stress corrosion cracking (SCC), and fatigue loading. The effects of mixed-mode loading depend on loading cycle (e.g., monotonic or fatigue) and thus, are described differently for each case.

A section on bond manufacture and testing details (Section 4) compares the phosphoric acid anodizing (PAA) aluminum adherend treatment to the chromic acid etch (FPL) on the basis of resistance to SCC in the wedge test. This section also describes the details of laboratory joint manufacture and testing for all specimen types. An appendix to this section (Appendix I) describes the PAA treatment for laboratory bonding.

Section 5 deals with the over all problem of the application of linear elastic fracture mechanics (LEFM) to adhesive bonds. This section discusses the finite element approach to this problem, as well as the energy analysis that has proved successful in using laboratory fatigue fracture data to predict structural life.

The last section (Section 6) is a set of summary conclusions taken from the text and selected references. These conclusions are meant to summarize the current status of Fracture Mechanics Methodology as applied to adhesive bonding.

These conclusions also contain suggestions concerning further research in defining the complex relationships between pure and mixed-mode loading for specimens and structures.

Abstract

The application of fracture mechanics methodology to adhesive bonds, described here, deals with the measurement of the energy lost to the growing crack. The use of this technique, primarily with aluminum adherends, has led to the development of several pure and mixed-mode specimen types that have been shown to be suitable for characterizing bond performance under both rapid and slow growth conditions. This methodology has also been used successfully to predict fatigue life in a bonded structural component. This prediction was made possible by the development of an empirical relationship describing the effect of mixed-mode loading on fatigue crack growth. (A relatively advanced finite element method has not permitted the fatigue life calculation to be made.)

Recent advances in adherend surface treatment and adhesive materials have eliminated bond separation at the interface for any service condition and, consequently, the description of environmentally assisted slow crack growth (SCC) has changed drastically. Pure mode-I SCC has a high threshold, $\mathcal{G}_{Iscc}$, and mixed-mode tests can show threshold values that are a substantial fraction of $\mathcal{G}_{Tc}$.

Fracture appearance is quite different for pure mode-I and mixed-mode crack growth only for rising load tests. All other test conditions have similar fracture conditions which may be resolved with scanning electron microscope (SEM) techniques.

Standard test methods have been described for three mode-I specimen types and three mixed-mode types. The MZKG specimen holds great promise for bond analysis and quality control. Verification of the relationships that have been found between pure and mixed-mode fatigue loading have yet to be confirmed by using other specimen shapes and types of adhesives. This relationship does not appear to hold for either rising load or SCC exposure.

1.0 Introduction

The load carrying capacity of adhesive bonds depends on both manufacturing and service variables. Manufacturing variables include adherend and adhesive materials, adhesive bond and adherend thicknesses, as well as processing history for the adherends and thermal treatments received by the finished part. Service conditions might include static or alternating loads in a variety of temperatures and environments. The complex state of stress, as well as the mode-mix of loading imposed on flaws, defects and bond-free edges, has not permitted accurate structural life predictions of bonded structures. These structures are currently designed using standard stress analysis techniques and a given level of bond quality is maintained by a rigid schedule of manufacture and inspection. This procedure has not always proved successful for such structures and occasional failures, especially in commercial airplanes, have been responsible for the continued search for a quantitative methodology that would enable laboratory tests to be used for structural life prediction.

One of the first steps to be accomplished is to design laboratory tests that model service conditions. Since the structural joint design is generally such that failure in the bond cannot occur due to overloads, i.e., failure occurs by yielding in the relatively thin adherends, the emphasis has been on modelling slow crack growth. The modelling of failure resulting from crack extension rather than plastic flow has been successfully done in monolithic systems using the techniques of fracture mechanics. Thus, fracture mechanics methodology was extended to bonded systems used for load bearing structures in an attempt to understand and avoid future failures. Laboratory test methods in current use today, e.g., "lap-shear" and "peel", while useful to rank adhesive materials, cannot be used to determine the load carrying capacity of a bond contained in a structure. In addition, fatigue and environmental effects pose serious problems that are difficult to define quantitatively with any of the relative ranking tests.

These simple lap-shear and peel tests have been extended to include slow crack growth phenomena, however, the data is used to discover serious problems that can occur in the adhesive material or in the processing of the adherends prior to bonding. Although the onset of slow crack growth for the simple tests generally occurs at lower loads than those needed for short term bond or adherend failure, there is no method currently available that enables the use of simple tests to predict structural bond performance. Similarly, no techniques, even heuristic ones, are available to translate actual service conditions into acceptable performance or quality control requirements for these simple tests.

Early in the history of the extension of linear elastic fracture mechanics (LEFM) of monolithic materials to adhesive bonds, it was realized that bonds were weakest in the presence of mode-I or cleavage loading. The evaluation of cleavage mode resistance was accomplished by several different test specimen configurations using highly elastic rigid and monolithic cantilever beam adherends. The specimens used for mode-I testing were uniform double cantilever beams (UDCB), contoured double cantilever beams (CDCB) and width tapered beams (WTB). The latter two of these specimen types are "crack-length-independent" over much of the bond area and require a knowledge of load alone to determine the applied value of crack extension force, $\mathcal{G}_i$, or stress intensity factor, K_i. All mode-I specimens are described and analyzed in Section 2. Data obtained using mode-I specimens has been described in a number of publications and a review article published in 1976[1].

These data indicated the differences between adhesives of different manufacture and the parameters of concern for slow crack extension which was considered the most serious problem in the design of bonded structure.

Concurrently, with the development of the pure mode-I specimen, work was also done on obtaining a pure mode-II or mixed modes I and II specimen[2]. Data on adhesives loaded primarily in shear indicated that mode-I was a "worst-case" condition, however, data obtained in 1975

on tough adhesives using small mixed-mode specimens appeared to show a serious toughness loss when mixed-mode loads were used[3]. Development work on large mixed-mode specimens (Section 3) has shown that combined mode crack growth does not result in less fracture energy absorption than pure mode-I. In fact, the data collected thus far shows that for monotonically increasing, mixed-mode loading the total crack extension force at onset of rapid fracture ($\mathcal{G}_{Tc}$) occurs when the mode-I component reaches the value of $\mathcal{G}_{Ic}$ determined in a pure mode-I test. This simple relationship does not hold for the slow growth tests of fatigue and stress corrosion cracking.

The work being done by MRL for NASC has been complemented and aided by the work done by MRL on a contract for AFML (e.g., see Ref. 13). This contract was awarded to the Lockheed California Company (CALAC) with MRL as the principal sub-contractor. The AFML work has been directed towards a determination of the suitability of fracture mechanics for design of aircraft bonded structure. In the two years since the start of the contract, the effect of various service conditions has been determined and an accurate prediction of fatigue life of a structural element (the single lap joint; SLJ), similar to the one to be used in the primary adhesive bonded structural technology (PABST) program, made. In the course of the work, the effect of mixed-mode loading was examined and specimens developed that showed that the mode-I case was always the most severe.

Testing of pure and mixed-mode specimens, as well as adherend surface preparation and bonding, covered in Section 4, includes the details of laboratory bond manufacture and fracture mechanics testing details for pure and mixed-mode loading in both onset of rapid fracture and slow growth tests.

2.0 Mode-I (Cleavage) Tests for Large Area Bonds

2.1 Introduction: Review of Analyzed Mode-I Specimens

Among the varieties of specimens used for measuring the mode-I toughness of adhesives, the simplest is the bonded pair of uniform thickness adherends that comprise a double cantilever beam (UDCB)[4]. This specimen type is simple to manufacture and can be used for testing of either adhesive bonds or, with the addition of crack directing face grooves, monolithic materials. As with all crack line loaded specimens, this specimen has the advantage that, with a fixed displacement, the crack extension force, $\mathcal{G}$, decreased with increasing crack length. Thus, an initiated crack will tend to be arrested without complete specimen separation. The crack arrest capability allows several determinations of both the initiation toughness, $\mathcal{G}_{Ic}$, and the arrest toughness, $\mathcal{G}_{Ia}$. Both of these values are thought to be material properties of the test material and can be used in design. Crack arrest data have been shown to be independent of loading rate and are thought to be the minimum value of $\mathcal{G}_i$ or K_i required for any loading situation. The ability of the test material to arrest a fast moving crack should be the major design consideration for materials likely to have local inhomogeneities or lower than normal $\mathcal{G}_{Ic}$ or K_{Ic} levels (e.g., welds in monolithic materials, bubbles or unbonded areas in adhesives or composites).

In addition to the UDCB specimen, several other types have been used successfully, especially for adhesives. These are the contoured double cantilever beam (CDCB) specimen and the width tapered beam (WTB) specimen[4].

This section deals with the compliance analysis of the three specimen types and defines the useful limits for specimen geometry.

2.2 Mode-I Analysis of UDCB Specimens

The error in determining the crack extension force, $\mathcal{G}$, depends on how accurately the compliance change with respect to crack length, dC/da, can be determined. In general, $\mathcal{G}$ is defined as:

$$\mathcal{G} = \frac{P^2}{2B_N}\frac{dC}{da} \qquad 2.2.1$$

where:

- P = applied load
- B_N = crack width
- a = crack length
- C = specimen or structure compliance at a given crack length, a (i.e., the inverse slope of load-displacement line at a given a)

Specifically the compliance for a pair of cantilever beams is

$$C = \frac{24}{EB}\int_o^a \frac{x^2}{H^3} + \frac{6(1+\upsilon)}{EB}\int_o^a \frac{1}{H}\,dx \qquad 2.2.2$$

where:

- E = Young's modulus
- υ = Poisson's ratio
- B = specimen width
- x = distance along the crack plane measured from the point loading and
- H = beam height at the distance x

The two terms in the expression are the contributions to compliance from bending and shear deflections, respectively. Taking $\upsilon = 1/3$

$$C = \frac{8}{EB}\int_o^a \left(\frac{3x^2}{H^3} + \frac{1}{H}\right) dx \qquad 2.2.3$$

In both of the expressions for compliance, H may be a function of x, i.e., the beam height need not be constant. Differentiation of the above expression gives:

$$\frac{dC}{da} = \frac{8}{EB}\left(\frac{3a^2}{H^3} + \frac{1}{H}\right) \qquad 2.2.4$$

where

a = crack length measured from the point of loading

H = beam height at a distance from the point of loading

This expression shows that dC/da depends only on the height of the beam at the crack front and that the equation holds independently of the specimen shape to the extent that beam theory is applicable.

For UDCB specimens where H is constant an integration of the compliance expression yields:

$$C = \frac{2}{3EI}(a^3 + H^2 a) \qquad 2.2.5$$

where

I = the moment of inertia of one of the pair of beams (e.g., $I = BH^3/12$)

Experimental measurements of compliance were obtained on UDCB specimens using uniform beams with machined cracks at a number of locations. The range of beam heights covered was 0.5 to 4 inches and the range of crack lengths used varied from 0.5 to 10 inches. For values of a/H greater than unity, it was found that, in addition to deflections due to bending and shear, some deflections occurred because of rotations at the assumed "built-in" end of the beam. Rewriting the above expression for compliance adding a rotation correction term representing a crack length increase:

$$C = \frac{2}{3EI}[(a + a_o)^3 + H^2 a] \qquad 2.2.6$$

where

a_o = an empirical rotation correction (0.6 H)

Rewriting 2.2.6 to include a_o and the definition of I for a rectangular cross section:

$$C = \frac{8}{EBH^3}[(a + 0.6\,H)^3 + H^2 a] \qquad 2.2.7$$

Two completely analytical methods have been used to define C and dC/da for UDCB specimens. The first, using boundary collocation[5], defined C in terms of an initial slope, I_o:

$$C = \frac{24}{EBH^3}\left(\frac{a^3}{3} + I_o a\right) \qquad 2.2.8$$

The value for the dimensionless parameter enabled calculation of $(d/da)(I_o a)$, but not C:

$$\frac{KBH^{\frac{1}{2}}}{P} = 3.46\left(\frac{a}{H} + 0.7\right) \qquad 2.2.9$$

or

$$\frac{K^2B^2}{P} = \frac{12}{H^3}\left(a^2 + 1.4\,aH + 0.5\,H^2\right) \qquad 2.2.10$$

where

$$K = \text{stress intensity factor} = \sqrt{\mathcal{G}E} \qquad 2.2.11$$

Thus

$$I_o = 1.4\,aH + 0.5\,H^2 \qquad 2.2.12$$

Rewriting the expression in terms of the crack extension force:

$$\mathcal{G} = \frac{K^2}{E} = \frac{12P^2}{EB^2H^3}\left(a^2 + 1.4\,aH + 0.5\,H^2\right) \qquad 2.2.13$$

or

$$\mathcal{G} = \frac{P^2}{2B}\,\frac{8}{EBH^3}\left(3a^2 + 3.6\,aH + 2.08\,H^2\right) \qquad 2.2.14$$

The difference in measured $\mathcal{G}$ values between the calculated and experimental curves results in errors varying from -0.3% to +2.7%. Between a/H of 2 and 12 the error averages 1.5%. The errors, intrinsic to compliance measurement, prevent making a conclusion regarding the more likely of the two expressions for $\mathcal{G}$.

A second method uses a one-dimensional finite length beam model which is partly free and partially supported by an elastic foundation[6]. For the case where the beam is assumed to be infinitely long:

$$C = \frac{\delta}{P} = \frac{4a^3}{EBH^3}\left(1 + 1.92\,\frac{H}{a} + 1.22\,\frac{H^2}{a^2} + 0.39\,\frac{H^3}{a^3}\right) \qquad 2.2.15$$

The derivation of this equation, however, contains a rather arbitrarily established foundation modulus and, consequently, the values of C as a function of a/H are quite close to those defined experimentally and in Ref. 5. The value for the constant involving dC/da is:

$$\frac{KBH^{3/2}}{P} = 2\sqrt{3}\,a\left(1 + 0.64\,\frac{H}{a}\right) \qquad 2.2.16$$

or

$$\frac{K^2B^2}{P^2} = \frac{12}{H^3}\left(a^2 + 1.28\,Ha + 0.4096\,H^2\right) \qquad 2.2.17$$

Rewriting this expression for $\mathcal{G}$

$$\mathcal{G} = \frac{K^2}{E} = \frac{12P^2}{EB^2H^3}\left(a^2 + 1.28\,Ha + 0.4096\,H^2\right) \qquad 2.2.18$$

or

$$\mathcal{G} = \frac{P^2}{2B}\,\frac{8}{EBH^3}\left(3a^2 + 3.84\,Ha + 1.288H^2\right) \qquad 2.2.19$$

If we compare the coefficients for Ha and H^2, we find that this calculation falls between the experimental (Ha = 3.6) and the collocation equation (Ha = 4.2) for the Ha coefficient, while the H^2 coefficient for the beam on elastic formulation calculation is lower than either the collocation (H^2 = 1.5) or the experimental value (H^2 = 2.08). Since these terms are small with respect to $3a^2$, as a/H increases above 1, the differences between both sets of calculations and the experimentally determined compliance represented by the experimental compliance equation is of the order of 1 to 2 percent.

The expression for compliance of the UDCB assumes infinite length, however, when the length of the uncracked ligament (W - a) or b is too short, the back end of the specimen begins to control the compliance[7]. Empirically, deviations from the infinite length b expression occur when:

$$1.25\ H \leq b \leq 1.5\ H \qquad 2.2.20$$

where H is the height of one of the pair of beams. Neither the Srawley and Gross[5] nor Kanninen[6] work deals quantitatively with end effects; thus, the approximate value of b at which end effects become important must be obtained from compliance calculations. However, one can use the compact specimen (CS) compliance calibration to approximately obtain the value of b/H at which back end effects become significant. If we write the CS calibration in terms of $\not{p}$ we obtain:

$$\not{p}_{CS} = \frac{P^2}{2B}\frac{8}{EBH^3}\,0.15\,[f(\tfrac{a}{W})]^2 \qquad 2.2.21$$

where

W = the distance from the loading holes to the end of the specimen

B = specimen thickness

H = height of one of the pair of beam

E = elastic modulus of the beam

f(a/W) = a polynomial fit expression specified by ASTM E399-78

a = crack length

Recall that for the UDCB specimen (see Eqs. 2.2.1, 2.2.4 and 2.2.6)

$$\not{p}_{UDCB} = \frac{P^2}{2B}\frac{8}{EBH^3}\,[3\,(a + 0.6\,H)^2 + H^2] \qquad 2.2.22$$

Thus, if we take the ratio of these:

$$\not{p}_{CS}/\not{p}_{UDCB} = R = 0.15\,[f(\tfrac{a}{W})]^2/[3\,(a + 0.6\,H)^2 + H^2] \qquad 2.2.23$$

Values of R have been determined for values of b ranging from 0.416 to 1.33, Table 1. For the example, H was taken equal to 1, thus, b = b/H and the point of deviation is at a b/H value of approximately 1.17. This demonstrates that the limits on b/H, i.e., $1.25 \leq b/H \leq 1.5$, are conservative as long as there is not substantial yielding prior to

crack extension. The limits on b/H were established empirically for adhesive joints some of which developed a substantial yield zone ahead of the crack tip. It is likely that with brittle materials the value of b/H could be reduced as low as 1.17.

Table 1

Comparison of dC/da Ratio* for Compact Specimens and Uniform Beam Specimens for a Decreasing Net Ligament, (W - a) or b
H = 1.0, W = 1.6667

a/W	a	b/H	R
0.20	0.333	1.33	1.12
0.25	0.417	1.25	1.07
0.30	0.500	1.17	1.11
0.33	0.550	1.12	1.16
0.35	0.583	1.08	1.22
0.40	0.667	1.00	1.38
0.50	0.833	0.83	1.93
0.60	1.000	0.67	3.77
0.70	1.167	0.50	6.64
0.75	1.250	0.41	10.50

*

$$\mathcal{G}_{UDCB} = \frac{P^2}{2B}\frac{8}{EBH^3}\left[3\,(a + 0.6\,H)^2 + H^2\right]$$

$$\mathcal{G}_{CT} = \frac{P^2}{2B}\frac{8}{EBH^3}\frac{H^3}{4W}\left[f\left(\frac{a}{W}\right)\right]^2$$

For the given dimensions and $R = \mathcal{G}_{CT}/\mathcal{G}_{UDCB}$:

$$R = 0.15\left[f\left(\frac{a}{W}\right)\right]^2/\left[3\,a + 0.6\right)^2 + 1\right]$$

Note that R remains approximately constant up an a/W of 3 and b/H of 1.17. Thus, the values selected for b/H, i.e., $1.25 \leq b/H \leq 1.5$, are conservative.

The shear-corrected beam formula (SCBF) expression for the rate of compliance change with crack length, dC/da, for a pair of UDCB specimens (eq. 2.2.4) can be rewritten in terms of the dimensionless term $\xi = a/H$:

$$\frac{dC}{da} = \frac{8}{EBa} \xi (3 \xi^2 + 1) \qquad 2.2.24$$

For UDCB specimens, it was found that some additional deflection occurred due to rotation at the built-in end which modified the compliance expression:

$$\frac{dC}{da} = \frac{8}{EBa} \xi (3 \xi [3 (\xi + 0.6)^2 + 1]) \qquad 2.2.25$$

The SCBF definition of m (the bracketed part of eq. 2.2.4) in terms of ξ is:

$$m = \frac{\xi}{a} (3 \xi^2 + 1) \qquad 2.2.26$$

The empirical, compliance-determined, shear and rotation corrected beam formula (SRCBF) definition of the same term, denoted m_1, is

$$m_1 = \frac{\xi}{a} [3 (\xi + 0.6)^2 + 1] \qquad 2.2.27$$

The expression for $\mathcal{G}$ is expressed in 2.2.1 and can be written in terms of m_1 as:

$$\mathcal{G} = \frac{P^2}{2B} \frac{8}{EB} m_1 \qquad 2.2.28$$

For the UDCB case, m_1 is equal to the m' described earlier and is the corrected compliance term that enables calculation of $\mathcal{G}$.

2.3 Mode-I Analysis of CDCB Specimens and Comparison to UDCB Specimens

Calculations concerning constant dC/da specimens often use a dimensionless expression that is related to the square root of the value of dC/da expected for a given specimen. A suitable expression for these specimens can be derived by rewriting expression 2.2.11:

$$\mathcal{G} = K^2/E \qquad 2.3.1$$

Combining eq. 2.3.1 with eq. 2.2.1 we obtain:

$$\frac{KB\sqrt{a}}{P} = 2\sqrt{m'a} = \tfrac{1}{4}\sqrt{\frac{dC}{da}\,EBa} \qquad 2.3.2$$

Since the UDCB specimen compliance calculation has shown that m_1 is equal to m' (see eq. 2.2.27):

$$\frac{KB\sqrt{a}}{P} = 2\sqrt{\xi\,[3\,(\xi + 0.6)^2 + 1]} \qquad 2.3.3$$

The equivalent expression taken from the boundary collocation analysis by Srawley and Gross[5] is:

$$\frac{KB\sqrt{a}}{P} = \sqrt{\xi}\,(3.46)\,(\xi + 0.7) \qquad 2.3.4$$

Both of the expressions, eq. 2.3.3, derived experimentally, and eq. 2.3.4, derived numerically, agree within one percent for ξ between 0.5 and 10.

Cantilever beam adherends that are height tapered in accordance with the bracketed part of eq. 2.2.4 and denoted m have been found to be independent of crack length. The parameter m is a shape factor having the dimensions of reciprocal length, e.g., $in.^{-1}$, which specifies a particular contour. While this constant has been shown to be sufficient in designing a linear dC/da or "constant-K" specimen, the actual value of dC/da is generally larger than the calculated value. For example, for adherends contoured to $m = 90\ in.^{-1}$, the experimental and calculated value of dC/da are identical. However, at lower values of m the deviation becomes substantial. Surprisingly, the shear and rotation corrected beam formula (SRCBF) cannot be used for CDCB specimens to define a value of m_1 that coincides with the m' value determined from compliance. Recalling that m' is an experimental value determined from a countoured double cantilever beam (CDCB) compliance calibration, a comparison can be made between the shear corrected beam formula (SCBF), m, and the experimental m', as shown in Table 2.

Table 2

Comparison of Calculated and Experimentally Determined Compliance Terms for CDCB Specimens

m $in.^{-1}$	m' $in.^{-1}$	Error %
90	90	0
8	13.7	31.4
4	5.45	38.8
3	4.13	37.7
1.33	2.22	66.9

It should be noted that the value of m obtained from the beam formula without any corrections, such as the rotation correction used for UDCB adherends, remains a suitable criterion for specimen contouring even for large differences between it and the value of m' determined from compliance calibration.

Re-examination of expression 2.2.26 shows that, although any value of m can be used for specimen design, its absolute shape will depend on the system of units chosen. For example, if we measure m in centimeters instead of inches, the height of the specimen for a given absolute value of crack length will be increased, since m will be multiplied by the ratio 1:2.54.

To avoid the question of dimensional units, specimen design can be accomplished using the dimensionless parameters mH and ma. This technique has the added advantage that the family of constant K specimens, defined by m, are reduced to a single curve shape, Figs. 1 and 2. For adhesive joint adherends, as well as monolithic fracture specimens, the specimen design criteria to be satisfied are (1) adequate adherend strength to resist adherend yielding during the test, (2) a suitable crack plane length so that fracture data can be obtained over as long a range as possible, and (3) a reasonable specimen size and cost. In addition, monolithic fracture specimens must be of sufficient height at a given crack length, i.e., a low enough m value, such that the crack will be confined to the center plane of the specimen. For adhesive joints the criteria are met with relatively small aluminum adherends, e.g., $m = 90\ in.^{-1}$, where the crack growth data is analyzed between $\underline{a}$ values of 1½ to 9¼ inches. Monolithic specimens of isotropic

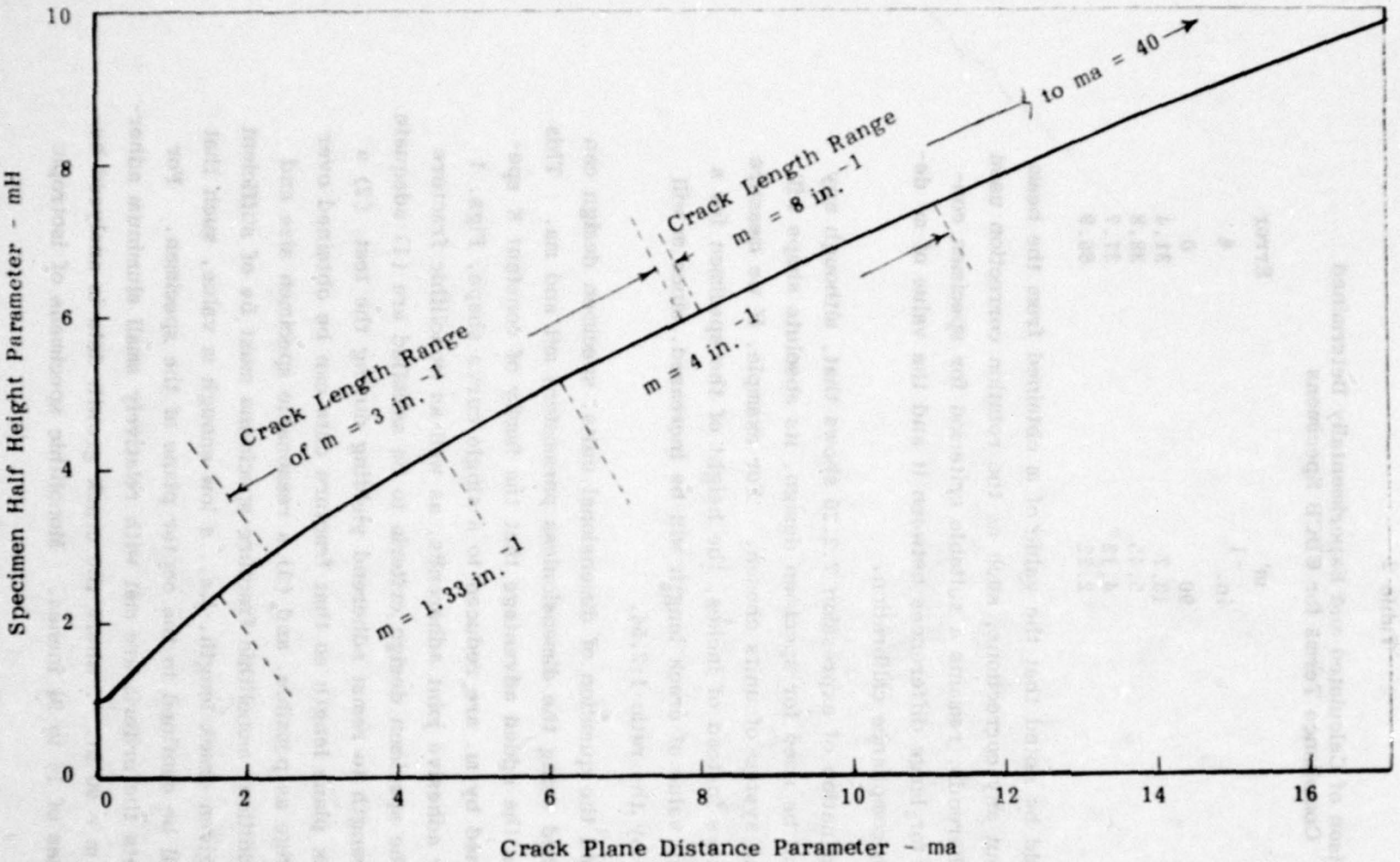

Fig. 1 Parameterized Constant Compliance Change (dC/da) or "Constant-K" Specimen Shape for ma Less Than 17. Note that the single curve describes the shape of the entire family of "Constant-K" specimens of which four are shown on this plot.

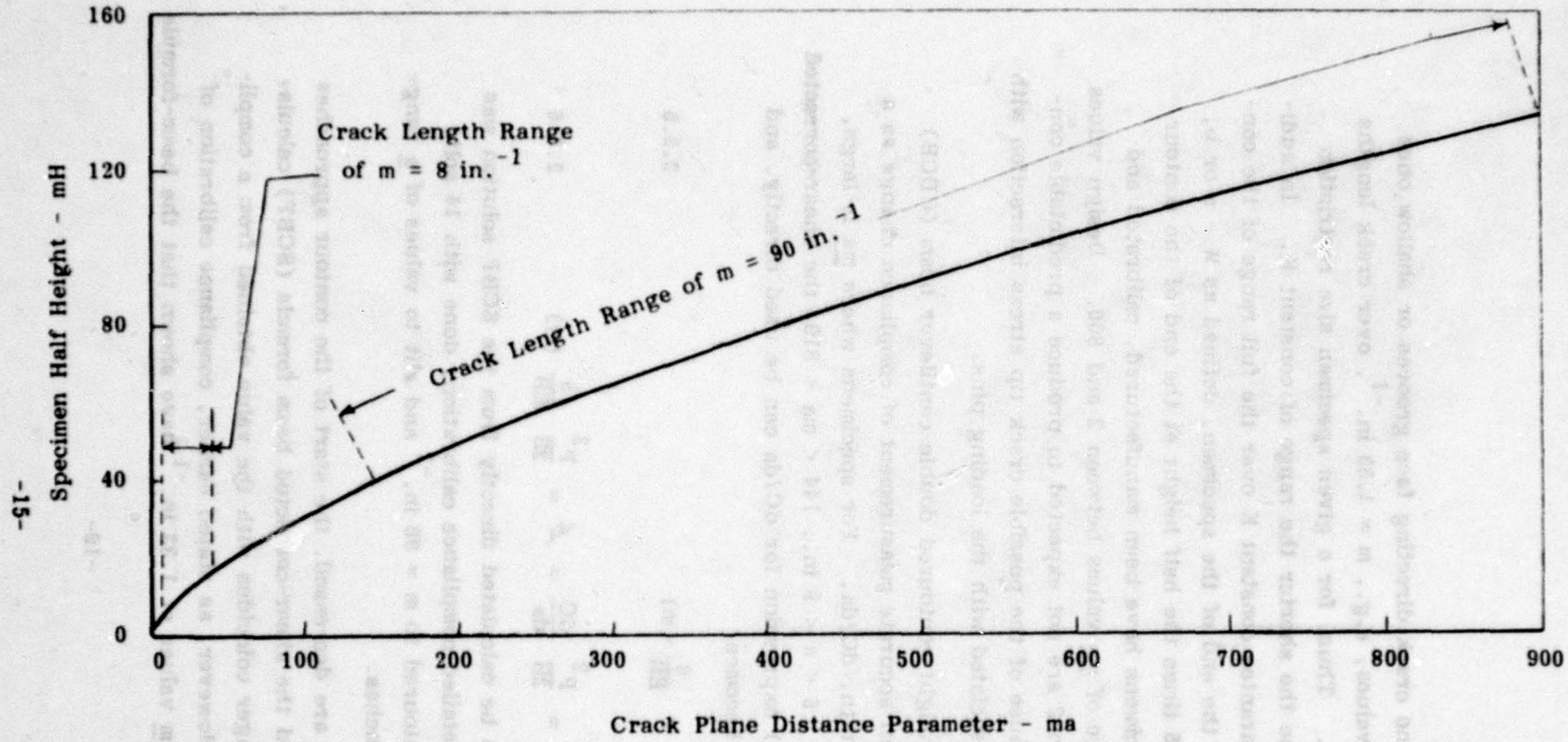

Fig. 2 Parameterized Constant dC/da of "constant-K" Specimen Shape for ma up to 900. Note the range used for m = 90 in.$^{-1}$ adherends used for adhesive testing.

material with either no crack directing face grooves or shallow ones require very low m values, e.g., m = 1.33 $in.^{-1}$, over crack lengths of 2.3 to 5.6 inches. Thus, for a given specimen size restriction the lower the m value the shorter the range of constant K. In addition, in order to guarantee constant K over the full range of the contour the distance to the end of the specimen, defined as W - a or b, must be at least 1.25 times the half height at the end of the contour (eg. 2.2.20). Specimens have been manufactured, calibrated and tested over the range of ma values between 2 and 800. Design values of ma much less than 2 are not expected to produce a predictable constant K contour because of the possible crack tip stress interaction with the local stresses associated with the loading pins.

The use of height contoured double cantilever beam (CDCB) specimens requires an accurate measurement of compliance change as a function of crack length, dC/da. For specimens where ma is large, e.g., m = 90 $in.^{-1}$; $1.6 < a < 9$ in.; $144 < ma < 810$, the shear-corrected beam formula (SCBF) expression for dC/da can be used directly, and eq. 2.2.4 or 2.2.24 becomes:

$$\frac{dC}{da} = \frac{8}{EB}\,(m) \qquad 2.3.5$$

and

$$\mathcal{G} = \frac{P^2}{2B}\,\frac{dC}{da} = \mathcal{G} = \frac{P^2}{2B}\,\frac{8}{EB}\,(m) \qquad 2.3.6$$

The fact that $\mathcal{G}$ can be calculated directly from the SCBF solution was determined from a detailed compliance calibration, done with 14 solid CDCB specimens contoured to m = 90 $in.^{-1}$ and slit to values of a ranging from 1.6 to 10 inches.

As m and ma are decreased, the start of the contour approaches the loading holes and the shear-corrected beam formula (SCBF) calculation of dC/da no longer coincides with the value obtained from a compliance calibration. However, as stated earlier, compliance calibration of CDCB specimens to m values of 1.33 $in.^{-1}$ have shown that the beam-formula

concept for specimen design is adequate to obtain constant dC/da over the ma range used for this program. For these cases, m is replaced in eq. 2.2.6 with m', an experimental value determined from a compliance calibration.

Several numerical solutions are available that enable calculation of dC/da that come closer than the SCBF to the value determined from compliance. The boundary value collocation (BVC) technique[5] uses straight contours to approximate the shape while the finite element technique[8] can be used for curved specimen contours. Each technique has been used to evaluate a range of the ma contour for ξ chosen, such that the contour can be approximated by a straight line. Thus, at the high ma values, used for the contoured m = 90 in.$^{-1}$ adhesive specimen, the finite element method (FEM) gives a calculated dC/da value closer to that determined from experimental compliance than does collocation.

At values of ma between 2 and 8 (for ξ between 0.7 and 1.5) both numerical solutions give similar values for the dimensionless compliance parameter $KB\sqrt{a}/P$. Experimental compliance measurements on straight-contour CDCB specimens in this range agree moderately well with the calculated values. A fit equation for the data can also be obtained from a combination of the modified beam formula equations developed for the straight sided DCB specimen. Recall (eq. 2.2.7) that dC/da for UDCB specimens could be calculated using an empirical shear and rotation corrected beam formula (SRCBF) expressed as a dimensionless parameter, (eq. 2.2.10) while the SCBF expression was somewhat simpler:

$$\frac{KB\sqrt{a}}{P} = 2\sqrt{\xi\,(3\xi^2 + 1)} \qquad 2.3.7$$

A combination of these two expressions (FITBF) can be obtained as follows:

$$\frac{KB\sqrt{a}}{P} = 2\sqrt{k\,[3\xi\,(\xi + 0.6)^2 + \xi] + (1 - k)(3\xi^3 + \xi)} \qquad 2.3.8$$

where

k = a fitting parameter to determine the amount of each term in the expression; e.g., $k = 1$ for the case where only SRCBF expression is valid, $k = 0$ for the SCBF alone.

Using the compliance calibration data for specimens in the ma range between 2.5 and 11, k was found to be equal to 1/3, thus:

$$\frac{KB\sqrt{a}}{P} = 2\sqrt{3\xi^3 + 4\xi\,(0.3\xi + 0.34)} \qquad 2.3.9$$

The compliance calibration range of possible cantilever beam specimens can be shown on a plot using the dimensionless variables ξ and $KB\sqrt{a}/P$, Fig. 3 (see also Table 3). Several curves and data points from constant dC/da specimens are included for comparison. The lower curve is calculated from beam theory, (eq. 2.3.7; SCBF) while the two curves above it are empirically obtained; the upper one being the rotation modified expression (eq. 2.3.5; SRCBF) and the middle one the weighted sum of the two (eq. 2.3.9; FITBF). The uppermost curve is obtained from the published compliance calibration of compact specimens, ASTM E399-78, and is used to demonstrate that end effects become important at (W - a)/H or b/H ratios of less than 1.19, eq. 2.2.20.

Data points from the compliance calibration of three specimen configurations, m = 1.33, 3 and 4 $in.^{-1}$, are included as are calculated values of $KB\sqrt{a}/P$ from FEM and BVC. An expanded plot of the data in the range $0.5 \leq \xi \leq 1.6$ is shown in Fig. 4.

At high values of ξ (e.g., $\xi > 3$) the shear corrected beam formula (SCBF) and FEM give essentially identical results while BVC, being based on a straight line approximation of the specimen shape, is somewhat higher (Fig. 3). For values of ξ between 0.6 and 1.6 (Fig. 4) which is the range for monolithic specimens requiring little or no crack directing face grooves, both the BVC and FEM points lie approximately on the line defined by the empirical beam formula fit expression (FITBF), eq. 2.3.7. Compliance data from two of the three CDCB specimens fall on this FITBF curve,

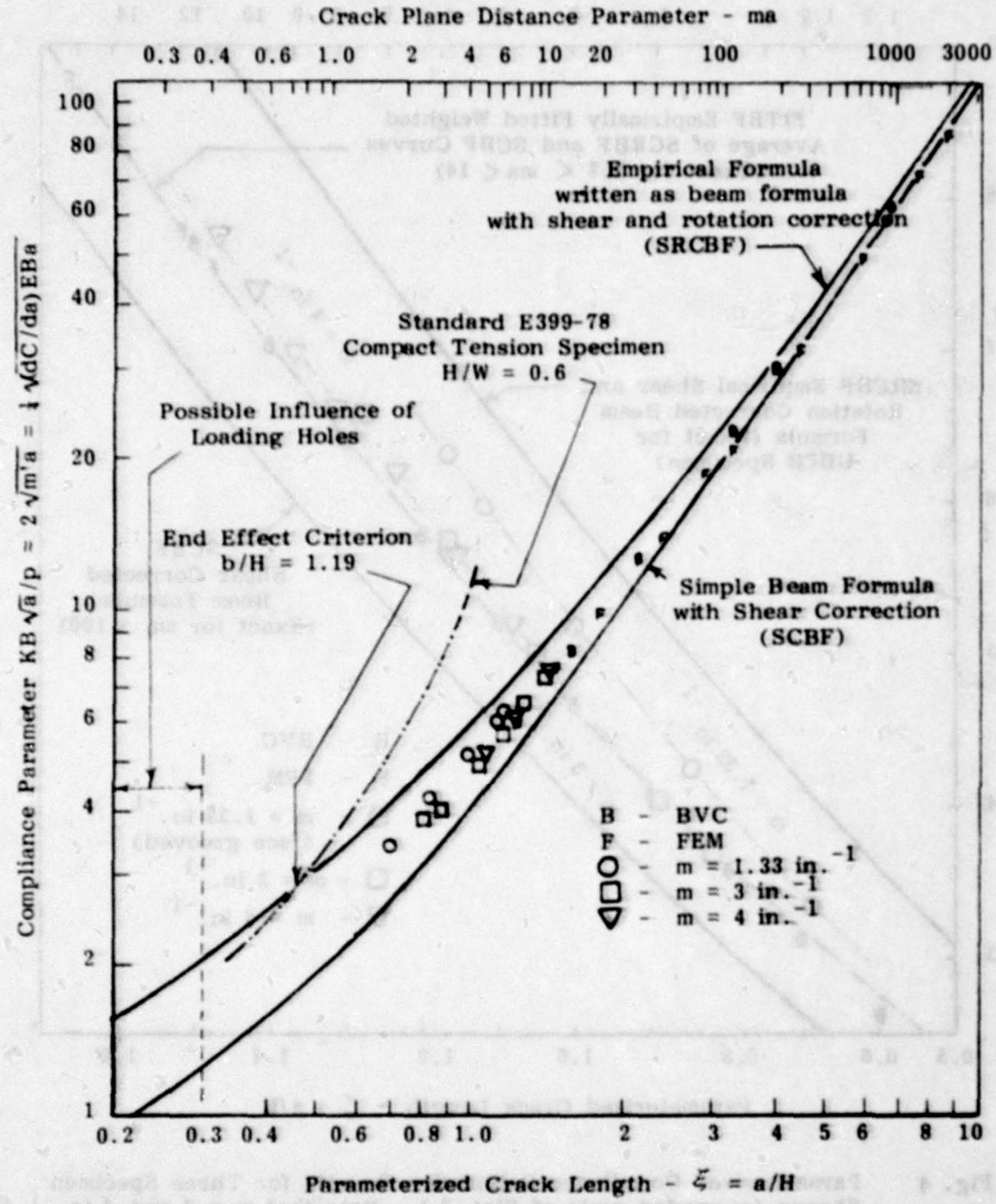

Fig. 3 Parameterized Compliance Calibration Results for Three Specimen Shapes. Data Lines Added are (1) Shear Corrected Beam Formula (SCBF) used for CDCB Specimens Above ma = 100 and (2) the Empirical Shear and Rotation Corrected Beam Formula (SRCBF) used for UDCB Specimens.

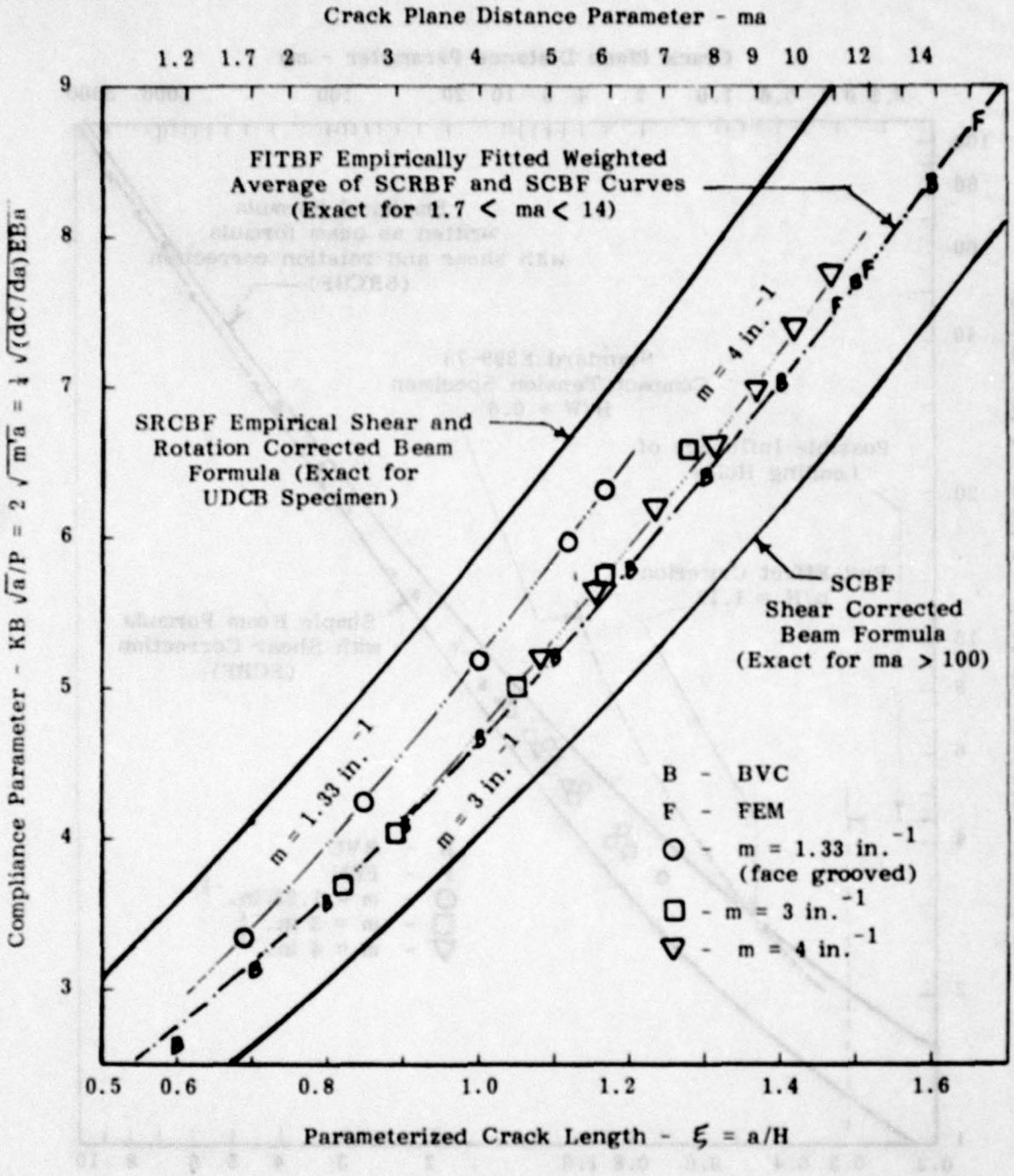

Fig. 4 Parameterized Compliance Calibration Results for Three Specimen Shapes (expanded scale of Fig. 3). Note that m = 3 and 4 in.$^{-1}$ Specimen Compliance Data the Numerical Boundary Value Collocation (BVC) and Finite Element Method (FEM) Points are Fitted by the Empirical Weighted Average Curve (FITBF). Note also that the m = 1.33 in.$^{-1}$ data is not fitted due to compliance calibration with 12.5 percent per side face grooves.

however, data from the m = 1.33 $in.^{-1}$ specimen lies somewhat above the others. This apparent anomaly can be understood in light of the fact that compliance data from these specimens were obtained on blanks having 25 percent face grooves to duplicate the actual specimen configuration. Thus, the displaced curve is related to the face groove depth and configuration. The position of the compliance curve as a function of face groove dimensions has been determined experimentally for each CDCB contour to be used in a given test program, however, no general numerical method has yet been applied to this task.

The use of the shear corrected beam formula (SCBF) in the design of constant dC/da specimens has been shown to be satisfactory. The actual value of dC/da cannot be predicted from the SCBF at values of ξ less than 3 ($\underline{m}a < 30$) and for non-face-grooved specimens. A very good estimate of the dimensionless, true compliance parameter, $KB\sqrt{a}/P$, can be obtained from BVC, FEM or FITBF, an empirical modification of the beam formula similar to that used for UDCB specimens. However, face grooving of a given specimen shape requires a new compliance calibration. Nevertheless, for modest face grooves, e.g., 12.5 percent per side, an approximate calibration can be calculated by using eq. 2.3.8 with a k value of 0.5. No BVC or FEM calculations are available that allow inclusion of face grooves.

The use of contoured double cantilever beam (CDCB), constant dC/da, specimens made from monolithic materials, e.g., bulk adhesive, is often limited because of non-planar crack growth. For $\underline{m}$ values greater than 2 $in.^{-1}$ face grooves must be provided along the desired crack plane to avoid a circumstance denoted "arm break-off". For non-side grooved specimens, as $\underline{m}$ increases, thre is an increased possibility that the crack will leave the crack plane in the center of the specimen and break off a small part of "arm" of the specimen near one loading hole. The tendency for this type of fracture is undoubtedly related to the magnitude of the bending stress, σ_x, parallel to the crack plane relative to the critical perpendicular stress, σ_y, which occurs during crack extension, e.g., the ratio σ_x/σ_y. Thus, a specimen design that would lower the bending stress

at a given fracture load, e.g., a lower m value, would be more likely to keep the crack in the center plane. The nominal bending stress, σ_x, can be calculated from strength of materials, i.e.:

$$\sigma_x = \frac{6Pa}{BH^2} \qquad 2.3.10$$

Rewriting this expression in terms of a/H or ξ

$$\sigma_x = \frac{6P}{BH}\,\xi = \frac{6P}{Ba}\,\xi^2 \qquad 2.3.11$$

Since the calculation of a nominal stress, σ_y, at the crack tip cannot be done simply, except when the crack front is near the free back edge of the specimen, the value of the applied K is used in place of σ_y in the calculation of a crack stability parameter, K/σ_x.

This ratio has the dimensions of the square root of length, e.g., $(\text{inch})^{\frac{1}{2}}$. which is consistent with laboratory experience using UDCB specimens. For monolithic uniform beam specimens tested at a given crack length, the greater the value of H (i.e., the smaller the value of the nominal σ_y stress) the greater the tendency of the crack to run straight. Additionally, the tougher the material (i.e., the greater the value of K_Q or K_{Ic}) the larger the plastic zone surrounding the crack tip and the greater the tendency for crack deviation. Both of these phenomena suggest that the dimensional quantity, K/σ_x, be used as the crack stability parameter. Since crack stability is expected to depend on a number of factors, the specification of a minimum K/σ_x cannot be made. Rather, the ratio K/σ_x is used as a qualitative estimate of the possibility of crack deviation for a given specimen. From an experimental point of view, should a given specimen present a problem controlling crack direction, modifying it so as to obtain a higher value of K/σ_x would tend to increase crack direction stability.

Calculation of K/σ_x can be done using the definition of σ_x and the three expressions for the dimensionless parameter $KB\sqrt{a}/P$. The first of these (eq. 2.3.2) is based on the empirical shear and rotation

corrected beam formula (SRCBF) for UDCB specimens and the second, (eq. 2.3.3), is based on the strength of materials shear corrected beam formula (SCBF) for CDCB specimens where ma is greater than 100. A third empirical beam formula, (eq. 2.3.9), (FITBF) was also shown to be reasonably exact for non-face grooved CDCB specimens for values of ma between 1.7 and 20.

The expression for σ_x shown in eq. 2.3.11 can be rearranged as follows:

$$\frac{\sigma_x aB}{P} = 6\xi^2 \qquad 2.3.12$$

Using expressions 2.3.11 and 2.3.7, we can obtain the dimensionless ratio:

$$\frac{K}{\sigma_x\sqrt{a}} = \frac{1}{3\xi^2}\sqrt{\xi(3\xi^2+1)} \qquad 2.3.13$$

This expression, to be used for large values of ma (eq. 2.3.13), can be scaled to K/σ_x using an arbitrary value of initial crack length as:

$$\frac{K}{\sigma_x\sqrt{a_o}} = \frac{K}{\sigma_x\sqrt{a}}\sqrt{\frac{a}{a_o}} = \sqrt{\frac{a}{a_o}}\,\frac{1}{3\xi^2}\sqrt{\xi(3\xi^2+1)} \qquad 2.3.14$$

Multiplying and dividing eq. 2.3.24 by $\sqrt{m}$:

$$\frac{K}{\sigma_x\sqrt{a_o}} = \frac{1}{\sqrt{ma}_o}\,\frac{\sqrt{ma}}{3\xi^2}\sqrt{\xi(3\xi^2+1)} \qquad 2.3.15$$

But

$$ma = \xi(3\xi^2+1) \qquad 2.3.16$$

Thus

$$\frac{K}{\sigma_x\sqrt{a_o}} = \frac{1}{\sqrt{ma}_o}\,\frac{\xi(3\xi^2+1)}{3\xi^2} = \frac{1}{\sqrt{ma}_o}\,\frac{(3\xi^2+1)}{3\xi} \qquad 2.3.17$$

or

$$\frac{K}{\sigma_x \sqrt{a}} = \frac{1}{\sqrt{ma_o}} \frac{ma}{3\xi^2} \qquad 2.3.18$$

To find the minimum in this expression, i.e., the value of ma where $K/\sigma_x \sqrt{a_o}$ is the lowest, we differentiate eq. 2.3.18 with respect to (ma) and set the derivative equal to zero:

$$\frac{d}{d(ma)} = \frac{1}{3\xi^2} - \frac{(ma)(2)}{3\xi^2} \frac{d\xi}{d(ma)} = 0 \qquad 2.3.19$$

$$0 = \frac{1}{3\xi^2} - \frac{2(3\xi^2 + 1)}{3\xi^2 (9\xi^2 + 1)} \qquad 2.3.20$$

$$1 = -2 \frac{(3\xi^2 + 1)}{9\xi^2 + 1} \qquad 2.3.21$$

and thus:

$$\xi = \frac{\sqrt{3}}{3} \qquad 2.3.22$$

Thus, the highest probability of crack deviation is found at an ma value where $\xi = \sqrt{3}/3$, i.e.

$$ma = \xi (3\xi^2 + 1) = \frac{2\sqrt{3}}{3} = 1.1547 \qquad 2.3.23$$

Expressions for $K/\sigma_x \sqrt{a_o}$ can also be found for UDCB specimens and CDCB's at low values of ma using eq. 2.3.11 and eqs. 2.3.3 and 2.3.9, respectively, for UDCB's,

$$\frac{K}{\sigma_x \sqrt{a_o}} = \frac{1}{\sqrt{ma_o}} \left\{ \frac{\sqrt{ma}}{3\xi^2} \sqrt{\xi[3(\xi + 0.6)^2 + 1]} \right\} \qquad 2.3.24$$

Substituting

$$\sqrt{ma} = \sqrt{\xi (3\xi^2 + 1)}$$

$$\frac{K}{\sigma_x \sqrt{a_o}} = \frac{1}{\sqrt{ma_o}} \left\{ \frac{1}{3\xi} \sqrt{3\xi^2 + 1} \sqrt{(\xi + 0.6^2 + 1)} \right\} \qquad 2.3.25$$

$$= \frac{1}{\sqrt{ma_o}} \frac{1}{3\xi} \sqrt{3\xi^2} + 1 \sqrt{3\xi^2 + 3.6\xi + 2.08}$$

$$\frac{K}{\sigma_x \sqrt{a_o}} = \frac{1}{\sqrt{ma_o}} \{\frac{1}{3\xi} \sqrt{3\xi^2} + 1 \sqrt{3\xi^2 + 1.2\xi + 1.36}\} \qquad 2.3.26$$

Expressions 2.3.25 and 2.3.26 are not as easily differentiable, however, the minimum values of $K/\sigma_x\sqrt{a_o}$ for both cases are found numerically at values of $\underline{m}a$ somewhat above 1.155, i.e., 1.323 and 1.522 for eqs. 2.3.26 and 2.3.25, respectively. For CDCB specimens at low $\underline{m}a$ values, eq. 2.3.26 can be used (after eliminating a_o) to generate a family of $\underline{a}$ vs. K/σ_x curves for $\underline{m}$ values of interest, Fig. 5. Although the improvement in K/σ_x goes as the square root of $\underline{m}$ the m = 1.33 $in.^{-1}$ specimen has demonstrated little tendency for crack deviation compared to that experienced using $\underline{m}$ values of 3 $in.^{-1}$ or greater in monolithic materials. It should be noted that when $\underline{m}$ is changed, both the size of the specimen is changed and its geometry relative to the $\underline{m}a$ curve is shifted. Fig. 5 also includes K/σ_x vs. $\underline{a}$ data for UDCB specimens with height, H, as a parameter obtained using eqs. 2.3.11 and 2.3.3:

$$\frac{K}{\sigma_x} = \frac{\sqrt{a}}{3\xi^2} \sqrt{\xi\,[3(\xi + 0.6)^2 + 1]} \qquad 2.3.27$$

The family of UDCB curves shows that the m = 1.33 $in.^{-1}$ shape is more stable than a 2-inch UDCB specimen when the crack length, $\underline{a}$ is 2.25 in., and a 4-inch UDCB when $\underline{a}$ is 7 inches. For comparison, the m = 4 $in.^{-1}$ shape is equivalent in stability to a 1-inch UDCB at a = 1.5 inches and a 3-inch UDCB at a = 8 inches. This comparison is useful in that it demonstrates the sensitivity of the stability parameter, K/σ_x. An estimate of the upper bound value of K/σ_x necessary for crack plane stability can be obtained from the successful compact tension specimen (CS) geometry. For a non-face grooved 1T CS specimen having a K_{Ic} of 45 ksi-$\sqrt{in.}$ and a yield strength, σ_o, of 100 ksi, the value of K/σ_x is about 1.4 $\sqrt{in.}$ at a/W = 0.55. This implies that a

non-face grooved $m = 1.33$ in.$^{-1}$ specimen could be tested without crack plane deviation using similar or tougher material.

A convenient representation of the effect on the stability parameter of moving along the ma curve is shown in Fig. 6. This is a plot of ma vs. mH with the superimposed, scaled dimensionless parameter $K/\sigma\sqrt{a_o}$ from eq. 2.3.26. For this plot the constant $\sqrt{ma_o}$ is 0.25. This plot shows that all specimens used to date are at or slightly beyond the minimum value of $K/\sigma_x \sqrt{a_o}$. Thus, crack stability should improve with increasing crack length. A tentative conclusion that might be drawn from Figs. 5 and 6 is that a value of K/σ_x equal to or larger than 1.3 $(\text{in.})^{\frac{1}{2}}$ is required for a substantial degree of crack stability, especially with low strength materials. Fig. 7, a plot of ξ vs. $KB\sqrt{a}/P$, similar to Fig. 4, includes the dimensionless parameter $10K/\sigma_x$ as calculated from eq. 2.3.24 for UDCB specimens. This figure shows that the bending stress, relative to K, decreases as the crack length parameter, ξ, increases. Thus, for uniform beam specimens, even though longer crack lengths require lower loads to produce a given value of K, the longer the crack length for a given value of H and K, the less the crack stability. This trend is opposite to that obtained on CDCB adherends where increases in ξ or ma result in increased stability.

Table 3

Tabled Values of ma[1], mH and ξ for
Double Cantilever Beam Specimens vs. Dimensionless
Crack Stability Parameter $10K/\sigma_x \sqrt{a}$[2]

ma	mH	ξ	$10K/\xi\sqrt{a}$
0.3	1.191	0.252	35.87
0.5	1.389	0.360	22.79
1.0	1.864	0.536	14.38
2.0	2.676	0.747	10.24
3.0	3.373	0.889	8.71
4.0	4.000	1.000	7.86
5.0	4.578	1.092	7.30
6.0	5.120	1.172	6.89
7.0	5.633	1.243	6.58
8.0	6.122	1.307	6.53
9.0	6.592	1.365	6.13
10.0	7.045	1.419	5.95
11.0	7.483	1.470	5.80
12.0	7.908	1.157	5.67
13.0	8.322	1.562	5.55
14.0	8.725	1.605	5.44

(1) $$m = \frac{3a^2}{H^3} + \frac{1}{H} = \frac{\xi}{a}(3\xi^2 + 1); \quad \xi = \frac{a}{H}$$

$$ma = \xi(3\xi^2 + 1); \; mH - (3\xi^2 + 1); \; \xi = \frac{ma}{mH}$$

(2) σ_x is the bending stress, $6Pa/BH^2$

$$\frac{K}{\sigma_x \sqrt{a}} = \frac{1}{6\xi^2}\left[2\sqrt{3\xi^3 + 4\xi(0.3\xi + 0.34)}\right]$$

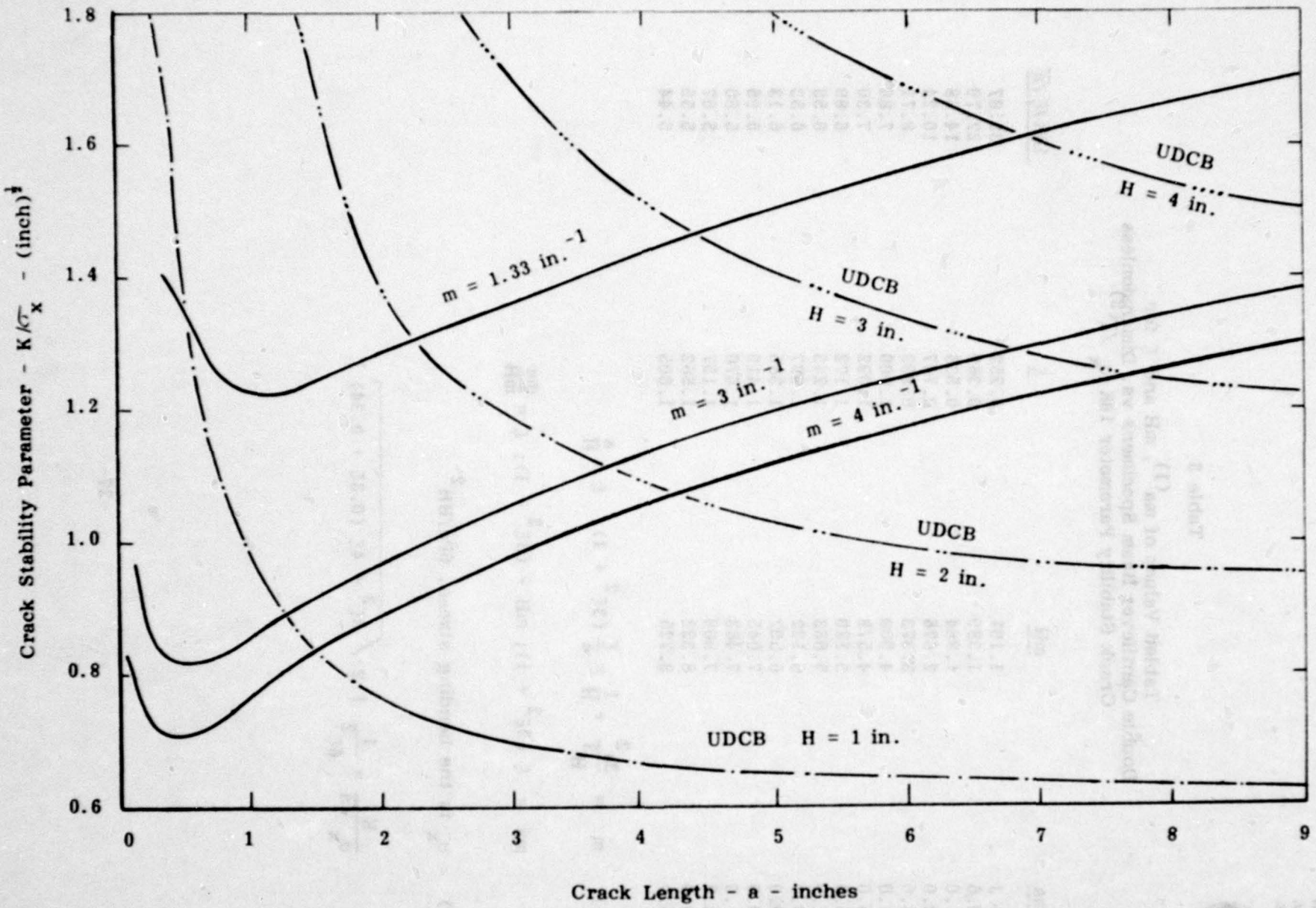

Fig. 5 Crack Length, a, versus Crack Stability Parameter, K/σ_x for Three CDCB Specimen Shapes and Four UDCB Specimens

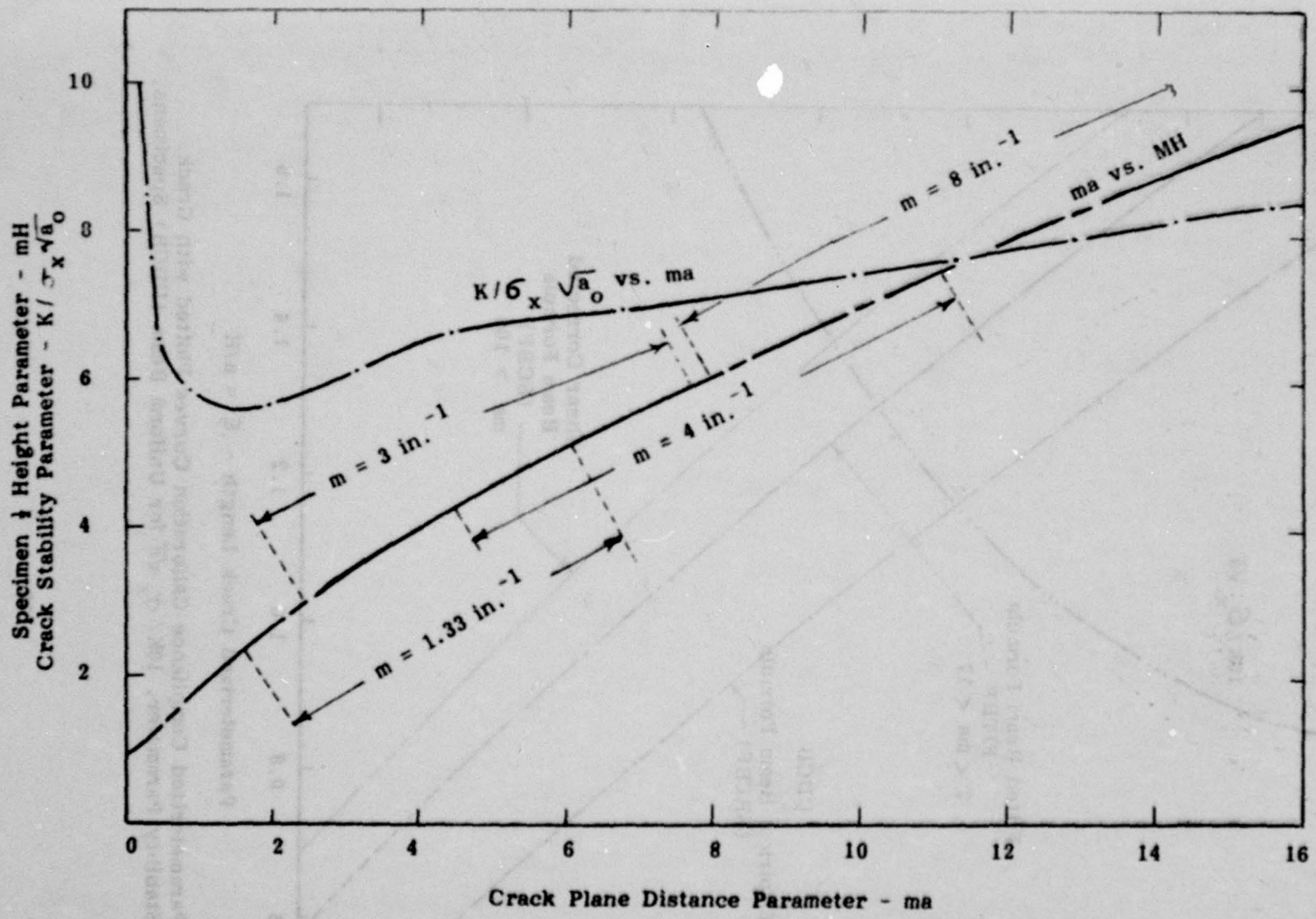

Fig. 6 Parameterized Constant dC/da ("constant-K") Specimen Shape for ma less than 17 plotted with parameterized crack stability factor $K/\sigma_x\sqrt{a_o}$.

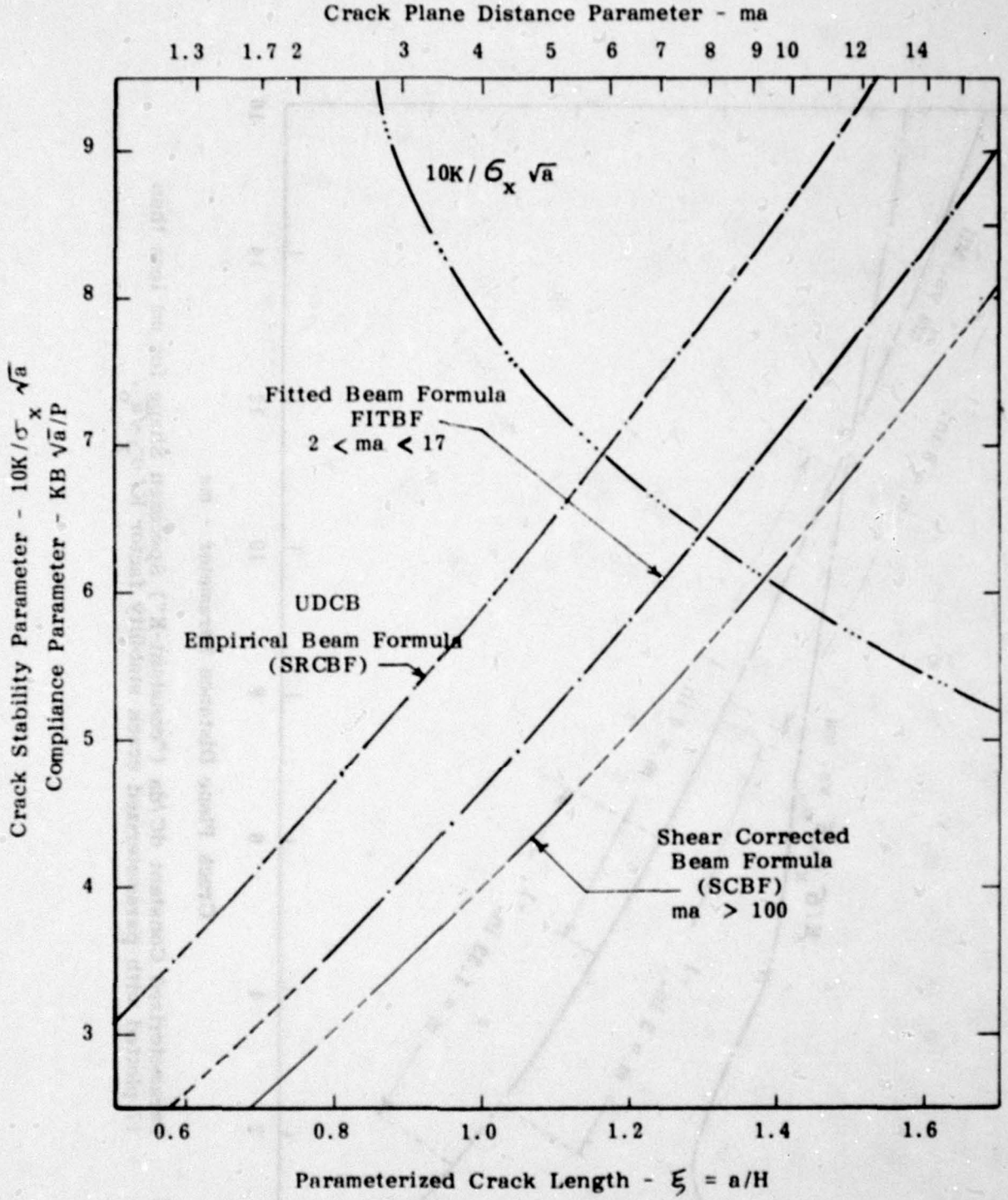

Fig. 7 Parameterized Compliance Calibration Curves Plotted with Crack Stability Parameter, $10K/\sigma_x \sqrt{a}$ for Uniform Beam (UDCB) Specimens.

2.4 Mode-I Analysis of Width Tapered Beam (WTB) Specimens

The toughness and loading response of large-area bonded aircraft panels was suspected to be different enough from narrow area specimens that a new mode-I "constant-K" specimen was designed to evaluate actual structurally bonded panels. While it was always possible to use a simple or moment loaded uniform DCB, the difficulty of each loading condition, (e.g., the need to know crack lengths or the more complex loading geometry) led to the development of a simply loaded, linearly-width-tapered beam (WTB) specimen.[4][9] Such a specimen, although "constant-K", does not have a constant value for the compliance change as a function of crack length, dC/da. Instead, the change in width, B, with crack length is such that the value of (dC/da)/B is constant over some region of crack length, thus giving "constant-K" (i.e., constant compliance change) for a given area, A, of crack motion, dC/dA.

Recall that the beam formula expression for $\mathcal{G}$, from eq. 2.2.1 and 2.2.4, neglecting the shear term is:

$$\mathcal{G} = \frac{P^2}{2B_N}\frac{dC}{da} = \frac{P^2}{2B_N}\left[\frac{8}{EB}\frac{3a^2}{H^3}\right] \qquad 2.4.1$$

For width tapered beams (WTB) where $B_N = B$, the loading holes are at the apex of the taper, and $\mathcal{G}$ is expressed as an a/B ratio:

$$\mathcal{G} = \frac{12P^2}{EH^3}\left(\frac{a}{B}\right)^2 \qquad 2.4.2$$

Because of data on uniform DCB specimens, it was not expected that the above expression for $\mathcal{G}$ would be accurate without some type of "rotation correction" to the beam formula used in the derivation. However, unlike the the height contoured DCB specimens (CDCB), correcting the equation alone was not sufficient to obtain "constant-K". For width tapered beams (WTB), it was necessary to manufacture compliance calibration specimens and measure the change in the value of (dC/da)/B

as a function of crack length. This enabled the loading holes to be moved from the apex of the taper in the direction of increased crack lengths so as to make the value of (dC/da)/B constant.

If the loading holes are moved, keeping the taper angle the same, eq. 2.4.2 must be modified to reflect the fact that a in the expression will not be correct. If the taper angle is given as k and defined as the value of a/B if the loading holes were at the apex of the taper; eq. 2.4.2 becomes:

$$\mathcal{G} = \frac{12P^2}{EH^3} k^2 \qquad 2.4.3$$

Assuming that the loading holes are moved to a position $B_o k$ where B_o is the width at a given distance from the apex of the taper the expression for the total compliance is:

$$C = C_o + \frac{12K}{EH^3} (2 [(B_o k + a)^2 - (B_o k + a_o)^2] \qquad 2.4.4$$

where

a_o = the approximate length of the grip end section of the specimen from the loading holes to the point where the taper begins

C_o = the compliance of the section of the specimen to a_o

The value of $B_o k$ was initially determined from compliance calibration to be 0.143 in. For the adherend height of the WTB specimens used (e.g., 0.377 in.) this value corresponds to a "rotation correction" to the beam formula, i.e., βH, of 0.38 H. Subsequent redetermination of (dC/da)/B from the same compliance specimens with loading holes relocated to 0.143 in. showed that the value of 0.38 H was still too small. Calculations of new loading hole placement indicated a value of 0.55 H or 0.207 in.[10]. Since relocating the loading holes to a third location could not be done, the value of 0.55 H is in some doubt. It should be noted that the total error in $\mathcal{G}$, calculated from eq. 2.4.3

and using a specimen prepared with loading holes at 0.38 H rather than a 0.55 H, is estimated at no more than 5 percent over the crack length range of 3 to 7 inches. In addition, it is expected that the value of βH will be close to 0.6 H as was found in uniform beam adherends.

Calculation by compliance of the absolute value of crack length, needed for determination of fatigue and/or stress corrosion cracking (SCC) rates at a given applied $\mathcal{G}$ or $\Delta\mathcal{G}$, is considerably more difficult than for CDCB height contoured specimens. For CDCB adherends a given change in compliance, in the "constant-K" region, is directly related to a given change in crack length, e.g.,

$$\Delta a = \left(\frac{dC}{da}\right) \Delta C \qquad 2.4.5$$

where

Δa = a given amount of crack extension

ΔC = a given change in compliance

dC/da = the constant compliance change for the particular CDCB geometry

For WTB specimens a given compliance change is not directly related to crack length change and, in fact, will mean a different value of crack length, depending on the initial crack position where the measurement was begun, i.e.,

$$\frac{dC}{da} = \frac{24}{EH^3} \frac{(a + \beta H)^2}{B} \qquad 2.4.6$$

The crack length can be determined from the total compliance rather than compliance change, and rewriting eq. 2.4.4 in terms of βH, we obtain:

$$C = C_o + \frac{12k}{EH^3} \left(2 \left[(\beta H + a)^2 - (\beta H + a_o)^2\right]\right) \qquad 2.4.7$$

The use of total compliance for calculation of crack motion requires a very accurately made compliance calibration using the value of βH

appropriate to this class of specimen (e.g., 0.6 H). However, this technique is commonly used for compact specimens with good accuracy. Presumably, if geometrically similar WTB specimen geometries are used one could scale values of C_o, however, a standard WTB specimen is yet to be manufactured and calibrated.

3.0 Mixed-mode, Crack Length Indifferent, Tests, Specimen Design and Analysis

3.1 Introduction: Review of Analyzed Mixed-Mode Specimens

Fracture toughness test specimens for monolithic materials have most often been made with the underlying assumption that fracturing will occur in mode-I or cleavage in a direction perpendicular to the *maximum normal stress*. *Even for monolithic material directional* properties, e.g., a weak plane, can result in crack growth with some combination of mode-I and one or both of the other shearing modes. For structural adhesive joint design the amount of shear loading is maximized, often by the use of added fasteners, so that as little of a mode-I component as possible appears on the bond line. Of course, not all of the mode-I loading can be eliminated, thus, test methods for adhesive bonds have been designed to include determination of the effect of mixed-mode loading where the amount of the shear components is high compared to the opening mode component.

Several specimens having the crack length indifferent or "constant-K" design, have been manufactured and tested by this laboratory. For this class of specimen were an accurate analysis for mixed-mode loading to be available, the values of the toughness parameters could be determined directly from the value of loads needed for onset of rapid fracture, crack arrest and the number of parameters used to characterize slow growth.

$\mathcal{J}$ or K analysis of mixed-modes I and II or II, or pure shear modes II and III, is substantially more complex than for pure mode-I alone because of the difficulty in defining the true amount of mode-I

present. This can be the case even though the specimen is designed for pure shear alone. For example, an examination of the load path for standard (not "constant-K") thick adherend lap shear (TALS) specimens appears to be one of pure shear, however, numerical analysis of the deformation of this specimen during loading shows that mode-I forces will occur at the free ends of each overlap. While the amount of mode-I in such specimens is likely to be the same for each test in this configuration, the percentage of the parasitic mode-I component cannot be readily calculated. The problem is less important for TALS specimens and others used for qualitative evaluation and quality assurance than for those designed for quantitative fracture control.

Four fracture mechanics specimens have been designed and/or used at this laboratory for evaluation of mixed-mode loading. The first, a CDCB loaded at an angle, was used to determine if a small mode-II component could be responsible for a loss in total toughness $\mathcal{G}_{Tc}$ or K_{Tc}. This specimen, although difficult to load, did show that when $\mathcal{G}_{II}$ was a small percentage of the total $\mathcal{G}$, $\mathcal{G}_T$, the critical crack extension force was not lowered or changed significantly.

The second specimen named the beam-column (BC) specimen, was a uniform DCB that could be loaded simultaneously with a moment to produce the mode-I component and an in-plane load to produce the pure mode-II component. This loading arrangement was designed for crack length independence or "constant-$\mathcal{G}$" and if the loads are put on independently and without interaction the approximate value of the two $\mathcal{G}$ values[11] are:

$$\mathcal{G}_{II} = \frac{P_{II}^2}{B^2 HE} \qquad 3.1.1$$

$$\mathcal{G}_I = \frac{12\, M^2}{B^2 H^3 E} \qquad 3.1.2$$

where

$\mathcal{G}_{II}$ = the applied $\mathcal{G}$ in the forward shearing mode, mode-II

$\mathcal{G}_{I}$ = the applied $\mathcal{G}$ in the cleavage or mode-I direction

B = UDCB adherend width

H = UDCB adherend height

M = the moment for the application of the mode-I load, e.g., $P_I L_I$; the force, P_I multiplied by a lever arm L_I of the particular fixture

E = the elastic modulus of adherends; e.g. 10^7 psi

Note that eqs. 3.1.1 and 3.1.2 are expected to be less accurate than the simply loaded UDCB case, which contain shear and rotation corrections to the beam formula to obtain a more correct value of dC/da. The calculation of the total $\mathcal{G}$ at fracture, $\mathcal{G}_{Tc}$, cannot be made with certainty without a determination of the compliance characteristics of the specimen for the given loading. Nevertheless, mixed-mode tests of several adhesive compositions were made with the beam-column (BC) specimen to evaluate large effects. Normal and shear loads were kept separate by measuring each separately using strain gages mounted to both arms of the specimen. Results from this specimen also indicated that the addition of a mode-II component did not alter the $\mathcal{G}_c$ more than a value indicated by

$$\mathcal{G}_I + \mathcal{G}_{II} = \mathcal{G}_{Tc}$$

Size limitations (the 1" tall, ½ inch wide BC specimen adherends had a 12 inch bond length) prevented increasing the $\mathcal{G}_{II}/\mathcal{G}_T$ ratio above 0.29, thus severely limiting its usefulness. Considering the statement of eq. 3.1.3, further compliance calibration of a small BC specimen does not appear to be warranted.

The third specimen type is the cracked lap shear (CLS) and the fourth is the modified zero K gradient (MZKG), both of which are covered in the following sections.

3.2 The Cracked Lap Shear (CLS) Specimen for Determination of Adhesive Fracturing Behavior for Combined Modes I and II Loading

The third and most well characterized of the mixed-mode specimens is the cracked lap shear or CLS specimen for mixed-mode I and II (Fig. 8)[9][11][12][13]. Testing and mode-mix analysis (amount of each of the two modes making up the total $\mathcal{G}$, $\mathcal{G}_T$) of this specimen were done concurrently; consequently, three sets of closed form analyses were performed. Predicted values of the $\mathcal{G}_I / \mathcal{G}_T$ ratios were obtained for each analysis and compared with fracture data on CLS specimens. The assumption was made in all cases that the calculated mode-I component in the mixed-mode test at onset of rapid fracture would approximate the value of $\mathcal{G}_{Ic}$ for a pure mode-I test. Each set of calculations agreed more closely with that assumption, i.e., the mixed-mode $\mathcal{G}_{Ic}$ was closer to the pure mode-I $\mathcal{G}_{Ic}$. However, at this time a more complex numerical analysis of the specimen would be needed to fix the $\mathcal{G}_I / \mathcal{G}_T$ ratio for this mixed-mode loading condition.

All of the analyses begin with a straightforward calculation of the total strain energy release rate, $\mathcal{G}_T$, using the calculation of the change in strain energy as the crack elongates.

$$\mathcal{G}_T = \frac{P^2}{2B_N E_2 A_2} \left[1 - \frac{E_2 A_2}{(EA)_o} \right] \qquad 3.2.1$$

where

P = applied load

B_N = bond width remaining after face grooving

E_2 = elastic modulus of the long adherend

A_2 = area of the long adherend

$(EA)_o$ = the modulus weighted area of the bonded adherends

For face grooved specimen:

$$A_2 = H_2 (B) + G/2 (B_N) \qquad 3.2.2$$

and

$$(EA)_o = E_2A_2 + E_1A_1 \qquad 3.2.3$$

$$(EA)_o = E_2 [H_2B + \frac{G}{2} B_N] + E_1 (H_1B + \frac{G}{2}B_N] \qquad 3.2.4$$

where

E_1 = elastic modulus of the short adherend

B = width of the CLS specimen prior to face grooving

A_1 = area of the short adherend

G = face groove width or gap

H_1 = full width height of the short adherend after face grooving ($H_1 = t_1 + G/2$)

H_2 = full width height of long adherend after face grooving ($H_2 = t_2 + G/2$)

t_1 = total height of short adherend

t_2 = total height of long adherend

For the face grooved specimens, eq. 3.2.1 can be written in terms of the average tension stress in the long adherend and the tensile stiffness parameter, viz.,

$$k = \frac{E_1t_1}{E_1t_1 + E_2t_2} \qquad 3.2.5$$

$$\sigma = \frac{P}{t_2B} \qquad 3.2.6$$

$$\mathcal{G}_T = \frac{\sigma^2t_2}{2E_2} k \qquad 3.2.7$$

In this calculation k ranges from 0 to 1 as the ratio of t_1/t_2 goes from 0 to infinity.

The calculation of the mode-I component of the $\mathcal{G}_T$ for the simplest case can be found using a compliance analysis similar to that used for pure

mode-I specimens. For a single beam, moment loaded (M) by a weight, W, at a lever arm, L, from the neutral axis moving a distance, Δ_1, to elastically load the specimen, the total energy, U_T, for the mode-I case is:

$$U_T = \frac{1}{2}\frac{W\Delta_1}{B_N} \qquad 3.2.8$$

Since the compliance of the system is defined as:

$$C = \Delta_1/W \qquad 3.2.9$$

$$U_T = \frac{1}{2}\frac{W^2}{B_N} C \qquad 3.2.10$$

We obtain $\mathcal{G}_I$ by taking the derivative of 3.2.10 with respect to crack length:

$$\mathcal{G}_I = \frac{W^2}{2B_N}\frac{\partial C}{\partial a} \qquad 3.2.11$$

The compliance of the system can be calculated from considering the change in angle at the load application point, Θ, as the crack length, a, changes.

$$\Theta = \frac{Ma}{E_2 I_2} \qquad 3.2.12$$

where

M = applied movement, e.g. WL
a = crack length
E = elastic modulus of the long adherend
I_2 = moment of inertia of the long adherend

The total displacement of the weight at any angle is:

$$\Delta_I = L\Theta = \frac{WL^2 a}{E_2 I_2} \qquad 3.2.13$$

thus

$$C = \Delta_1/W = \frac{nL^2}{E_2 I_2} \qquad 3.2.14$$

and

$$\frac{\partial C}{\partial a} = \frac{E^2}{L_2 I_2} \qquad 3.2.15$$

The expression for the $\mathcal{G}_I$ component is obtained using 3.2.15 and 3.2.11:

$$\mathcal{G}_I = \frac{(WL)^2}{2B_N} \frac{1}{(EI)_2} = \frac{M^2}{2B_N} \frac{1}{(EI)_2} \qquad 3.2.16$$

For non-side grooved rectangular adherends:

$$\mathcal{G}_I = \frac{12M^2}{2B^2 t_2 E_2} = \frac{6M^2}{B^2 t_2 E_2} \qquad 3.2.17$$

This formula agrees with the one presented on Page 29.1 in the Tada handbook[14].

The calculation of M at the crack tip, i.e., M_o, requires a consideration of the location of the centroid near the crack tip[11] and leads to the expression

$$M_o = \frac{P\lambda_2 \, k(t_1 + t_2)}{(\lambda_1 + \lambda_2)^2} \qquad 3.2.18$$

where

P = total tensile load

$\lambda_1 = [12P/(B\, t_2^3\, E_2)]^{\frac{1}{4}}$

$\lambda_2 = \{12P/([E_1 t_1^3 + E_2 t_2^3 + 3k\, E_2 t_2 (t_1 + t_2)^2]B)\}^{\frac{1}{4}}$

Substituting eq. 3.2.18 into 3.2.17 and forming the ratio of $\mathcal{G}_I/\mathcal{G}_T$ using 3.2.7:

$$\frac{\mathcal{G}_I}{\mathcal{G}_T} = \left[\frac{\lambda_2 (t_1 + t_2)}{(\lambda_1 + \lambda_2)\, t_2}\right]^2 3k \qquad 3.2.19$$

For equal modulus adherends:

$$\frac{\mathcal{G}_I}{\mathcal{G}_T} = \frac{3k\,(1-k)}{[1 + (1-k)^{3/2}]^2} \qquad 3.2.20$$

For equal thickness adherends $\mathcal{G}_I/\mathcal{G}_T$ is 0.41 and the maximum value of $\mathcal{G}_I/\mathcal{G}_T$ (0.48) occurs at a k value of 0.66 ($t_1/t_2 = 2$) (see Table 4a).

The value of $\mathcal{G}_I/\mathcal{G}_T$ of almost 50 percent of the total for adherends where t_1/t_2 is 2 does not agree with the assumption of constant $\mathcal{G}_{Ic}$ for the case of mixed mode fracturing of CLS specimens. For a deeply side grooved CLS specimen where t_1/t_2 was about 2, $\mathcal{G}_{Tc}$ was between 63 and 76 lbs/in. Were expression 3.2.20 to be correct, it would imply that the $\mathcal{G}_{Ic}$ component of $\mathcal{G}_T$ was of the order of 35 lbs/inch rather than the 12.5 lbs/in. value of pure mode I $\mathcal{G}_{Ic}$.

Because of this apparently anomalous value of $\mathcal{G}_{Ic}$, from the mixed-mode test, the specimen was re-examined considering the case where the beam was not "built-in" at the crack tip. Such a calculation takes into account the strain energy on both sides of the crack tip[12]. Thus, expression 3.2.16 becomes modified by the moment of inertia term $(1 - I_2/I_o)$, i.e.,

$$\mathcal{G}_I = \frac{M_o^2}{2B_N} \frac{1}{(EI)_2} \left(1 - \frac{I_2}{I_o}\right) \qquad 3.2.21$$

For equal modulus adherends without face notches eq. 3.2.20 is changed to:

$$\frac{\mathcal{G}_I}{\mathcal{G}_T} = \frac{3k\,(1-k)(1-k^3)}{[1 + (1-k)^{3/2}]^2} \qquad 3.2.22$$

For practical thicknesses and ratios of moduli, the minimum ratio is of the order of 0.100, Table 4b. The plot of k vs. $\mathcal{G}_I/\mathcal{G}_T$ (eqs. 3.2.5 and 3.2.2) shown in Fig. 9 illustrates the ratios of importance for the same

adherend material over a range of thicknesses. For this calculation the $\mathcal{G}_I/\mathcal{G}_T$ ratios most easily accessible with adherends of the same material are 0.2 to 0.35. If lower amounts of $\mathcal{G}_I$ are required, adherends of different moduli can be used to obtain a $\mathcal{G}_I$ equal to 10 percent of the total. Testing of equal moduli specimens has been limited, however, to $\mathcal{G}_I/\mathcal{G}_T$ ratios no lower than 0.27. In addition, CLS specimens bonded with tough adhesives require load values for onset of rapid fracture, $\mathcal{G}_{Tc}$, above the value of yield strength for 7075 T 651 aluminum when the adherends used are less than 5/8 in. thick.

In light of the measured values of $\mathcal{G}_{Tc}$, the above solution was also thought to give values of the $\mathcal{G}_I/\mathcal{G}_T$ ratio that were too high. For example, the value of the $\mathcal{G}_{Ic}$ component for the test cited above was of the order of 23 lbs/in. ($\mathcal{G}_I/\mathcal{G}_T$ was calculated at 0.33 for t_1/t_2 of 2) which was still substantially above the pure mode-I $\mathcal{G}_{Ic}$ value of 12.5 lbs/in. A third, but approximate, solution was then obtained by considering an equal adherend thickness, the same adherend material, CLS specimen subjected to a uniform bending moment, Fig. 10. The total strain energy release rate for this loading is calculated in a similar manner to that for the tension case shown in eq. 3.2.1 and leads to[13]:

$$\mathcal{G} = \frac{M^2}{2B_N (EI)_2} \left[1 - \frac{(EI)_2}{(EI)_o} \right] \qquad 3.2.23$$

For this case, where loading and geometry are not symmetric about the crack plane, the CLS specimen in pure bending is not a pure mode-I condition. For the special case of similar material adherends of equal thickness the problem can be separated into symmetric and asymmetric parts (Figs. 11-b and 11-c) each of which can be solved by the same virtual strain energy procedure:

$$\mathcal{G}_I = \frac{M^2}{4 B_N (EI)_2} \qquad 3.2.24$$

$$\mathcal{G}_{II} = \frac{3 M^2}{16 B_N (EI)_2} \qquad 3.2.25$$

For this case, this calculation results in a $\mathcal{G}_I/\mathcal{G}_T$ ratio of 4/7. In order to use these calculations to estimate $\mathcal{G}_I$ for a CLS specimen loaded in tension it is assumed: (1) that the $\mathcal{G}_I$ value resulting from the tension induced bending moment is equivalent to that produced by an equal uniform bending moment and (2) that the $\mathcal{G}_I/\mathcal{G}_T$ ratio of 4/7 found for equal thickness adherends can be used as a starting point to define the $\mathcal{G}_I/\mathcal{G}_T$ ratio for unequal thickness adherends.

Calculation of the equation for $\mathcal{G}_I$ for tension loading using the above formulation requires a redefinition of M_o, the tension induced bending moment, from eq. 3.2.18 in terms of the values of $\bar{Y}_2$, $\bar{Y}_o$ (the centroid position of the cracked long adherend and uncracked specimen, respectively), λ_o and λ_2. For this case the definitions of λ_o and λ_2 are:

$$\lambda_o = \sqrt{P/(EI)_o} \qquad 3.2.26$$

$$\lambda_o = \sqrt{P/(EI)_1} \qquad 3.2.27$$

and the expressions for $\bar{Y}_2$ and $\bar{Y}_o$ are:

$$\bar{Y}_2 = \frac{\frac{BH_2^2}{2} + \frac{B_N H_2 G}{2} + \frac{B_N G^2}{8}}{BH_2 + B_N (G/2)} \qquad 3.2.28$$

$$\bar{Y}_o = \frac{B_N(H_2 G + G^2/2) + B(H_2^2/2 + H_1 H_2 + H_1 G + H_1^2/2)}{B(H_1 + H_2) + B_N G} \qquad 3.2.29$$

Thus, a redefinition of M_o from eq. 3.2.18 becomes:

$$M_o = \frac{P(\bar{Y}_2 - \bar{Y}_o)\lambda_o}{\lambda_2 + \lambda_o} \qquad 3.2.30$$

The equation for $\mathcal{G}_I$ for the tension loaded CLS specimen is then:

$$\mathcal{G}_I = \frac{2M_o^2}{7B_N(EI)_2}\left[1 - \frac{(EI)_2}{(EI)_o}\right] \qquad 3.2.31$$

Using the definition of k stated earlier, eq. 3.2.31 can be used with eq. 3.2.1 to obtain a table showing the effect on the $\mathcal{G}_I/\mathcal{G}_T$ ratio of varying the thickness of the adherends, Table 5. This table also shows the substantial effect of side groove geometry on the ratio. Two cases from this table are plotted on Fig. 12. The first one is for an ungrooved specimen and the second is for a deeply grooved case where $B_N/B = 1/8$ and G is 3/16 inch. For the CLS configurations used in this test series $\mathcal{G}_I/\mathcal{G}_T$ is raised by about 15 percent for deep side grooves.

Recalculation of the mixed mode $\mathcal{G}_{Ic}$ from the earlier case using the above formulas gives a value of about 30 lbs/in. ($\mathcal{G}_I/\mathcal{G}_T = 0.3$; $t_1/t_2 = 2$) which is still above the pure mode-I case, but is the lowest value obtained from any of the calculation methods. These data indicate that the value of the mixed mode $\mathcal{G}_{Ic}$ may be above the value for the pure mode-I case showing that the addition of shear loading is more beneficial than indicated from the standpoint of geometry changes in the mode of loading.

Table 4a

Variation in $\mathcal{G}_I/\mathcal{G}_T$ for CLS Specimens
Having Equal Moduli Adherends as a Function of Adherend Thickness
(Uncorrected Virtual Strain Energy Method)

t_1/t_2	k	$\mathcal{G}_I/\mathcal{G}_T$
0.1	0.091	0.071
0.2	0.167	0.134
0.5	0.333	0.280
0.8	0.444	0.370
1.0	0.500	0.409
1.2	0.546	0.436
1.5	0.600	0.459
1.952	0.661	0.469
2.0	0.667	0.469
3.0	0.750	0.444
4.0	0.800	0.404
6.0	0.857	0.331
8.0	0.889	0.276
10.0	0.909	0.235
20.0	0.952	0.133
50.0	0.980	0.057

$$k = \frac{E_1 t_1}{E_1 t_1 + E_2 t_2}$$

Table 4b

Variation in $\mathcal{G}_I / \mathcal{G}_T$ for CLS Specimens
As a Function of Elastic Modulus and Adherend Thickness
(Simply Corrected Case)

$$\mathcal{G}_I / \mathcal{G}_T \text{ as } f\,[(t_2/t_1),\ (E_2/E_1)]$$

t_2/t_1	6.93	4	2.32	2	1	0.5	0.431	0.25
$E_2/E_1 = 1$	0.100	0.162	--	0.269	0.358[1]	0.330	--	0.197
(k)	(0.126)	(0.20)	--	(0.333)	(0.50)	(0.667)	--	(0.8)
$E_2/E_1 = 3$	--	0.060	0.100	0.114	0.204	0.314	--	0.365[2]
(k)	--	(0.077)	(0.126)	(0.143)	(0.25)	(0.40)	--	(0.571)
$E_2/E_1 = 1/3$	--	0.330	--	0.360[3]	0.257	0.122	0.100	0.044
(k)	--	(0.429)	--	(0.60)	(0.75)	(0.857)	(0.874)	(0.923)

$$\frac{\mathcal{G}_I}{\mathcal{G}_T} = \frac{3k\,(1-k)\,(1-k^3)}{[\,1 + (1-k)^{3/2}\,]^2}$$

$$k = \frac{E_1 t_1}{E_1 t_1 + E_2 t_2}$$

(1) Peak at $t_2/t_1 = 0.806$)
)
(2) Peak at $t_2/t_1 = 3.703$)
)
(3) Peak at $t_2/t_1 = 0.413$)

$\mathcal{G}_I / \mathcal{G}_T = 0.365$

$k = 0.554$

Table 5

Variation in $\mathcal{G}_I / \mathcal{G}_{II}$ for CLS Specimen As Obtained from Applied Moment Calibrations As a Function of Adherend Thickness, Face Groove Depth, B_N, and Face Groove Width, G. (E = constant, B = 1 in.)

		$\mathcal{G}_I / \mathcal{G}_T$									
	t_1/t_2	10	6-2/3	5	2.5	1-2/3	1	½	1/3	1/5	1/10
	k	0.91	0.87	0.833	0.714	0.625	0.5	0.33	0.25	0.166	0.091
G	B_N -										
1	1	0.134	--	0.208	0.257	0.252	0.205	0.112	0.068	0.032	0.010
1/16	3/4	0.132	0.178	0.210	0.262	0.256	0.208	0.114	0.069	0.024	0.010
	½	0.129	0.178	0.213	0.267	0.261	0.212	0.115	0.070	0.024	0.010
	¼	0.126	0.179	0.216	0.272	0.266	0.215	0.117	0.070	0.024	0.010
	3/16	0.125	0.180	0.217	0.274	0.267	0.216	0.117	0.070	0.024	0.010
	1/8	0.124	0.180	0.218	0.275	0.268	0.217	0.118	0.071	0.024	0.010
1/8	½	0.118	0.176	0.215	0.275	0.269	0.218	0.118	0.071	0.024	0.010
	¼	0.107	0.175	0.220	0.286	0.279	0.225	0.121	0.072	0.024	0.010
	3/16	0.103	0.175	0.222	0.289	0.282	0.227	0.122	0.073	0.024	0.010
	1/8	0.100	0.175	0.224	0.292	0.285	0.229	0.123	0.073	0.024	0.010
0.155	0.190	0.086	0.169	0.222	0.296	0.289	0.232	0.124	0.074	0.024	0.010
3/16	½	0.100	0.168	0.214	0.282	0.276	0.224	0.121	0.072	0.024	0.010
	¼	0.071	0.161	0.218	0.298	0.292	0.235	0.126	0.074	0.024	0.010
	3/16	0.061	0.159	0.220	0.302	0.296	0.238	0.127	0.075	0.024	0.010
	1/8	0.050	0.157	0.222	0.307	0.300	0.241	0.128	0.075	0.025	0.010

$$\mathcal{G}_I = \frac{2 M_o^2}{7 B_N (EI)_2} \left[1 - \frac{(EI)_2}{(EI)_o} \right]$$

$$\mathcal{G}_T = \frac{P^2}{2 B_N E_2 A_2} \left[1 - \frac{(EA)_2}{(EA)_o} \right]$$

$$M_o = \frac{P (\bar{Y}_2 - \bar{Y}_o) \lambda_o}{\lambda_2 + \lambda_o}$$

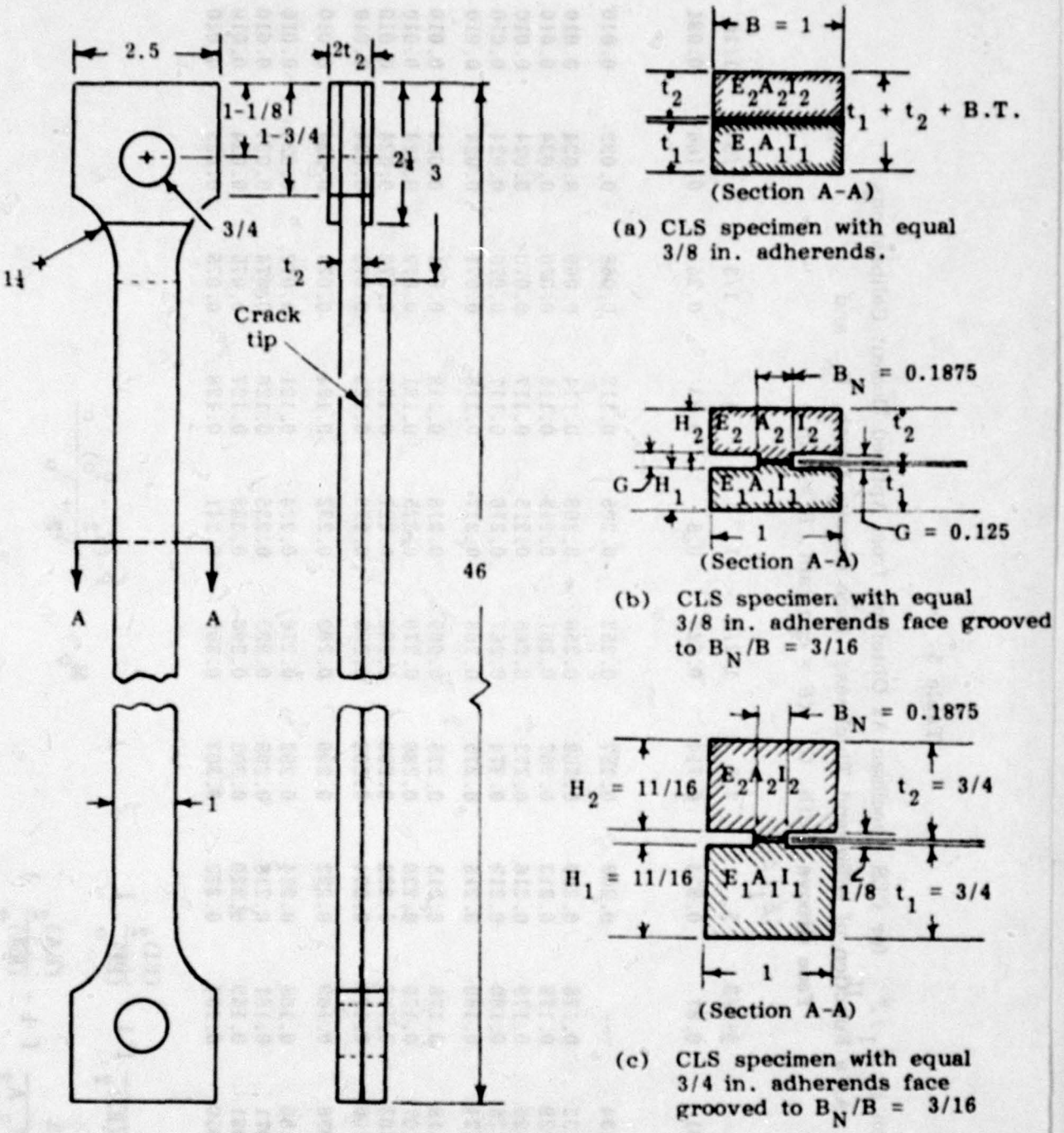

Fig. 8 Cracked lap shear (CLS) specimen showing three different adherend configurations.

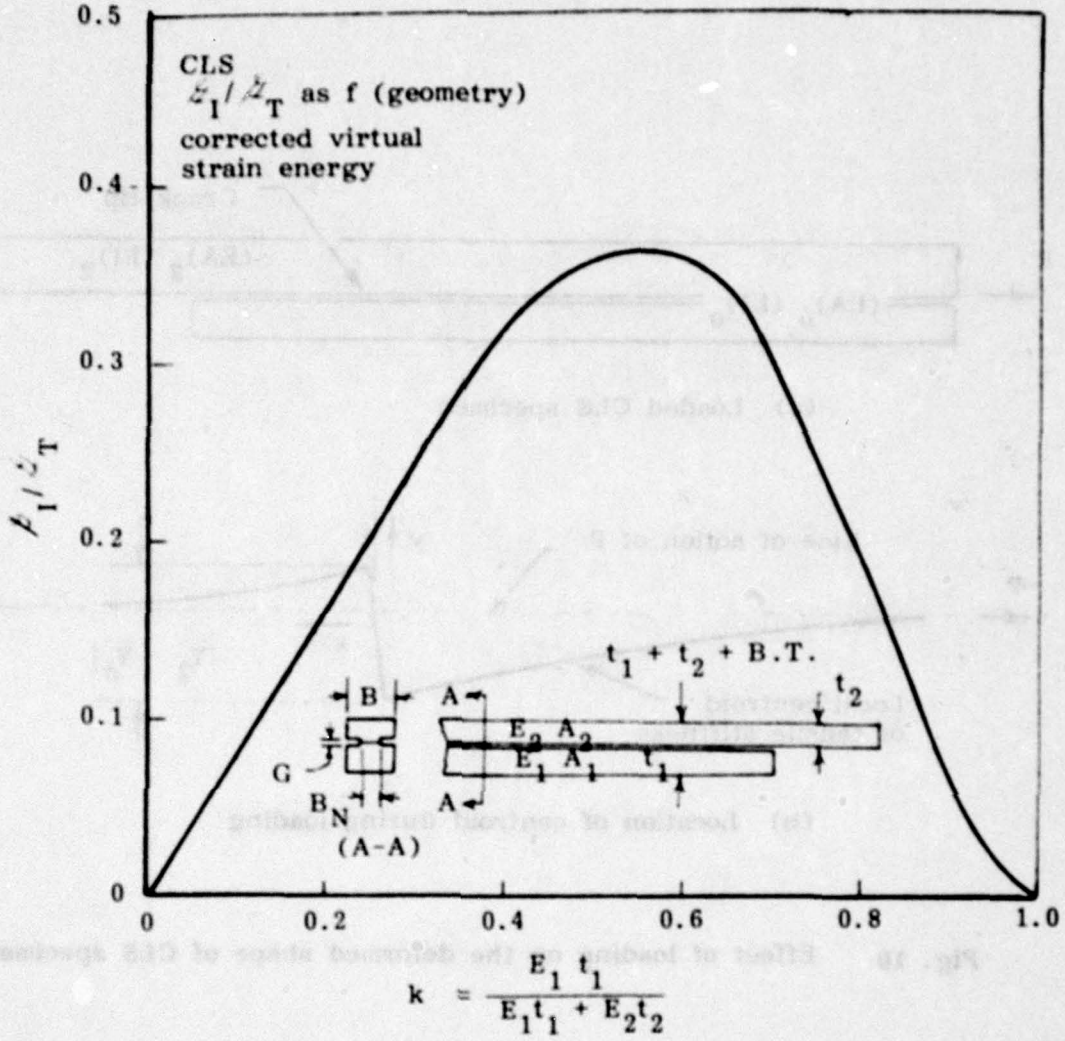

Fig. 9 CLS specimen $\mathcal{G}_I / \mathcal{G}_{II}$ ratio as a function of combined modulus, thickness parameter, k, from equations 5 and 22 (corrected virtual strain energy calculation).

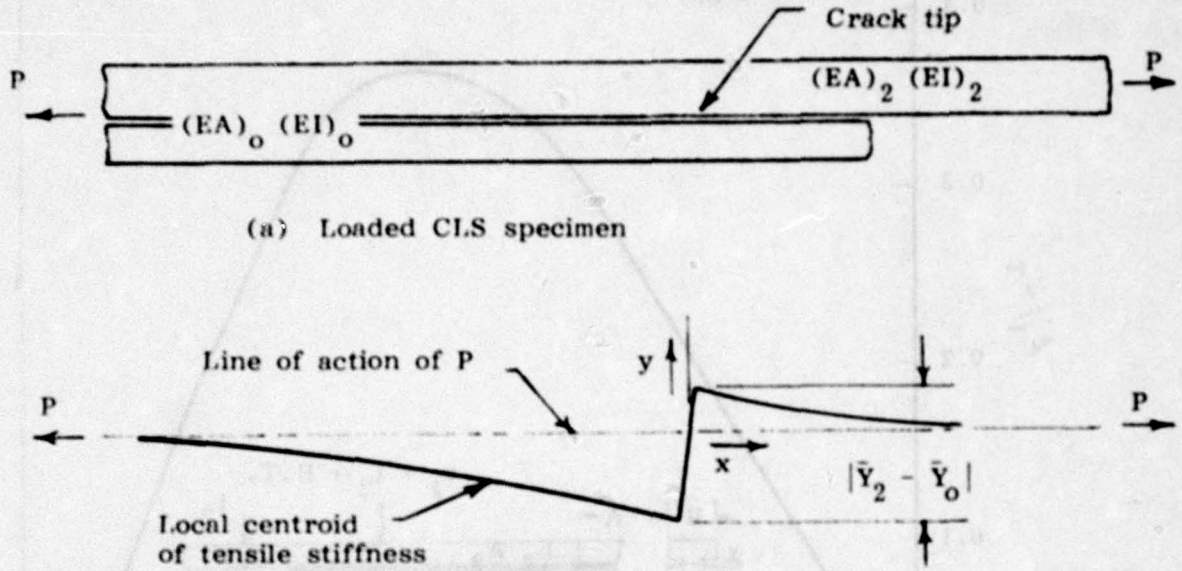

(a) Loaded CLS specimen

(b) Location of centroid during loading

Fig. 10 Effect of loading on the deformed shape of CLS specimens.

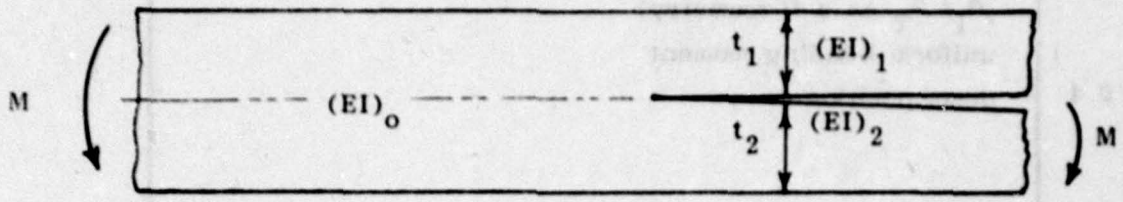

(a) CLS specimen loaded in pure bending.

(b) Symmetric half of bending moment decomposition.

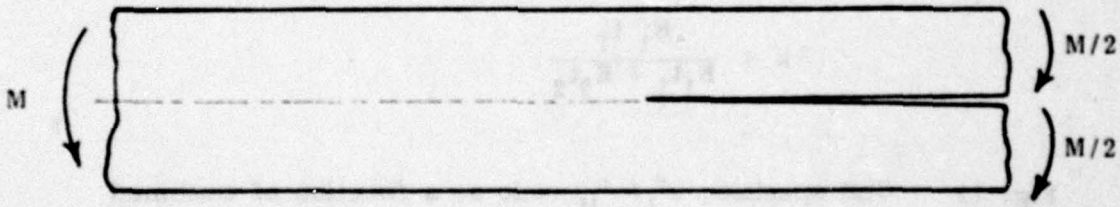

(c) Antisymmetric half of bending moment decomposition.

Fig. 11 CLS specimen loaded in pure bending and analyzed by bending moment decomposition into symmetric and antisymmetric parts.

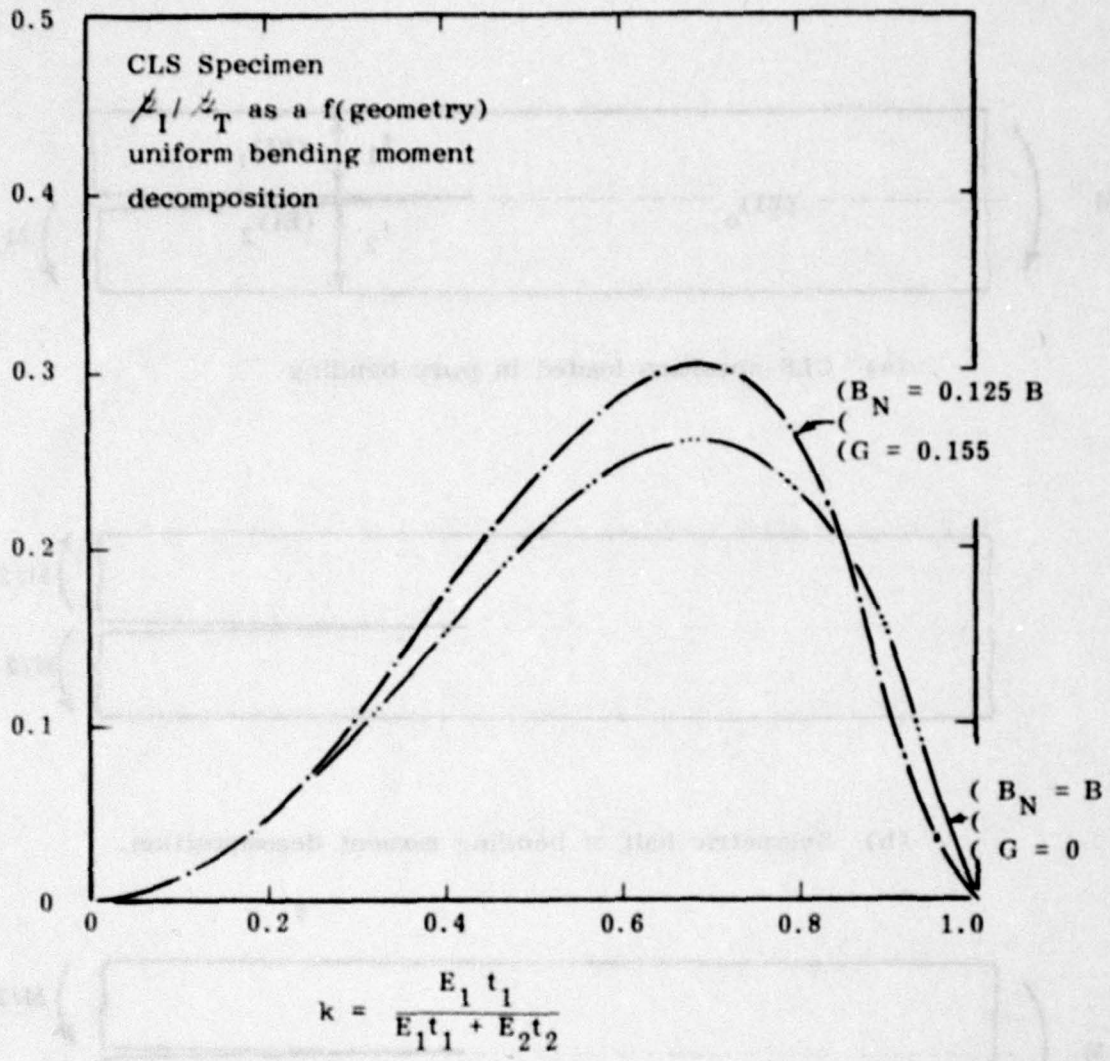

Fig. 12 CLS specimen $\mathcal{G}_I / \mathcal{G}_{II}$ ratio as a function of combined modulus thickness parameter, k, for two adherend face groove geometries (uniform bending moment decomposition).

3.3 The Modified Zero K Gradient (MZKG) Specimen for Determination of Adhesive Fracturing Behavior for Combined Modes I and III Loading

A fourth mixed-mode crack length indifferent adhesive specimen design is one where the shearing forces are primarily edgewise sliding or mode-III directed. This type of design has great promise in quantitatively evaluating the effect of high shear loading on crack growth parameters with the use of relatively small specimens. Recall that the mixed-mode-I and II, BC specimen (Section 2), although large, was inadequate for ratios of $\mathcal{G}_{II}/\mathcal{G}_T$ above 0.29. The mode-III adhesive specimen was manufactured by modifying a design used for plane strain testing of thin sheet[15]. The original thin sheet specimen was denoted the "zero-K-gradient" or ZKG specimen, and its modification for mode-III adhesive testing was denoted the "modified ZKG" or MZKG specimen.

The development of the specimen shape for each of these designs required taking into consideration the stepped cross section of each.

In a manner similar to that shown in eqs. 2.2.2 and 2.2.3, the compliance derivative in the expression for $\mathcal{G}$ (eq. 2.2.1) can be written as

$$\frac{dC}{da} = \frac{2}{3\,EI_x}\,(3a^2 + H^2) \qquad 3.3.1$$

For the stepped cross section, I_x is the moment of inertia about the center of gravity (CG). If we rewrite eq. 3.3.1 so that the term I_x/B appears inside the brackets:

$$\frac{dC}{da} = \frac{2}{3EB}\left(\frac{3a^2 + H^2}{I_x/B}\right) \qquad 3.3.2$$

Additionally, the term H in the brackets is the shear correction term which for the ZKG and MZKG cross sections is replaced by $2\bar{y}$ where $\bar{y}$ is the distance from the top of the beam to CG. Note that for uniform cross section beams $2\bar{y}$ equals H. Replacing H by $2\bar{y}$ in 3.3.2:

$$\frac{dC}{da} = \frac{2}{3EB}\left[\frac{3a^2 + (2\bar{y})^2}{I_x/B}\right] \qquad 3.3.3$$

Both ZKG and MZKG specimen sketches are shown in Fig. 15. One difference in nomenclature should be pointed out. Eq. 2.2.1 is generally written for the case where the crack plane width is B_N. This is correct for the ZKG specimen, but not for the MZKG specimen where the bond area is defined by B_3 (see Fig. 15). Thus, for the MZKG, eq. 2.2.1 is rewritten as:

$$\mathcal{G} = \frac{P^2}{2B_3}\frac{dC}{da} \qquad 3.3.4$$

Note that the $\mathcal{G}$ written in eq. 3.3.4 is not defined as $\mathcal{G}_{III}$ because of the uncertainty in the amount of parasitic modes-I and II likely to be present but whose amounts cannot be readily calculated.

In order to contour the specimen for constant dC/da the bracketed part of eq. 3.3.3, denoted M_o, must be made constant:

$$M_o = \frac{3a^2 + (2\bar{y})^2}{I_x/B} \qquad 3.3.5$$

Note that M_o is equal to 12 $\underline{m}$ where

$$m = \left(\frac{3a^2}{H^3} + \frac{1}{H}\right) \qquad 3.3.6$$

the value kept constant for CDCB specimen described earlier (e.g., eq. 2.2.4 and 2.2.26).

We first define the instantaneous position of the CG, $\bar{y}$, from the top of the contour.

$$\bar{y} = \frac{A_1\bar{y}_1 + A_2\bar{y}_2 + \ldots}{A_1 + A_2 + \ldots} \qquad 3.3.7$$

$$\bar{y} = \frac{H_1\left(\frac{H_1}{2}\right)B_N + H_o\left(\frac{H_o}{2}\right)(B - B_N)}{B_N(H_1) + (B - B_N)H_o} \qquad 3.3.8$$

or

$$\bar{y} = \frac{\frac{B_N}{2}(H_1)^2 + \frac{B - B_2}{2}(H_o)^2}{B_N(H_1) + (B - B_N)H_o} \qquad 3.3.9$$

Eq. 2.2.1 is for the general ZKG case where B_N can take any value. For the MZKG specimen B_N would be equal to B/2, thus;

$$\bar{y} = \frac{H_1^2 + H_o^2}{2(H_1 + H_o)} \qquad 3.3.10$$

The moment of inertia referred to the CG is most easily found using the parallel axis theorem:

$$I_x = I_x' - Ad^2 \qquad 3.3.11$$

where

I_x = the moment of inertia referred to the CG

I_x' = moment of inertia referred to the bottom of one adherend (MZKG) or to the crack plane (ZKG)

A = *total area of one adherend cross section*

d = distance from the CG to the bottom of one adherend (MZKG) or to the crack plane (ZKG)

For ZKG specimen:

$$A = BH_o + B_N L = B\left(H_o + \frac{B_N}{B} L\right) \qquad 3.3.12$$

For the MZKG specimen when $B_N = B/2$;

$$A = B\left(H_o + \frac{L}{2}\right) \qquad 3.3.13$$

Since d is $(H_1 - \bar{y})$ eq. 3.3.10 can be rewritten using eq. 3.3.11 for the ZKG specimens as:

$$I_x = \frac{B}{3}\left[H_1^3 - \left(1 - \frac{B_N}{B}\right) L^3\right] - B\left[H_o + \frac{B_N}{B} L\right][H_1 - \bar{y}]^2 \qquad 3.3.14$$

thus;

$$\frac{I_x}{B} = \frac{H_1^3}{3} - (1 - \frac{B_N}{B})\frac{L^3}{3} - (H_o + \frac{B_N}{B}L)(H_1 - \bar{y})^2 \qquad 3.3.15$$

For the MZKG specimen where $B_N = B/2$;

$$\frac{I_x}{B} = \frac{H_1^3}{3} - \frac{L^3}{6} - (H_o + \frac{L}{2})(H_1 - \bar{y})^2 \qquad 3.3.16$$

Equations 3.3.5, 3.3.9 and 3.3.15 can then be used to obtain an expression for $\underline{a}$ as a function of H_o, H_1 and L for purposes of specimen design: i.e., for the ZKG specimen;

$$a = [\frac{M_o}{3}\{\frac{H_1^3}{3} - (1 - \frac{B_N}{B}\frac{L^3}{3} - (H_o + \frac{B_N}{B}L)(H_1 - \bar{y})^2\} - \frac{(2\bar{y})^2}{3}]^{\frac{1}{2}} \qquad 3.3.17$$

For the MZKG specimen;

$$a = [\frac{M_o}{3}\{\frac{H_1^3}{3} - \frac{L^3}{6} = (H_o + \frac{L}{2})(H_1 - \bar{y})^2\} - \frac{(2\bar{y})^2}{3}]^{\frac{1}{2}} \qquad 3.3.18$$

Since B_3, the mode-III bond width, can vary, a table of dimensions has been calculated for B_3 values between ¼ and 3/4 in., for specimens having a maximum total height of 7.00 inches and a gap width, g, of 1/16 inch. Table 6a. This table illustrates the changes in H_T as a function of B_3 are modest, i.e., between 0.030 and 0.094 in. (0.8 to 1.3%) for $\underline{a}$ values between 3 and 7 in. Typical specimens are shown in Figs. 6, 7 and 8 for B_3 values of ½, 5/8 and 3/4 inch, respectively.

Determination of the numerical values to be used to calculate λ in eq. 2.2.1 for MZKG specimens require an accurate compliance calculation, as was done for ZKG specimens in Ref. 15, however, CDCB compliance data can be used to estimate the likely value of dC/da once the specimen

has been contoured according to eq. 3.3.3. The value of M_o used for the contours shown in Figs. 14, 15 and 16 was 48 in.$^{-1}$. This value corresponds to a CDCB contour value of m = 4 in.$^{-1}$. From calibration data over approximately the same crack length range, the corrected value of m, i.e., m', was 5.45 in.$^{-1}$. Using this correction for M_o the calculated value of M_o' would be 65.4 in.$^{-1}$. For the dimensions shown in the three MZKG specimen figures (e.g., B = 0.526 in., E = 10×10^6 psi),

$$\mathcal{G}_c = \frac{P_c^2}{2B_3} \frac{2}{3EB} M_o' = \frac{2.18 \times 10^{-6}}{B_3 B} P^2 \qquad 3.3.19$$

or

$$\mathcal{G}_c = \frac{P_c^2}{2B_3} 8.29 \times 10^{-6} \qquad 3.3.20$$

Eq. 3.3.20 can be used to calculate a value for $\mathcal{G}_c$ for the MZKG specimens having the wide range of overlap values shown in Table 13.

Fracture toughness data[16] is shown in Table 6b and Fig. 17 for overlap dimensions, B_3, ranging from ¼ to 3/4 in. This data was obtained using M_o' rather than M_o in the dC/da expression for $\mathcal{G}_c$. The plot (Fig. 17) shows that there is a minor, if any, effect of changing values of B_3 on $\mathcal{G}_c$ and the value of $\mathcal{G}_c$ ranges from 82.1 to 97.5 lbs/in. with the average $\mathcal{G}_c$ equal to 90.1 lbs/in. Scatter in $\mathcal{G}_c$ values is less for larger overlap values. Fracture toughness tests on predominantly mode-II specimens[17] has indicated that the value of the mode-I components in a mixed-mode test at onset of rapid fracture is approximately equal to the pure mode-I $\mathcal{G}_{Ic}$ value. If we assume that the amount of the unknown mode-I component in this mixed mode III-mode I test is equal to $\mathcal{G}_{Ic}$, then the value of the ratio of mode-I $\mathcal{G}$ to the total $\mathcal{G}$ ($\mathcal{G}_T$), i.e., $\mathcal{G}_I/\mathcal{G}_T$, is approximately 14%.

Fatigue test data reworked from reference 16 are tabled and replotted for specimens having overlap lengths, B_3, of 3/8 and 5/8 in.

Tables 7 and 8 contain the corrected R = 0.1 room temperature fatigue data on two specimens. Fig. 18 is the corrected plot with three fitted curves; one through each set of specimen data points and a third through all points. Table 9 has all plotted points plus the three sets of power law constants. Examination of Fig. 18 indicates that fatigue data from different values of overlap, B_3, give similar da/dN vs. $\Delta\mathcal{K}_i$ results.

The earlier work on mixed mode I and II indicated that both fatigue growth rates as well as onset of rapid fracture were strongly influenced by the amount of the mode-I component present. An empirical equation using an effective alternating crack extension force, $\Delta\mathcal{K}_{eff}$, was developed that fitted the mixed-mode fatigue data rather well for the limited range of mode mix tested;

$$\Delta\mathcal{K}_{eff} = \Delta\mathcal{K}_i \left(1 + 2 \frac{\mathcal{K}_{II}}{\mathcal{K}_T}\right) \qquad 3.3.21$$

or

$$\Delta\mathcal{K}_{eff} = \Delta\mathcal{K}_I \left(1 + \frac{2\,(\mathcal{K}_T - \mathcal{K}_I)}{\mathcal{K}_T}\right)$$

where $\mathcal{K}_T$, the total $\mathcal{K}$ on the specimen, is made up of $\mathcal{K}_I$ plus $\mathcal{K}_{II}$.

If it is assumed that $\Delta\mathcal{K}_{eff}$ will be equal to the pure mode I $\mathcal{K}_I$ at a given da/dN and that $\mathcal{K}_{II}$ can be replaced by $\mathcal{K}_{III}$ in eq. 3.3.21, i.e., $\mathcal{K}_{III} = \mathcal{K}_T - \mathcal{K}_I$, the value of $\Delta\mathcal{K}_{III}$ and the ratio $\mathcal{K}_I/\mathcal{K}_T$ can be calculated directly as follows:

The power law expression for pure mode-I fatigue is:

$$\left(\frac{da}{dN}\right)_I = 6.90 \times 10^{-8}\, \Delta\mathcal{K}_I^{5.31} \qquad 3.3.22$$

and that for the mode-III MZKG specimen is:

$$\left(\frac{da}{dN}\right)_i = 3.42 \times 10^{-9}\, \Delta\mathcal{K}_i^{3.95} \qquad 3.3.23$$

Thus, using equations 3.3.21, 3.3.22 and 3.3.23 at a $\Delta \mathcal{G}_T = \Delta \mathcal{G}_i$ of 5.43 lbs/in., the value of the $\mathcal{G}_I / \mathcal{G}_T$ ratio for the MZKG specimen is 14%, irrespective of overlap dimensions. Although this value agrees exactly with that obtained for onset of rapid fracture results, there are not sufficient data to assume that the $\mathcal{G}_I / \mathcal{G}_T$ ratio has been determined exactly for either case.

It is concluded that this very promising mixed-mode specimen requires a great deal of additional work in order to make it quantitatively useful. At the least, an accurate compliance calibration and additional data detailing the effect of overlap on properties would be needed.

Table 6a

MZKG Specimen Dimensions for M_o = 48 in.$^{-1}$, g = 1/16 in.,
as a Function of B_3 (maximum total height, H_T, is 7.00 inches)

	B_3 = 1/4 L = 5/16		B_3 = 3/8 L = 7/16		B_3 = 1/2 L = 9/16		B_3 = 5/8 L = 11/16		B_3 = 3/4 L = 13/16	
a	H_1	H_T	H_1	H_T	H_1	H_T	H_1	H_T	H_1	H_T
1.696	1.50	2.75								
1.762	--	--	1.562	2.75						
1.967	--	--	--	--	1.688	2.875				
2.000	1.653	3.056	1.684	2.993	1.705	2.910				
2.186	--	--	--	--	--	--	1.813	3.00		
2.540	--	--	--	--	--	--	--	--	2.00	3.25
3.000	2.108	3.966	2.145	3.915	2.176	3.852	2.198	3.772	2.214	3.678
4.000	2.511	4.772	2.553	4.731	2.589	4.678	2.618	4.611	2.641	4.532
5.000	2.881	5.512	2.925	5.475	2.965	5.430	2.998	5.372	3.026	5.302
6.000	3.226	6.202	3.273	6.171	3.315	6.130	3.351	6.078	3.383	6.016
7.000	3.552	6.854	3.600	6.825	3.644	6.788	3.683	6.742	3.710	6.670
7.232	3.625	7.00								
7.274	--	--	3.687	7.00						
7.333	--	--	--	--	3.75	7.00				
7.403	--	--	--	--	--	--	3.812	7.00		
7.488	--	--	--	--	--	--	--	--	3.875	7.00

$H_T = 2H_1 - L + g = 2H_1 - B_3$

$\not{L}_c = \frac{P_c^2}{2B_3} 8.29 \times 10^{-6}$

For B = 0.526 in.

$(\not{L}_c)_{1/4} = 16.6 \times 10^{-6} P^2$

$(\not{L}_c)_{3/8} = 11.1 \times 10^{-6} P^2$

$(\not{L}_c)_{1/2} = 8.29 \times 10^{-6} P^2$

$(\not{L}_c)_{5/8} = 6.63 \times 10^{-6} P^2$

$(\not{L}_c)_{3/4} = 5.53 \times 10^{-6} P^2$

Table 6b

Mode III MZKG Specimen Data for 0.526 inch Thick Laminated Specimens Using AF 55S Adhesive

Overlap Width B_3 (inches)	Equilibrium Crack Extension Load, P_c (lbs.)	Multiplier of P^2 Term (10^{-6}/in.-lb.)	Calculated Value of $\mathcal{G}_c$ (lbs./in.)
1/4	2425	16.6	97.5
3/8	2725	11.1	82.1
1/2	3375	8.29	94.4
5/8	3650	6.63	88.3
3/4	4000	5.53	88.4

Average $\langle \mathcal{G}_c \rangle$ = 90.1 lbs/in.

$\mathcal{G}_{Ic}$ = 12.5 lbs/in.

Calculated Mode I Contribution to Mode III Test

$$\frac{\mathcal{G}_{Ic}}{\mathcal{G}_c} = \frac{12.5}{90.1} = 14\%$$

Table 7

MZKG, R = 0.1, Room Temperature, 3 Hz, Fatigue Data
(M_o = 48, M_o' = 65.4 $in.^{-1}$, B_3 = 0.375, B = 0.518, E = 10^7 psi)
For Specimen 2-08

Max. Load	$\Delta\mathcal{J}_i$	Calc. a	Δa	Cycles at Load	$\frac{da}{dN}$	$\frac{da}{dN}$ (Plot)
lbs.	lbs/in.	in.		N	μ-in/cycle	μ-in/cycle
1200	13.8	2.00	0	0	--	
		2.75	0.75	12288	61	
		3.13	1.13	20130	56	53
1000	9.09	3.23	0	0	--	
		3.25	0.02	2500	8	
		3.31	0.08	5700	13	
		3.57	0.34	15975	21	
		3.76	0.53	19787	27	18
800	5.50	3.86	0	--	--	
		3.94	0.08	28050	2.66	
		3.96	0.10	33824	2.86	
		3.94	0.08	42872	1.74	2.4
600	2.81	4.04	0	0	--	
		4.04	0	231093	0	0
800	5.50	4.14	0	0	--	
		4.31	0.17	28739	6	6
700	4.04	4.74	0	0	--	
		4.74	0	1185488	0	0
800	5.50	4.74	0	0	--	
		5.08	0.34	76129	4.4	
		5.22	0.48	293403	1.6	
		5.54	0.80	858717	0.9	1.5
700	4.04	5.80	0	0	--	
		5.93	0.13	163496	0.75	
		5.95	0.15	253023	0.59	
		5.99	0.19	425583	0.45	0.56

$$\Delta\mathcal{J} = \Delta P^2 = \frac{2.18 \times 10^6 P^2}{B_3 B} = 11.2 \times 10^{-6} P^2$$

Table 8

MZKG, R = 0.1, Room Temperature, 3 Hz, Fatigue Data

(M_o = 48, M_o' = 65.4, B_3 = 0.655, B = 0.518, E = 10^7 psi)

For Specimen 2-09

Max. Load lbs.	ΔS_i lbs/in.	Calc. a in.	Δ a in.	Cycles at Load N	da/dN μin/cycle	da/dN (plot) μin/cycle
1000	6.70	2.81	0	0	--	
		2.86	0.048	1547	31	
		2.88	0.070	3433	21	
		3.00	0.194	6238	31	
		3.15	0.343	14808	23	
		3.18	0.365	24574	15	24
800	4.31	3.18	0	0	--	
		3.23	0.045	41886	1.1	
		3.60	0.417	291600	1.4	
		3.64	0.455	343071	1.3	
		3.83	0.648	372083	1.7	1.4
800	4.31	3.83	0	0		
		3.87	0.037	51471	0.72	
		4.06	0.231	80483	2.91	1.8
700	3.30	4.06	0	0	--	
		4.23	0.171	603157	0.28	
		4.43	0.365	784300	0.46	
		4.54	0.484	951347	0.51	
		4.49	0.432	1038926	0.42	0.42
600	2.42	4.47	0	0	--	
		4.52	0.052	168235	0.31	
		4.59	0.119	436830	0.28	
		4.59	0.119	681522	0.17	
		4.61	0.142	787541	0.18	
		4.66	0.194	860230	0.22	
		4.59	0.119	2367559	0.05	0.05
800	4.31	4.37	0	0	--	
		4.61	0.238	80422	2.91	
		4.80	0.432	253814	1.64	
		4.78	0.410	262519	1.49	1.5
600	2.42	4.83	0	0	--	
		4.83	0	657708	--	
		4.83	0	759233	--	
		4.95	0.119	1023773	0.45	

Table 8, Continued

Max. Load	$\Delta \not{P}_i$	Calc. a	Δa	Cycles at Load	$\frac{da}{dN}$	$\frac{da}{dN}$ (plot)
lbs.	lbs/in.	in.	in.	N	μin/cycle	μin/cycle
		4.97	0.142	1210206	0.31	
		4.93	0.097	1277977	0.19	0.19
700	3.30	4.98	0	0	--	
		5.15	0.171	986125	0.17	0.17

$$\Delta \not{P} = \Delta P^2 \frac{2.18 \times 10^{-6}}{B_3 B} = 6.73 \times 10^{-6} \Delta P^2$$

Table 9

MZKG Data from Tables 7 and 8 Used for Regression Analysis for Power Law Expression[1]

Specimen 2-09		Specimen 2-08	
ΔK lb/in.	da/dN μ in/cycle	ΔK lbs/in.	da/dN μ in/cycle
6.70	2.4	13.8	53
4.31	1.4	9.09	18
4.31	1.8	5.50	2.4
4.31	1.5	5.50	6.0
3.30	0.42	5.50	1.5
3.30	0.17	4.04	0.56
2.42	0.05		
2.42	0.19		

B = 5.39
A = 6.23×10^{-10}
S = 0.273

B = 3.59
A = 5.33×10^{-9}
S = 0.200

Values for the Power Law constants for all data

B = 3.95
A = 3.42×10^{-9}
S = 0.273

(1) $\frac{da}{dN} = A\ \Delta K^B$

S = standard deviation of y on x

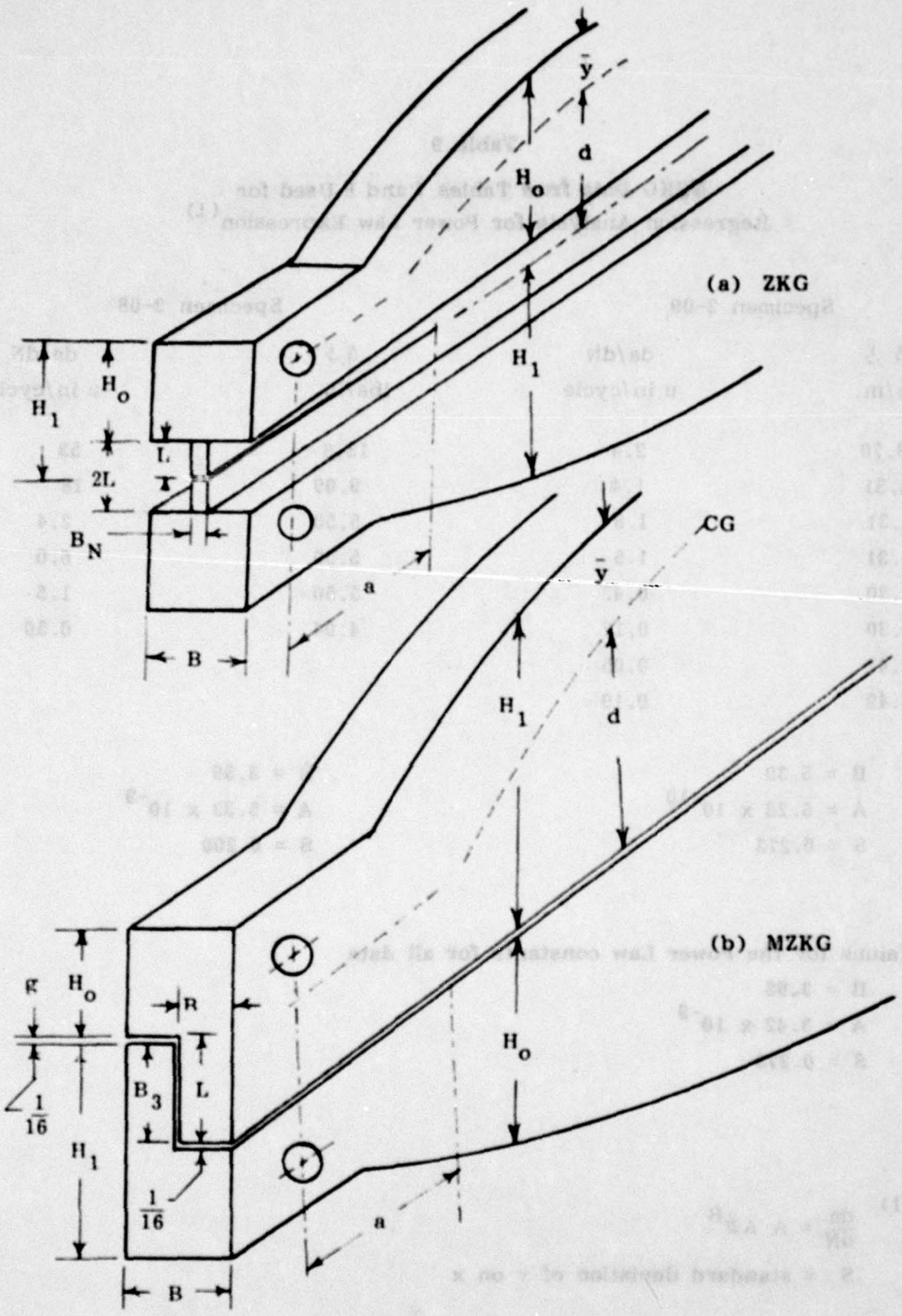

Fig. 13 Zero-K-Gradient Specimens for (a) Plane Stress, Mode I, R Curve, Thin Sheet Testing (ZKG) and (b) Mode III Adhesive Bond Evaluation (MZKG).

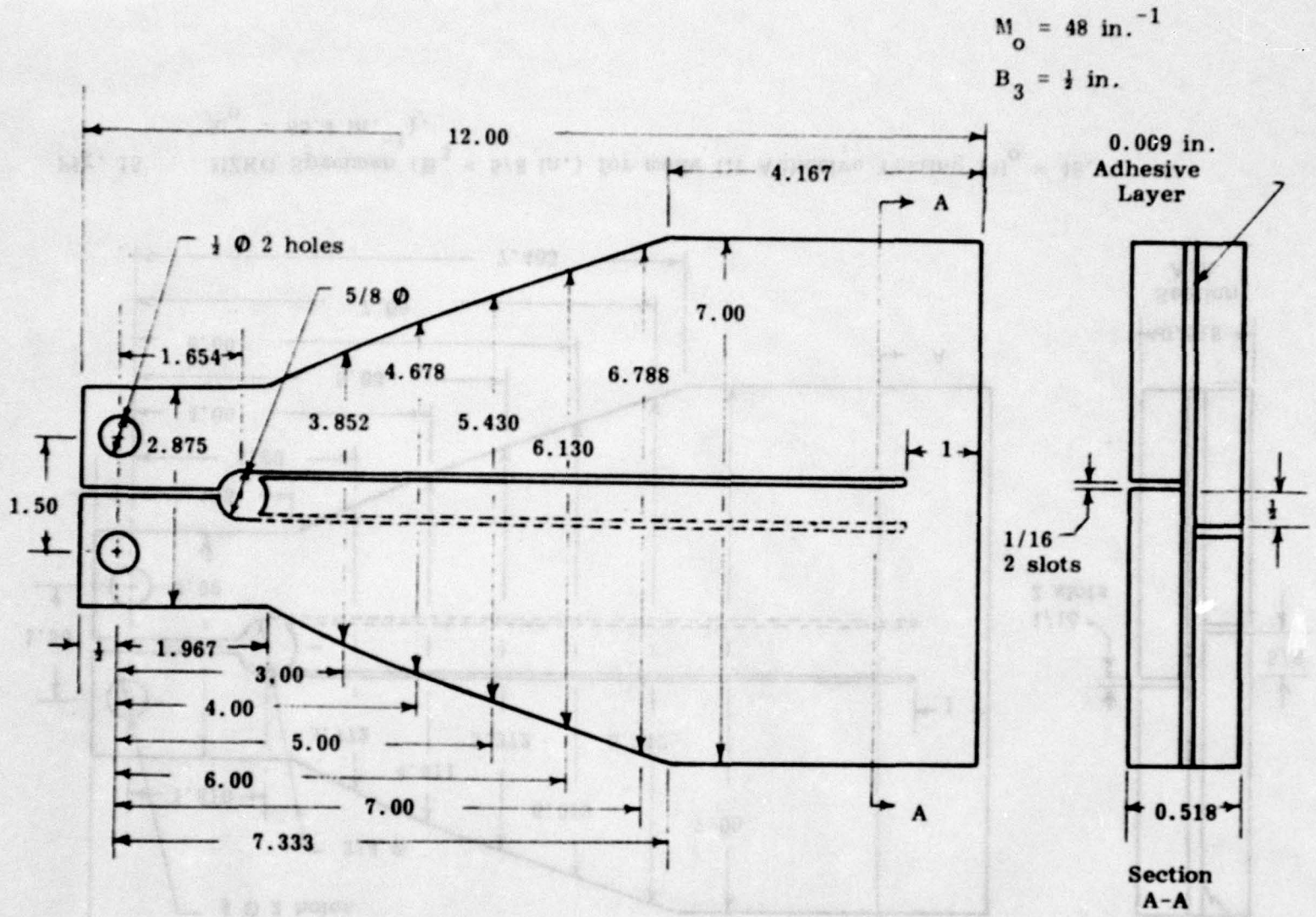

Fig. 14 MZKG Specimen (B_3 = ½ in.) for Mode III Adhesive Testing (M_o = 48, M_o' = 65.4 in.$^{-1}$).

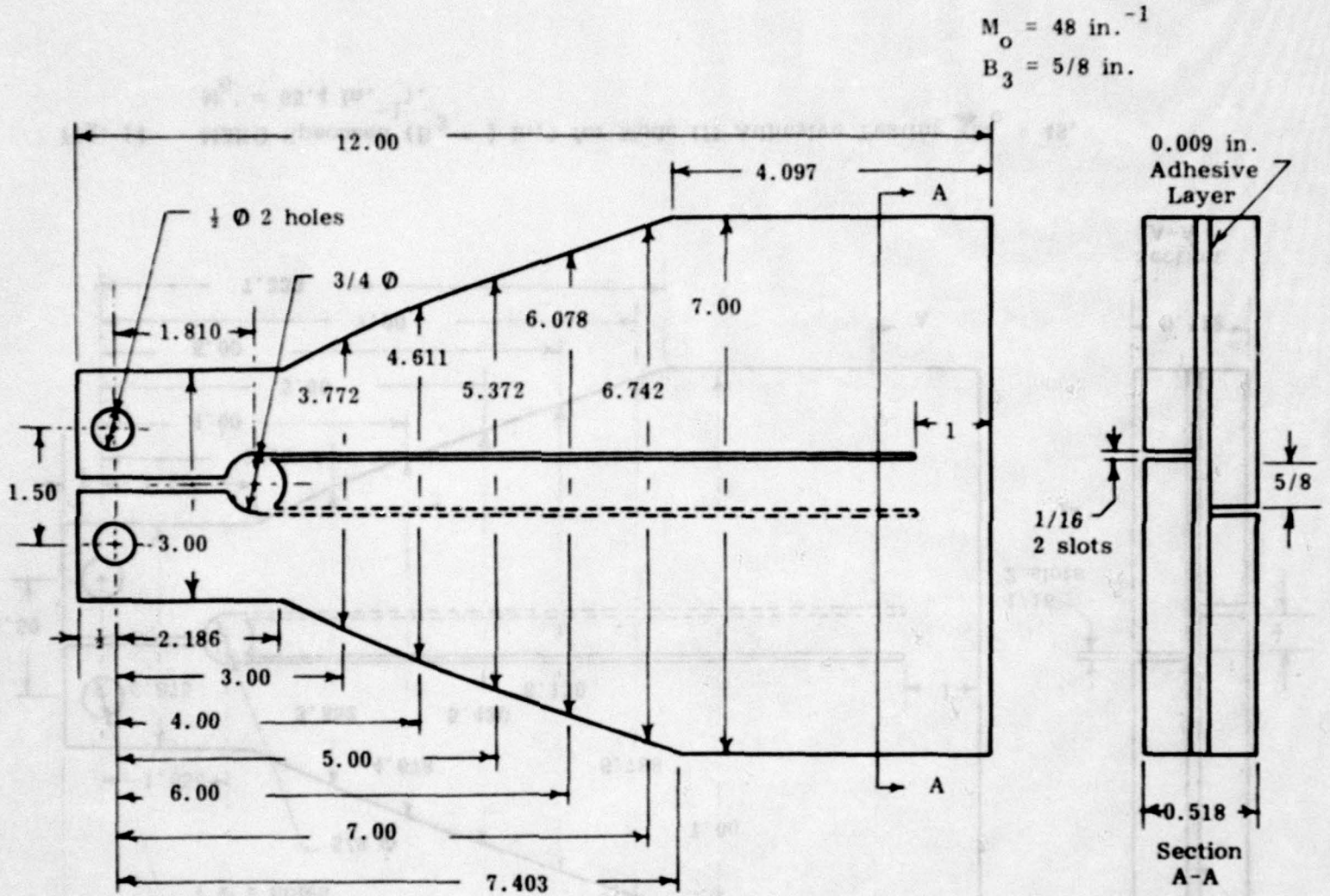

Fig. 15 MZKG Specimen (B_3 = 5/8 in.) for mode III Adhesive Testing (M_o = 48, M_o' = 65.4 in.$^{-1}$).

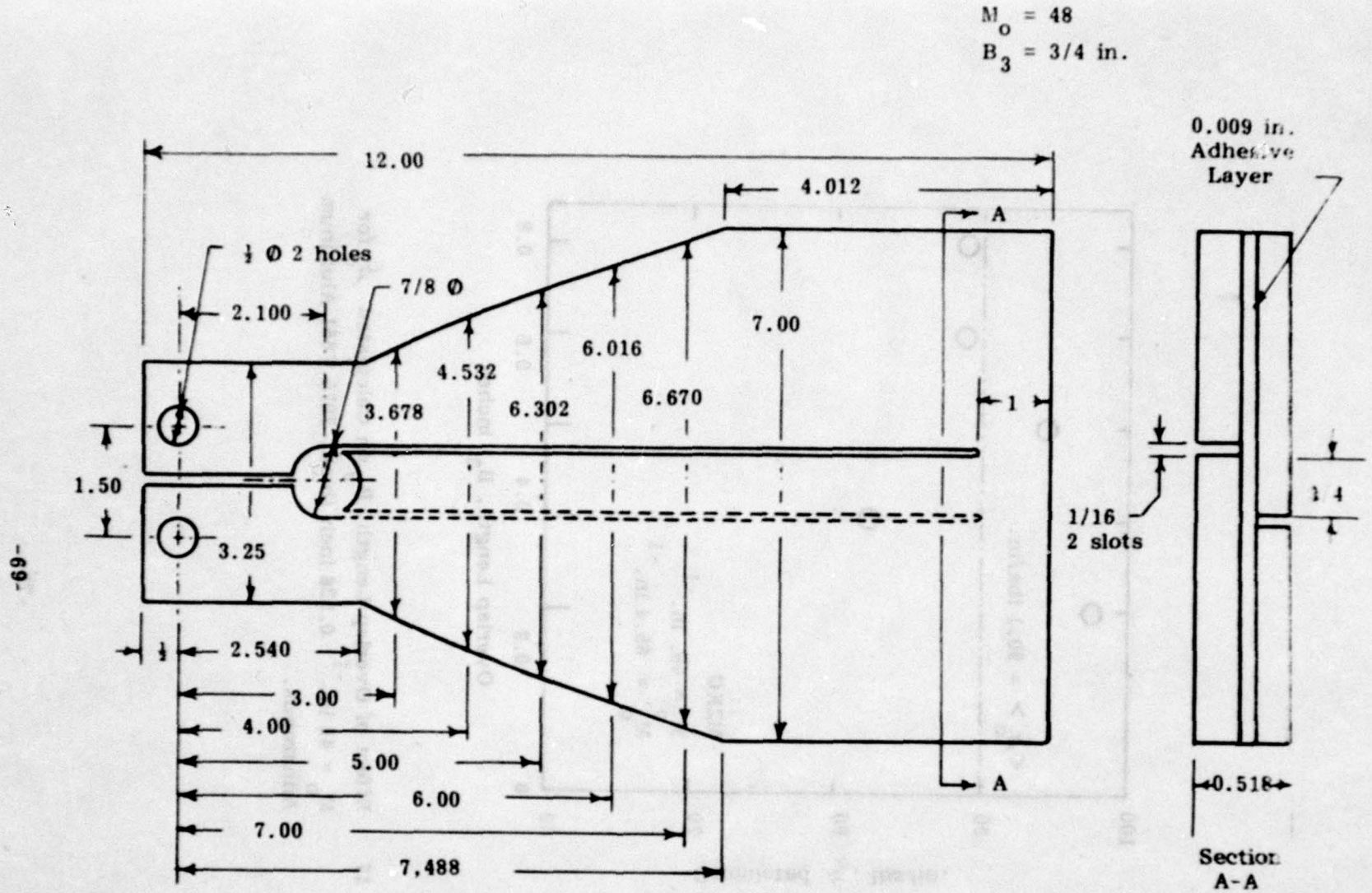

-69-

Fig. 16 MZKG Specimen (B_3 = 3/4 in.) for Mode III Adhesive Testing (M_o = 48, M_o' = 65.4 in.$^{-1}$).

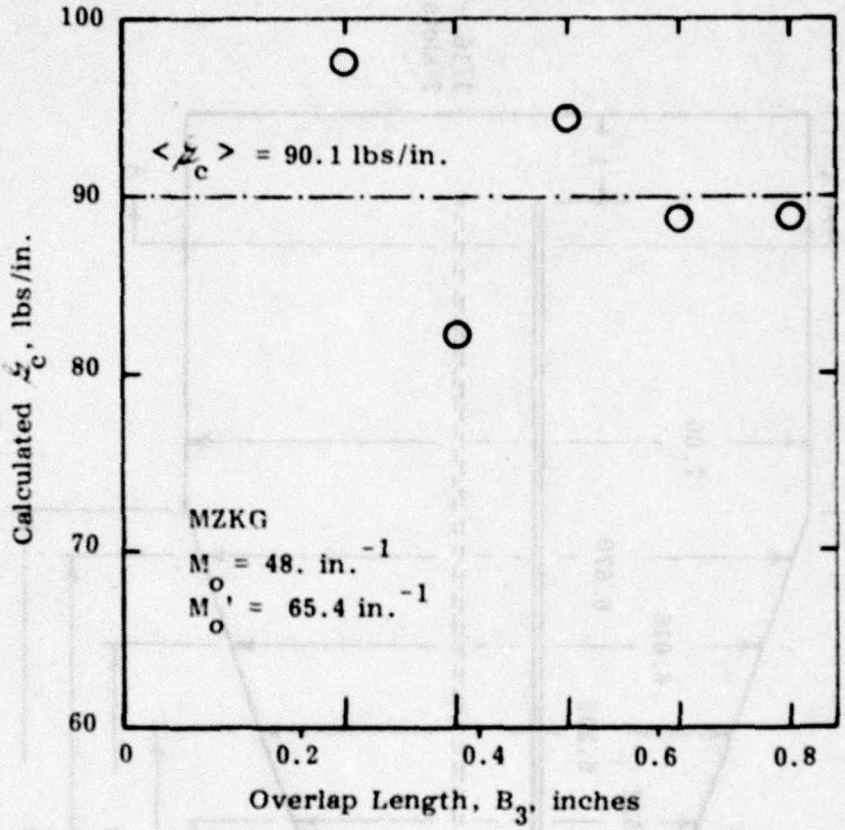

Fig. 17 Effect of Overlap Length, B_3 on Calculated $\mathcal{L}_c$ for M_o = 48 in.$^{-1}$, 0.526 inch thick, 7075 T651 Aluminum Adherends.

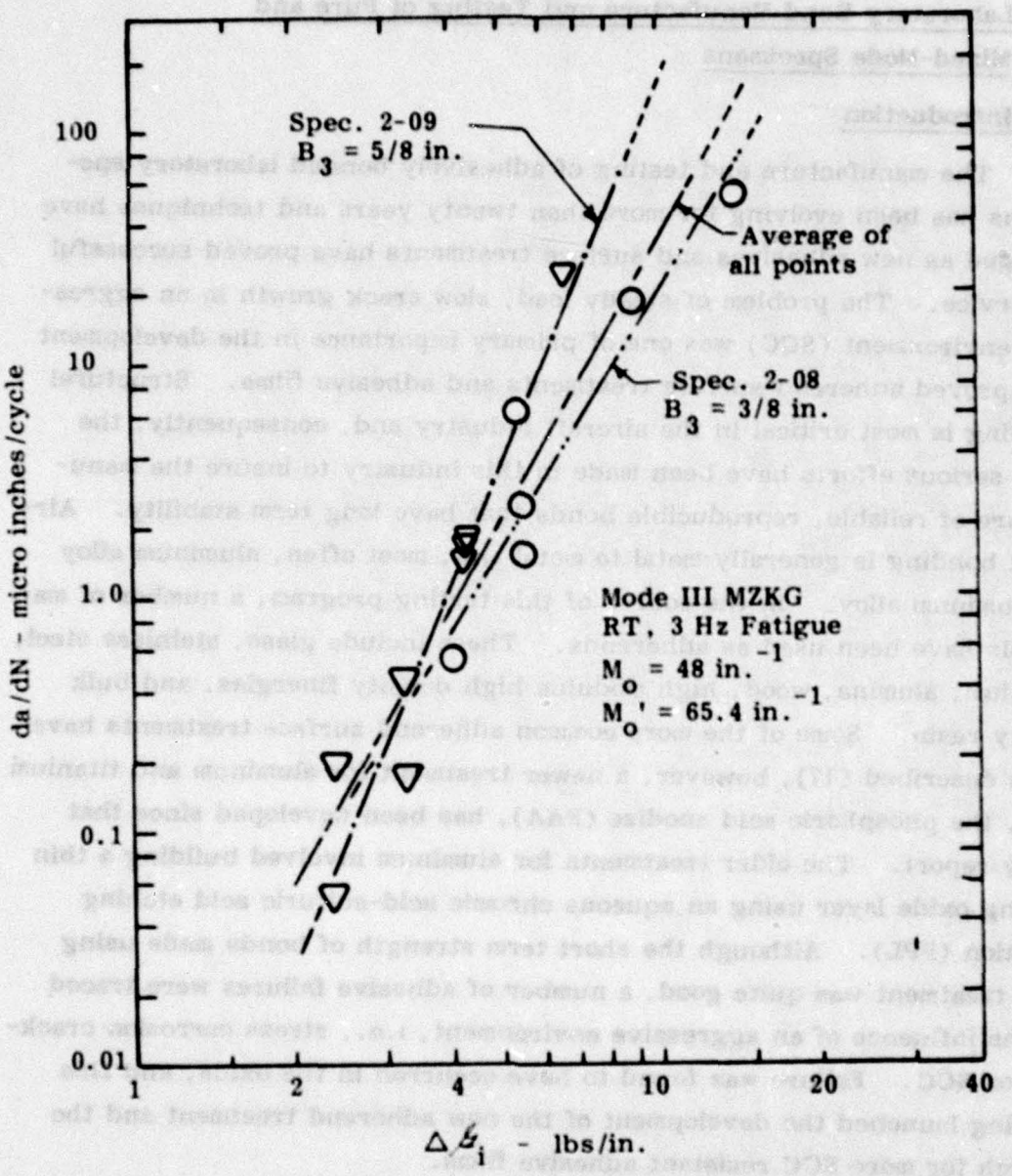

Fig. 18 MZKG Mode III, Room Temperature (RT) Fatigue Crack Growth Curves at 3 Hz for Two Values of the Overlap, B_3.

4.0 Laboratory Bond Manufacture and Testing of Pure and Mixed-Mode Specimens

4.1 Introduction

The manufacture and testing of adhesively bonded laboratory specimens has been evolving for more than twenty years and techniques have changed as new adhesives and surface treatments have proved successful in service. The problem of steady load, slow crack growth in an aggressive environment (SCC) was one of primary importance in the development of improved adherend surface treatments and adhesive films. Structural bonding is most critical in the aircraft industry and, consequently, the most serious efforts have been made in this industry to insure the manufacture of reliable, reproducible bonds that have long term stability. Aircraft bonding is generally metal to metal and, most often, aluminum alloy to aluminum alloy. In the course of this testing program, a number of materials have been used as adherends. These include glass, stainless steel, titanium, alumina, wood, high modulus high density fiberglas, and bulk epoxy resin. Some of the more common adherend surface treatments have been described (17), however, a newer treatment for aluminum and titanium i.e., the phosphoric acid anodize (PAA), has been developed since that early report. The older treatments for aluminum involved building a thin strong oxide layer using an aqueous chromic acid-sulfuric acid etching solution (FPL). Although the short term strength of bonds made using this treatment was quite good, a number of adhesive failures were traced to the influence of an aggressive environment, i.e., stress corrosion cracking or SCC. Failure was found to have occurred in the oxide, and this finding launched the development of the new adherend treatment and the search for more SCC resistant adhesive films.

The manufacture of laboratory adhesive test specimens has generally been done with small area bonding. Early specimen manufacture, using the liquid resin-hardener mixtures, was done by casting the heated mixed liquid in place using shims between the adherends to maintain bond thickness. The manufacture of laboratory specimens with the partially cured,

high performance, adhesive films was done initially using CDCB specimens made individually. The narrow area bonding condition that results differs substantially in the pressure-temperature history from that used in wide area structural bonding. Consequently, this section reviews the manufacture and testing of pure and mixed-mode specimens made as wide or narrow area bonds. It should be noted that test results are given for sound bonds (low void content) where good bonding practice is followed; e.g., the use of properly prepared adherends and a proprietary adhesive film where the specified pressure-temperature cycle produces bonds of a given thickness.

The testing of both pure and mixed-mode specimens is divided into two categories: onset of rapid fracture, i.e., fracture toughness testing and slow crack extension. In general, the latter is strongly influenced by temperature and environment while the former is not.

4.2 Development of the Phosphoric Acid Anodizing (PAA) Treatment (Boeing 5555)

The SCC failure of FPL treated structurally bonded aluminum panels was first investigated by the Boeing Airplane Company in an attempt to improve bond reliability. The test of proper adhesion was a highly stressed SCC exposure for a specified period, i.e., the Boeing wedge test. In this test, bonded strips were wedge loaded in cleavage and then exposed at elevated temperature to a moist environment or water. The criteria for acceptance of a given bond fabrication was (1) that an opening mode load approximately equal to the failure load be applied to the test coupon, (2) that slow crack growth over a 100-hour time period did not proceed more than a specified distance, e.g., 0.250 inch, and (3) that the fracture plane be mostly within the adhesive layer and not near the interface region. A scanning electron microscope investigation of the SCC failed bonds of specimens having conventionally treated adherends indicated that failure occurred cohesively in the oxide layer, rather than adhesively at the adhesive-adherend interface. This oxide layer produced by the FPL etch was found to be hydrophillic. This observation led to the development of a

hydrophobic oxide, e.g., that produced by the phosphoric acid anodizing (PAA) treatment (see Appendix I). The SCC resistant oxide surface is obtained by a conversion of the 80 Å FPL oxide to a 4000 Å thick "forest" of vertically oriented fragile oxide rods. Current bonding practice suggests that this layer requires adhesive primer to fill in the spaces to render the surface useable for bonding.

In recent tests on PAA treated adherends, no evidence of separation near one interface (IF) has been observed. These tests have included elevated temperature (140°F) SCC and fatigue tests, as well as combined effects of fatigue in an aggressive environment. For example, SCC tests have been carried out for more than six months at 140°F with little evidence of IF penetration, although exposed aluminum surfaces have become quite corroded.

Thus, service simulation requires that laboratory specimens using aluminum adherends be prepared with the PAA treatment for slow crack growth studies. This is particularly important with mixed-mode specimens where the locus of fracture tends to be near the interface.

4.3 Bonding Practice for Toughness Specimens Using Proprietary Film Adhesives

Wide area bonding using commercial film adhesives is done according to the manufacturer's specifications regarding temperature and pressure cycle. In general, PAA treated and primed adherend panels and adhesive film are assembled as a sandwich and mechanically held together. Pressure is applied either with a heated platen press or for aircraft panels in an autoclave where the vacuum bagged assembly is automatically cycled through the specified temperature-pressure profile. Fracture toughness specimens that can be machined from wide area bonds include the cracked lap shear (CLS), the modified-zero-K gradient (MZKG) and the width tapered beam (WTB). The advantage of using specimens made from wide area bonds results from testing the adhesive bond in the condition as it exists in the structure. Aside from the pressure-temperature history, bond thickness is the most important property of the structure. A common cure cycle for

250°F curing adhesives bonded in aluminum consists of a heating rate of 2°F/min. to a minimum of 220°F and a maximum of 270°F. Cooling rates are also about 2°F/min. Pressure is maintained during the cycle at 25 psi. Even though the adhesive becomes quite fluid during the high temperature part of the bonding cycle, very little change in thickness occurs in wide area bonding because of mechanical entrapment. For example, typical adhesive film thicknesses, both before and after bonding, are 0.008 to 0.010 in. Aircraft structure is generally made up of bonds between relatively thin gage metal, e.g., 0.070 in. and, while this adherend thickness is suitable for low load, slow crack growth studies, its low stiffness makes it unsuitable for onset of rapid fracture determination. Thus, for complete adhesive characterization, relatively thick panels (e.g., 3/8 to ½ in.) must be bonded separately, rather than removing specifically designed sections of bonded aircraft panels.

An alternative to the relatively expensive and difficult wide area, thick-panel bonding is the narrow area bonding used successfully for liquid adhesive systems. For narrow area bonds, care is taken to reduce the pressure during cure, so that for the recommended temperature cycle the bond thickness remains above 0.005 in. Bond thickness can also be kept constant by the use of shims. In this case, care must be taken to avoid leakage of the adhesive out of the bond cavity, thus creating voids. All toughness specimens can be made in this way, however, narrow area bonding is must suitable for the CDCB adherends. Specimens such as the MZKG and WTB would actually be somewhat less convenient to manufacture as a narrow area bond. Evaluation of the differences in mode-I toughness as a function of bond preparation has shown that bond thickness is more important than absolute pressure in obtaining high values of $\mathcal{G}_{Tc}$. Thus, it is concluded that suitable toughness specimens can be prepared using either method. Although the effect on slow growth has not been studied, it is assumed that the bulk properties of the adhesive will not be changed substantially by the pressure differences during the cure cycle, as long as a bond thickness above 0.005 in. is maintained.

4.4 Testing of Pure and Mixed-Mode Adhesive Fracture Specimens

Three load-time profiles are possible in simulating the service loading that may result in crack extension: (1) monotonically increasing, (2) steady, and (3) alternating. The first is used to obtain onset of rapid fracture, $\mathcal{G}_{Ic}$ (or $\mathcal{G}_{Tc}$ for mixed-mode loading) and the toughness at arrest ($\mathcal{G}_{IA}$ or $\mathcal{G}_{TA}$). The second is applied to obtain slow crack growth data during exposure to an aggressive environment (i.e., SCC), and the third to develop fatigue slow growth data with and without the environment.

4.4.1 Increasing Load Testing

Standard increasing load or fracture toughness testing, described in ASTM SRP 3433-75 for pure mode-I CDCB specimens, is similar for all pure and mixed-mode specimens. In general, loading is such that onset of rapid fracture occurs in a minute or less and $\mathcal{G}_{Ic}$ (or $\mathcal{G}_{Tc}$) and $\mathcal{G}_{IA}$ (or $\mathcal{G}_{TA}$) are determined from the load at onset and the load at arrest coupled with the crack length at onset and arrest. For "crack-length-indifferent" or "constant-K" specimens only the two loads need be known to determine initiation and arrest toughness, as long as the crack remains within the "constant-K" region. Another advantage of the "constant-K" specimen for fracture toughness testing is that, ordinarily, many determinations of onset and arrest toughness can be made on a single specimen. The response to loading is sensitive to loading rate, temperature, adhesive type, and loading mode. The brittle behavior seen at standard crosshead rates, shown by unmodified epoxy adhesives tested at room temperature (RT) or the tough, modified-epoxy, proprietary film adhesives tested at low temperature is much the same. The load-displacement (P-Δ) record is elastic up to onset of rapid fracture at maximum load, followed by arrest at a lower load ("peaked" P-Δ curve). Standard rate testing of the tough adhesives at RT often shows an elastic P-Δ record to maximum load where crack extension occurs at constant load at a rate dictated by the crosshead ("flat" P-Δ curve). High rate testing has shown that the arrest toughness is the lowest value of crack extension force for material showing peaked

behavior. Flat behavior is more complex since some materials show a transition from flat to peaked behavior with a lowered arrest toughness at high rates. Thus, the evaluation of tough adhesives should include some high rate testing to determine the amount of toughness loss.

The measured toughness of many of the adhesives is related to fracture appearance, therefore, a description of the fracture surface is appropriate to any toughness survey. For example, peaked P-Δ curves are generally associated with flat, shiny, featureless fractures; while flat P-Δ curves are associated with fracture surfaces that show evidence of plastic flow during crack growth. Of particular interest is the fracture surface resulting from high-shear mixed-mode ($\mathcal{J}_I$ plus $\mathcal{J}_{II}$) loading. For this case, both brittle and tough adhesives show multiple origin fracturing that results in a rough fracture surface with a dense pattern of inclined "flakes". Increasing load fracturing of high-shear, mode-III MZKG specimens does not show those obtained from mode-II specimens. For the one tough adhesive examined with the MZKG test specimen, fracturing occurred near the interfaces (IF) at the boundaries and partly cohesive or center of bond (COB) away from the boundaries. These differences in shear fracture morphology remain to be resolved.

4.4.2 Stress Corrosion Cracking (SCC) Testing

The measurement of steady load, environmentally assisted slow crack growth (SCC) depends greatly on specimen design. For example, SCC exposed specimens where crack extension force due to compliance change increases with crack length (e.g., dC/da increasing) will show increased crack growth rates with increased crack lengths. Constant-K specimens do not show increasing crack extension force as the crack grows and, thus, are easier to use for both SCC and fatigue testing. The SCC characterization of adhesive bonds and monolithic materials is quite similar in experimental practice. The parameters are (1) the threshold value of applied crack extension force at which a stationary crack begins to extend ($\mathcal{J}_{Iscc}$ or $\mathcal{J}_{Tscc}$) and (2) the SCC rate-extension force behavior ($\mathcal{J}_i$ vs. $\dot{a}$).

For many monolithic materials, e.g., metals, the $\mathcal{G}_i$-vs. $\dot{a}$ relationship shows a rate plateau. In this plateau region crack growth rate is independent of applied crack extension force for forces ranging from just above the threshold to more than half the $\mathcal{G}_{Ic}$ value. This rate independence is thought to be due to a transport or diffusion limited process. The SCC exposure in 140°F water of mode-I, PAA treated, adherend, film-ahdesive specimens shows the rate plateau with a relatively high threshold ($\mathcal{G}_{Iscc}/\mathcal{G}_{Ic} \approx 0.1 - 0.2$). However, earlier work with FPL etched adherends and the same adhesive showed a lower threshold and a steep $\mathcal{G}_I$-$\dot{a}$ curve, i.e., a small increase in force gave a large increase in crack length. The two distinct behaviors result from a difference in the location of fracture. For PAA treated adherends the fracture is cohesive in the center of the bond (COB), while for FPL etched adherends crack growth occurs near an interface (IF). These results confirm those originally found with the Boeing wedge test used to develop the PAA treatment. The plateau behavior is also observed for PAA treated mixed-mode CLS specimens.

The constant load SCC testing of mode-I CDCB specimens requires only that changes in displacement be monitored with time. For this case, dC/da is constant and equal to 8m'/EB. Thus, at constant load, the crack growth rate can be obtained directly from the rate of change of displacement of the load ($\dot{\Delta}$) with time:

$$\dot{a} = \frac{EB}{8Pm'} \dot{\Delta} \qquad 4.1$$

Displacement rate, $\dot{\Delta}$, is monitored continuously for several specimens with a multipoint recorder, and crack growth rates are determined over $\frac{1}{4}$ inch of crack length change or more. These tests at a single load can take over a month or more, especially if the $\mathcal{G}_i$ values are near the threshold. In addition, constant applied crack extension force seldom gives constant $\dot{a}$ and variations of a factor of two or more are not uncommon. Thus, the constant-K specimen is also quite useful in determining the range of variation in threshold and crack growth rate at a given $\mathcal{G}_I$ above the threshold.

The SCC testing of mode-I width tapered beam (WTB) specimens is somewhat more difficult, because dC/da is not constant, even though the WTB is a constant-K specimen (see Section 3). In this case, the testing practice is much the same, however, the conversion of displacement data to crack length requires a knowledge of the initial compliance and absolute displacement at the SCC load in order to obtain the initial crack length, a_o, and crack growth rate, $\dot{a}$. This is in contrast to the CDCB specimen where only the change in displacement with time, $\dot{\Delta}$, need be known in order to determine $\dot{a}$. The absolute displacement data is obtained at the beginning of the test and interim compliance data is periodically checked, using both the change in displacement with time at fixed load and by a periodic instrumented loading and unloading sequence. This procedure also corrects for the changes in displacement not connected with crack growth. These displacement changes not related to crack growth are thought to be a plastic or viscoelastic flow ahead of the crack tip. For mode-I SCC tests, this flow is highest immediately after the application of the fixed load and it decreases to near zero after about a day. The errors in $\dot{a}$ caused by flow are most obvious at loads near the threshold, G_{Iscc}, where the magnitude of flow relative to crack extension is largest.

The SCC testing of the mixed-mode cracked lap shear (CLS) specimen is similar to that described above for the mode-I WTB specimen. The additional compliance data is especially necessary here because, although the CLS specimen is independent of crack length as it is for all mixed-mode specimens in Section 3, the flow problem is more severe. Loading for the CLS specimen is such that both adherends and much more of the bond length is loaded than for mode-I specimens. For example, CLS displacement change data taken at constant load over a nine month period under conditions that were expected to cause SCC slow crack growth showed apparent crack length increases of 4 to 5 inches. However, verification compliance checks, taken periodically during the test duration, showed that crack length had remained unchanged.

Two observations were made on the basis of SCC testing of CLS specimens: (1) the substantial flow that occurs during steady mixed-mode loading makes the sole use of displacement change with time, $\dot{\Delta}$, to calculate $\dot{a}$ impractical, and (2) the threshold crack extension force for mixed-mode loading, $\mathcal{G}_{T_{scc}}$, is substantially above the calculated value, based on the assumption that crack growth begins when the mode-I component is above the pure-mode-I $\mathcal{G}_{I_{scc}}$. Both of these effects may be the result of the flow, evidenced by values of $\dot{\Delta}$ not associated with crack growth.

The modified-zero-K-gradient (MZKG) specimen differs from the CLS specimen in that loading is all applied at the leading edge of the crack, and the remainder of the adherend area away from the influence of the singularity is free of loading. In addition, dC/da is a constant for the MZKG specimen as it is for the CDCB specimen and, thus, compliance and crack length calculations from load and displacement requirements are much less involved than for the CLS specimen. This specimen has not been fully evaluated for SCC testing because of the lack of an analysis that is suitable to separate $\mathcal{G}_I$ and $\mathcal{G}_{III}$ components from the total $\mathcal{G}$, $\mathcal{G}_T$. Recall that the MZKG loading is all edgewise sliding mode-III and the amount of parasitic mode-I cleavage that occurs at the free edges, deduced experimentally as approximately 14 percent of $\mathcal{G}_T$, has not been determined by any analysis.

4.4.3 Fatigue Testing

The parameters that affect slow crack growth exposed to alternating load are (1) loading frequency (2) loading cycle shape and pattern (spectrum) (3) range ratio, R (P_{min}/P_{max}), (4) loading mode (pure or mixed-mode) (5) temperature and (6) environment (e.g., water). Fatigue testing in this program has not dealt with spectrum loading, however, some data have been obtained for the other parameters in an attempt to describe the areas of importance. For all of the adhesives and loading modes, room temperature (RT), environment free, fatigue tests showed decreased crack growth rates per cycle, da/dN, as loading frequency was increased above 3 Hz or R ratio was raised from 0.1 to 0.6. Thus, standard baseline fatigue data have been collected at an R of 0.1 and a frequency of no more than

3 Hz. The fatigue curve obtained for adhesive bonds shows the same general features observed for monolithic materials: (1) a power law area where da/dN is proportional to $\Delta\mathcal{G}^n$ and (2) a lower limit (e.g., threshold) on the applied alternating crack extension force, $\Delta\mathcal{G}_1$, below which slow crack growth does not occur, $\Delta\mathcal{G}_{TH}$. The value of n for adhesive bonds is 5 to 10, whereas for metals n is 1½ to 3. In light of this steep fatigue behavior, the threshold value is more important for adhesives than for metals.

Mixed-mode (I and II) fatigue data (CLS specimen) show the same steep slope when log da/dN is plotted versus the log of the total applied crack extension force, $\Delta\mathcal{G}_T$, however a given value of da/dN occurs at a higher value of $\Delta\mathcal{G}_T$ than for the pure mode case. An empirical fitting procedure defining an effective $\mathcal{G}$, $\mathcal{G}_{eff}$, has been used to allow pure and mixed-mode data to be plotted on the same curve:

$$\Delta\mathcal{G}_{eff} = \left[1 + \frac{2\Delta\mathcal{G}_{II}}{\Delta\mathcal{G}_T}\right] \Delta\mathcal{G}_I \qquad 4.2$$

where

$\Delta\mathcal{G}_{eff}$ = the effective $\mathcal{G}$ value used for the data plot

$\Delta\mathcal{G}_{II}$ = the value of $\Delta\mathcal{G}_{II}$ for the test specimen

$\Delta\mathcal{G}_I$ = the value of $\Delta\mathcal{G}_I$ for the test specimen

$\Delta\mathcal{G}_T$ = the sum of $\Delta\mathcal{G}_I$ and $\Delta\mathcal{G}_{II}$

Verification of this relationship would have to be made with other adhesive-adherend systems and other mixed-mode combinations in order to allow its use in design.

Fatigue of the mode-III, MZKG, specimen also shows the same high n value seen for both pure mode-I and CLS specimens and the use of eq. 4.2 permitted an estimation of the parasitic mode-I component (i.e., 14 percent). Fatigue fracture appearance for either pure or mixed-mode slow crack growth for all adhesives tested to date is cohesive, center of bond (COB), and essentially flat and featureless when examined with an optical microscope at 50X or less.

Fatigue crack growth in the presence of an environment (e.g., water) depends on the adherend treatment, the adhesive system, the loading cycle and the test temperature. For PAA treated aluminum adherends, failure of commercial film adhesives exposed to 140°F water occurs cohesively (COB), rather than near the interface (IF). If the adhesive itself is sensitive to hot water, decreased cyclic rate and increased R ratio will result in increased da/dN at a given ΔG.

Standard fatigue cycling is done at an R ratio of 0.1 and a sinusoidal frequency of 3 Hz using a closed loop, servo-hydraulic test machine in load control. Using constant-K specimens, constant load gives constant G and a given minimum increment of crack growth is selected for determination of da/dN (e.g. 0.1 to 0.25 in.). For increasing-K specimens, such as the uniform beam (UDCB) or compact specimen (CS), crack growth is determined at constant load until the value of da/dN is above 0.01 in./cycle. Should sufficient crack length remain at this point, the load is dropped and a new test started. The da/dN data are then obtained using the ASTM seven point incremental method developed for CS fatigue testing. Crack length is measured either visually or using compliance. Fatigue growth in monolithic metal fatigue tests can be followed equally well using either technique and often both are used: compliance for measurement of instantaneous crack length and visual to discover grossly uneven growth that can cause scatter in the rate data.

Crack growth in adhesive specimens is more difficult to follow visually than in metals: the crack extension forces are lower, and the crack is not opened as far during cycling. One of the techniques used for following fatigue cracks in metals, which has been successfully used for adhesives, involves slow cycling (e.g., 1/3 to 1 Hz.) after spraying a volatile inert solvent e.g., 1, 1, 1, trichloroethane) at the crack tip. The pumping action of the closing crack reveals the crack tip as a renewed, fast drying wet spot on each cycle. This pulsing wet spot can be easily seen with a 5X loupe or a toolmaker's microscope (Gaertner Scientific) often used for visual crack length measurement. This visual measurement

technique is satisfactory for pure mode-I testing, but is substantially more difficult for mixed-mode fatigue growth. It is possible to follow crack growth visually in a side grooved CLS specimen, but virtually impossible in the MZKG specimen, where the bond line cannot be seen from the side. Thus, compliance calculated crack lengths have been used almost exclusively for mixed-mode fatigue testing.

The displacement measurement used in the compliance calculation is obtained in several ways depending on the specimen being tested. Pure mode-I specimens have an LVDT or eddy current displacement gages mounted on the loading clevises such that the displacement of the load is measured. This arrangement is satisfactory even though loading pin bending is not eliminated, because of the relatively large fatigue displacements observed for standard WTB or CDCB specimens (e.g., 0.05 to 0.25 in.) in the "constant-K" range of crack lengths. Displacement measurements for the mode-III, MZKG specimen are made using similar clevis mounted gages, however, the total displacement is somewhat lower and requires a greater transducer gage sensitivity. Crack growth of the CLS specimen is calculated from the mode-I displacement using the specimen mounted non-contacting eddy current gage.

Compliance data for any specimen type can be obtained during the test in several ways depending on the available instrumentation. One satisfactory method uses a load vs. displacement, X-Y, pen recorder (frequency response $\leq$ 1 Hz) and an X-Y, X-time oscilloscope, which measures load versus displacement and load vs. time simultaneously (frequency response $\geq$ 10 K Hz). A precracked specimen is initially loaded slowly (e.g. $\approx$ 0.3 Hz) for a single cycle to obtain a load-displacement, X-Y compliance record on the pen recorder. A maximum load is selected (R ratio is 0.1) and fatigue cycling begun at 3 Hz at test machine settings slightly below this load. The proper amplitude and maximum load are then set using the oscilloscope load traces. Total displacement made as an alternate or second trace on the scope is used to indicate crack length change during cycling. The intial value of total displacement is used as

a reference and a given increase in displacement, for a given load range, corresponds to a given crack length change. Verification of exact crack length increase is done by compliance, taking periodic, slow rate, X-Y pen recorder traces and visually observing the crack, if possible.

Data reduction consists of determining crack length (compliance and/or visual) versus number of cycles at the loads applied in the test and converting the load-crack length-cycles data to $\Delta\mathcal{P}$ versus da/dN using the analysis for the specimen. Data collection includes repetition of given da/dN - $\Delta\mathcal{P}$ areas to determine reproducibility and confidence limits on the threshold and power law expression constants fitted routinely to the experimental points.

Fatigue data collection and reduction have been made somewhat more efficient using more automated test machines, instrumentation and data reduction equipment. Recent improvements in servo-hydraulic test machine instrumentation permit a given load range to be maintained over a wide frequency limit. A digital peak reading meter has increased accuracy in measurement of load and displacement during high speed cycling and has eliminated the need for an oscilloscope. The most advanced test machines use computer program driven, closed loop electronics and can be programmed for a complete cycle of data collection. The automated test machine has the capability to permit fatigue data to be completely reduced to a set of tabled values, which include raw and processed information, as well as the statistical values, without involvement of the engineer or test machine operator. A semi-automated test machine has been used successfully in this test program for both pure mode-I and mixed-mode fatigue testing. It is most useful for long time tests near $\Delta\mathcal{P}_{TH}$ where crack growth is zero or very small.

5.0 Application of Linear Elastic Fracture Mechanics to Adhesive Bondline Fracture Analysis

5.1 Introduction

The application of fracture mechanics to monolithic materials, begun in earnest in the third and fourth decade of this century, has gone through

several evolutionary changes. Beginning with linear elastic fracture mechanics (LEFM), which was concerned with the stress analysis of a cracked structure, the technology advanced from a condition where only relatively brittle materials could be toughness evaluated to one where a wide range of commercial materials used in structures can be included. This evolutionary process has not been free of controversy. Those materials that did show substantial yielding prior to crack extension had to be analyzed for plane strain conditions rather carefully prior to validating or invalidating the measured toughness, K_{Ic}. Because of the controversy and because of the importance of the toughness value in commerce, those concerned with establishing standards worked through the ASTM and specifically through the ASTM E-24 Committee. The work of this committee resulted in specimen and size requirements for toughness testing for tougher and tougher materials. At each stage arguments have been heard that would reject LEFM out of hand because of the non-applicability of the mathematical model in the vicinity of the crack tip during substantial plastic flow. Two approaches have been used to counter these arguments. The first suggests that fracture mechanics is an engineering discipline and that if the specimen models the way in which cracks will grow in the structure, then it is a useful methodology. This first approach has proved very successful in both post-mortem examination of failed structures and in design criteria for new ones.

More recently, the total-energy-lost concept of $\mathcal{J}$, the strain energy release rate or crack extension force, which developed concurrently with the K concept, was updated so that tougher materials could be evaluated. This concept, the J integral, has been substantially investigated and has shown to be satisfactory from an engineering point of view in describing plane strain behavior on substandard specimens that show substantial yielding. The use of this concept is not as unsettling as that of LEFM because no assumptions concerning the shape of the stress field at the tip of the crack are made.

The investigation of adhesive bonding from a fracture mechanics point of view was begun in the early 1960's and has continued to the present with most of the work being done at this laboratory. The energy approach was used here since suitable stress analyses of cracks in adhesive bonds had not been written. The recent success of computer assisted stress analyses for monolithic materials has led to its use for adhesive bonding.

5.2 Computer Assisted Stress Analysis of Cracks in Adhesively Bonded Structures

One of the most advanced stress analysis techniques involves a very special kind of finite element analysis that uses a number of super-elements to describe the stress situation approaching the crack tip. This stress analysis technique, used by Wang, et al. (8) at MIT, apparently does not agree with the energy analysis used at MRL. For example, a quote from the MIT work states "Any yielding of the material in a zone at the crack tip must be sufficiently localized, compared to the characteristic dimensions, that the yield zone is embedded in an elastic unyielded continuum of the bulk material." "Furthermore, the classical elastic singular stress distribution associated with the sharp crack prior to yielding must still obtain in the elastic domain surrounding the yield zone." "Only under these conditions will the singular stress field described by the stress intensity factor, K_I, (and the associated strain energy release rate, $\mathcal{G}_I$), control the fracture process at the crack tip and be useful as a criterion of brittle fracture."

In response to the MIT Report which was presented to ASTM Committee D-14 (adhesives), our laboratory and several others presented the current fracture mechanics thinking on analysis of fracturing adhesive bonds to ASTM Committee D-14 which are part of the official record of that committee.

The successful extention of MRL laboratory data to cracked adhesively bonded structures (9) suggests that the analysis used in Ref. (8),

AD-A075 541 MATERIALS RESEARCH LAB INC GLENWOOD ILL F/G 13/5
FRACTURING CHARACTERISTICS OF ADHESIVE JOINTS.(U)
SEP 78 S MOSTOVOY , E J RIPLING N00019-77-C-0256

UNCLASSIFIED NL

2 OF 2
AD-
A075541

END
DATE
FILMED
11-79
DDC

although sophisticated, is not adequate to describe adhesive bond failure by crack growth.

The general conclusions reached by all those responding to Ref. 8 was that the computer data contained in the report are the result of an analysis that does not have the degree of sophistication required to deal adequately with the problem of adhesive bonding.

It is to be hoped that further refinements of the computer program will produce analytical results more in keeping with that observed experimentally. Such a computer analysis would aid in the examination of bonded structure using fracture mechanics methodology and the criteria developed from laboratory tests to predict bond performance and areas of concern.

It should be noted that the compliance data obtained from the analysis was used in Section 2 and Fig. 3 to show that all of the analyses gave results similar to the simple shear corrected beam formula when ξ the parameterized crack length ($\xi = a/H$) was above 3.

5.3 The Comparison Between the Total Energy Concept and the Numerical Stress Analysis Approach

When the program to determine the fracture resistance of adhesive bonds was begun (in 1961) the problem of obtaining an analytical stress analysis in the process zone of the adhesive bond, i.e., the plastic or damaged area ahead of the crack tip, was considered too complex due to the nature of adhesive fracturing. Thus, the total energy concept of $\mathcal{G}_I$ was used to enable calculation of the loads at onset of rapid fracture for any cracked adhesive structure, $\mathcal{G}_{Ic}$. The thrust of this work was to enable calculation of the failure load for a given crack position in a specimen or structure without presumption as to the adhesive failure process.

Those familiar with the energy approach realize that if the plastic strains are surrounded, as has been assumed, by an elastic strain field, then after a small increment, da, of crack extension the recovery of the

elastic elongation, e, is complete when the plate is unloaded. By using adherends that are very large compared to the scale of the adhesive, this criterion has been met and the value of $\mathcal{G}_{Ic}$ has been measured for a variety of adhesive materials, adherend materials, cracking rates, bond thicknesses and temperatures.

The compliance techniques for defining $\mathcal{G}_I$ in an adhesive bond as a function of adherend material and crack length may be directly related to a K_I that is obtained in a monolithic material ignoring the contribution of the adhesive layer. The value of $\mathcal{G}_I$ thus obtained will not be related to that value of the K_I that results from finite element linear elastic calculations.

Essentially, the two techniques are concerned with different problems. The energy approach states that the details of the stress distribution in the adhesive bond are not going to be examined on a fine scale. Thus, the characterization of crack extension in bonds will be done much the same way, wherever the locus of failure, e.g., center of bond or near an interface. This means that the numbers obtained must be coupled with information concerning manufacturing (e.g., bond thickness) service (e.g., loading rate) and fracture morphology. This approach is analogous to the J-integral measurements made on ductile metal systems. The energy losses are measured relative to the loading holes, however, a J-integral calculation could be made that should be identical to $\mathcal{G}$ as long as the path of the integral is in the elastic surroundings of the process zone of the crack. In this approach the path over which the integral is taken is in the metallic adherends except for a small region of the adhesive bond remote from the influence of the crack. The value of the integral in this small region would have to be modified using the elastic properties of the adhesive, however, considering the linearity of the compliance data, (e.g., Fig. 3) the contribution of this part to the total value of the integral is expected to be insignificant. The numerical analysis approach directs itself to the process zone itself in an attempt to understand the fracturing process. Differences between $\mathcal{G}_{Ic}$ measurements and finite

element calculations occur because of the complexity of the strain field in the process zone. The properties used in the finite element calculations are linear elastic, although there is a great awareness of the large plasticity, crazing and damage that is ahead of the visible crack front. In energy calculations for both metals and adhesives, this problem is sidestepped by the use of an effective crack length. In the finite element calculation, no such attempt has been made.

As a result of the differences in point of view, there are large discrepancies in the conclusions which are not discrepancies from a continuum mechanics point of view. The problem of determining the shape of the stress fields near the crack tip using finite element techniques is not unique to adhesive systems. For example, some of the FEM discrepancies may be related to the choice of super-elements that have the built-in inverse-square-root function. In monolithic materials we have not yet been able to closely approach the crack tip. What is done is to determine the relationship as a function of position and attempt to fit the curve ahead of the crack tip. The difficulty that must be inherent in the analytical approach can be seen by a review of data collected by our laboratory. If a given adhesive is compared as bonded, first to aluminum adherends and then to steel adherends, we find that the measured value of $\mathcal{G}_{Ic}$ is the same (all other bonding parameters such as thickness being equal). When we attempt to deduce a K_{Ic} by using the simple expression $K = \sqrt{\mathcal{G}E}$, we find that the K value for the steel adherends is 1.73 times higher than the case for the aluminum adherends. This shows that the load carrying capacity of a bonded structure depends on the adherend modulus, not the adhesive modulus. Thus, while $\mathcal{G}_{Ic}$ remains constant the K calculated by this FEM analysis varies. This fact becomes the basis for presuming that the energy approach is in error.

Such a presumption is implied in the statement of Ref. 8 that "invalid K_c or $\mathcal{G}_c$ measurements are not useful in predicting failure for other geometries or loading conditions." This implies that "validity" only obtains when a specific FEM mathematical model of linear elasticity predicts

the stresses at distances from the crack tip, r, approaching the bond thickness.

The term valid, extensively used with test procedures, implies conformity to a referenced standard. Thus, "validity" as used above, is without meaning, i.e., it is not relevant in mechanical testing unless comparison is made to a referenced standard. As yet, there is no referenced standard which allows us to say under what conditions LEFM applies in mechanical testing. One could use the very strict interpretation of LEFM, as has been proposed in Ref. 8, to show that the application to any real structure is invalid. Nevertheless, the fracture mechanics community accepts the term "engineering usefulness" where consensus agreement on the value of LEFM has been achieved for monolithic materials. This point seems to be conceded in Ref. 8 in their discussion of monolithic materials. For engineering purposes, one need not follow crack extension on a fine scale, since we are concerned only with the loading point at which a stationary or slow moving crack begins to extend rapidly. The engineering usefulness of this method of measurement is determined by how well the fracture load in a structure can be predicted from a laboratory test on a much different geometry. In terms of this definition, measurements of $\mathcal{G}_{Ic}$ for adhesive bonds fulfill the requirements of engineering usefulness and it is our belief that continued use of the technique will lead to an improved adhesive bonding technology.

Perhaps the major problem with the computational approach presented here is that it is not dedicated to the problems connected with the design of bonded structures, i.e., it has little engineering usefulness. The results of the computation based on the simplified model do not agree with experimental results and will have to be modified considerably to model the process zone in order to enable calculation of fracture loads.

Of course, it is possible to use the strain-energy-release-rate concept to predict the load carrying capacity of a structure. This can be done in several ways. First, using computational methods, either a J integral or the compliance vs. crack length characteristics can be calculated

for bonded structure so that for a given loading and crack position the applied $\mathcal{G}_I$ (or J_I) can be calculated. The second method uses an experimental technique developed for fatigue of complex monolithic structure.

Two specific areas of difference between the numerical approach (FEM) and the energy method (LEFM) involve the area of compliance calibration and validity of $\mathcal{G}_{Ic}$ test results.

In the LEFM method, beam theory is used only to define a specimen shape. The determination of $\mathcal{G}_{Ic}$ using this specimen is based on an extremely accurate compliance calibration which must provide the base against which any computation, beam theory or FEM, must be checked. The shape of the specimen does not matter, as long as a compliance calibration is made prior to obtaining experimental data. The value of beam theory is that it can be used to design a constant-compliance-change specimen over a wide range of crack lengths.

The FEM can be used to determine a compliance curve, however, for values of ξ above 3, it is not significantly different from that found from a corrected beam formula prior to compliance calibration. Of course, the calibration value is the one used in testing, irrespective of any analysis.

Of particular concern in the FEM report is the question of the validity of $\mathcal{G}_{Ic}$ as determined from the LEFM approach. The meaning of "validity" here also appears to be used in the mathematical sense, described earlier in this section and does not pertain to the engineering basis used to define $\mathcal{G}_{Ic}$ experimentally.

The FEM paper examines the plastic work of fracture which may occur in a volume that is ahead of the crack tip by as much as ten bond thicknesses and concludes that the LEFM $\mathcal{G}_{Ic}$ determined experimentally does not apply.

The energy method does not deal with specimen micro-dimensions and the $\mathcal{G}_{Ic}$ value can be valid in an engineering sense even when the

dimensions of plastic flow in the adhesive ahead of the crack are much longer than the bond thickness of the adhesive. While this does make a fine scale stress analysis difficult, it does not diminish the engineering usefulness of the $\mathcal{G}_{Ic}$ concept. In addition, the FEM paper states that the measured value of toughness is no more descriptive of the crack resistance in structures than the peel adhesion value might be. In contrast, it has been shown (1) that the value of $\mathcal{G}_{Ic}$ obtained for a given set of adhesive parameters (e.g., bond thickness, curing conditions, etc.) is the same for structural adherends having a wide variety of geometries and moduli. It should be noted that although the $\mathcal{G}_{Ic}$ value may not be a linear elastic fracture mechanics (LEFM) parameter in the strictest mathematical sense, the engineering usefulness of the fracture mechanics concept both for monolithic systems and adhesive joints in fracture control has been amply demonstrated.

An area where the two approaches may give similar results is in the area of slow crack growth. For example, most highly loaded adhesively bonded structural elements are to be found in new design aircraft components. These bonded elements are seldom more than 0.1 in. thick. Even if the loadings were pure mode-I, as in a peel test, the toughness of the adhesives used today would be such that yielding in the metal would precede crack growth except for flaws in the adhesive that were many orders of magnitude larger than those observed. Thus, for the range of adherend thicknesses used and the initial flaw sizes common to adhesively bonded structures, failure by rapid flaw growth in the adhesive is prohibited. If the adhesively bonded structure is to fail, one of the initial flaws must extend by a slow growth process to a critical value in a similar fashion to what is observed in monolithic structures. This can occur by fatigue, stress corrosion cracking (SCC) and both in combination. The values of the fracture mechanics parameters for these service conditions can be much lower than $\mathcal{G}_{Ic}$. For example, the adhesive material discussed in the FEM report having a RT toughness of 9 lbs/in., has a fatigue threshold, $\Delta\mathcal{G}_{TH}$, of 0.5 lbs/in. This level of toughness is likely to be in the range of usefulness of the FEM analysis

even though $\mathcal{G}_{Ic}$ is out of the FEM range. This level of fatigue performance relative to $\mathcal{G}_{Ic}$ is somewhat poorer than seen for metals and implies that the fatigue properties of adhesives can be improved.

5.4 Summary of the LEFM-FEM Comparison

For structural adhesives, the K characterization of stresses as described by FEM within the adhesive layer is invalid, because the plastic zone is not small in relation to the bondline thickness. Therefore, a fracture mechanics approach which regards the bondline thickness as a specimen macro-dimension is not expected to be reliable without additional refinement.

The FEM results that show significant differences with LEFM data relate to this difference in approach. However, fracture mechanics appears to be applicable if the bondline thickness is regarded as a controlled microstructural property rather than a specimen macro-dimension. In this case, the only requirement is that the plastic zone be confined to the adhesive layer and be small compared to crack size and specimen macro dimensions. The FEM results are not pertinent to this type of approach, although it is the approach most commonly used. For mode-I increasing load (static) tests the plastic zone size seems to be small enough, because static data tend to correlate on a $\mathcal{G}_{Ic}$ basis when the adhesive properties and bondline thickness are constant. The plastic zone size is even smaller at the lower loads used in fatigue and environmental, sustained load testing, so LEFM should tend to be even more readily applicable.

Thus, in view of the current level of FEM development, one cannot appropriately conclude that LEFM is inapplicable to bondline cracks in structural adhesives, because at this point FEM has been restricted to a narrow view of the topic. More to the point, the FEM results are irrelevant to the way in which LEFM has already been applied successfully to structural adhesives.

6.0 Conclusions

One of the major conclusions of this work concerns the relevancy of a fracture mechanics methodology to the design and analysis of structures. The direct applicability of fatigue crack growth data has been shown by the ability to give a good estimate of structural fatigue life. Although both the structure and the analyses were somewhat simpler than the bonded components anticipated for aircraft, the technique has been adequately demonstrated.

The methodology used here began with a determination of the fracturing properties of one adhesive system for fatigue and environmentally assisted fatigue loading. The change in the fracturing properties as a function of the amount of shear was determined using the "constant-K" mode-I specimens (e.g., WTB and CDCB) and a mixed-mode specimen (CLS). These data were used to successfully predict crack growth in a full scale structural model using a rudimentary virtual energy analysis.

The success of this predicted life study has shown that the methodology can be of potentially great value in predicting the life of bonded structure. More refined analysis and testing techniques should be able to be used to develop proof tests and inspection schedules for bonded structure, as well as to provide design information on the most suitable bond geometry.

Still to be determined is the non-experimental solution that will enable calculation of the stress field around the tip of the crack in a bonded structure. To date the available numerical (finite element) analyses have been unable to reconcile observed energy measurements shown to dictate fracture properties in either laboratory specimens or structure.

When pure mode-I and mixed modes I and II were compared, it was found that no combination of mixed-mode loading resulted in a lower $\mathcal{G}_c$ than that for pure mode-I loading along. In fact, monotonically increasing load fracture under any mixed-mode combination has never been

shown to occur at fracture energy values less than $\mathcal{G}_{Ic}$. Second, for structural adhesive materials presently used in aircraft for wide area structural bonding, monotonically increasing loads will cause permanent deformation in the adherends prior to adhesive crack growth, unless the size of the debond is a substantial fraction of the bond area. This conclusion suggests that the value of $\mathcal{G}_{Ic}$ is of concern for bonding of thin sections only when it is below a minimum value, i.e., 2 lbs/in. This conclusion is valid for the case of aircraft structural bonding where the design and manufacture of bonded elements as well as the measurements of debond sizes are strictly controlled.

One of the most important results is that the well characterized mixed-mode, CLS, specimens ($\mathcal{G}_I / \mathcal{G}_{II} \cong 1$) show $\mathcal{G}_{Tc}$ values four to five times the pure mod-I value. In fact, the value of $\mathcal{G}_I$ in the mixed-mode tests at $\mathcal{G}_c$ is approximately equal to $\mathcal{G}_{Ic}$.

The most important fracture property for aircraft structure is fatigue resistance. The effect of 3 Hz mixed-mode loading on fatigue crack growth rate (at R = 0.1 and 0.6) has been studied with two structural adhesive systems and the threshold level of total $\mathcal{G}$ for mixed-mode crack growth is always above that for pure mode-I loading. Because of the mixed-mode fracture data, it was thought that mixed-mode fatigue crack growth was directly related to the amount of mode-I present in the total loading and predicted by the pure mode-I fatigue growth properties. Data collected recently indicates that a high shear loading (i.e., the $\mathcal{G}_I / \mathcal{G}_{II}$ ratio is low), requires considerably less of a $\Delta\mathcal{G}_I$ to cause crack growth than the amount predicted from pure mode-I data. This lower $\Delta\mathcal{G}_I$ threshold for mixed-mode loading requires that both the total $\mathcal{G}$, $\mathcal{G}_I / \mathcal{G}_{II}$ ratio and R ratio be known in order to calculate fatigue lives. In general, crack growth is slower at higher frequencies and higher R ratios.

The effect of environment on crack growth is strongly affected by the amount of shear present on the bondline. For PAA treated adherends, where interface (IF) failure is difficult, no mixed-mode SCC growth (which

occurs cohesively) was seen at values of crack extension force that were well above the calculated $\mathcal{G}_{Iscc}$ value determined from $\mathcal{G}_{eff}$ obtained from the fatigue analysis. Mixed-mode fatigue tests in elevated temperature (140°F) water showed no change in the $\Delta\mathcal{G}$ vs. da/dN behavior. This data implies that (1) the effect of shear loading on SCC tests is to limit crack extension much more than in environmentally assisted fatigue, (2) the calculated value of an effective $\mathcal{G}$ is unique to fatigue, and (3) correlation is expected to be as different for SCC as it is for rising load tests.

These conclusions support the empirical evidence that high shear loading for structural adhesive bonds is beneficial for both fatigue and SCC.

Future fatigue and static load studies of adhesive joints using a number of adhesive systems and potentially aggressive environments should be directed towards verification of the conclusions stated in the text in pure and mixed-mode loading. The determination of the combined loading effects for structures will require a determination of an effective $\mathcal{G}$ for all laboratory cases used to model structural service. The $\Delta\mathcal{G}_{eff}$ mixed-mode tests have been done for a few cases to allow its use in structural design without further study. The acceptance of the concept of $\Delta\mathcal{G}_{eff}$ would justify a fatigue characterization of structural bonds on the basis of pure mode-I data.

The further development of pure and mixed-mode specimens is required for several reasons. Pure mode-I specimens can be manufactured either as narrow (CDCB) or wide (WTB) area bonds. Differences in fracturing behavior between them should be studied to define the important variables in the bonding process (e.g., bond thickness). The large CLS specimens, while well characterized, are too large to be practical in a quality assurance program. Thus, the smaller MZKG, with its advantage of size, loading arrangement and ease of compliance measurement, should be examined with regard to making it a standard for mixed-mode testing.

A catalog of low magnification fracture appearances (light microscope) has shown some differences between pure and mixed-mode crack growth mostly for rising load tests. For PAA treated aluminum adherends the plane of crack growth is primarily cohesive or center of bond (COB) irrespective of testing condition. The rising load, pure mode-I crack growth plane is essentially smooth and featureless, except for traces of scrim cloth and arrest markings where the crack was stopped and restarted. BC or CLS mixed-mode, rising load tests are also COB, but very different. Both fracture surface halves show a dense pattern of inclined "flakes" indicating response to maximum cleavage forces prior to gross crack extension. Rising load tests on the MZKG specimen shows some interface separation near the area edges, as well as a more minor shear load fracture pattern in the center of the specimen. Surprisingly, fatigue fracture surfaces for both pure and mixed-mode loading are very similar and independent of environment. Static load, SCC tests on pure mode-I specimens are also COB and, except for some attack at the edges, are flat and featureless. Mixed-mode SCC tests have indicated that cracks do not extend except at loads approaching the critical crack extension force, $\mathcal{G}_{Tc}$. The purpose of the appearance catalog is to provide a data base for understanding service failures as has been done for metal fracture studies. The nature of the fracture surfaces are such that a more complete determination of the surfaces will have to be done using the scanning electron microscope.

References

1. S. Mostovoy and E. J. Ripling, "Flaw Tolerance of a Number of Commercial and Experimental Adhesives," Adhesion Science and Technology, Vol. 9B, pp. 513-562.

2. Sheldon Mostovoy and E. J. Ripling, Final Report, "Factors Controlling the Strength of Composite Structures," Contract No. N00019-70-C-0137, for the period March 1, 1970 through February 28, 1971.

3. S. Mostovoy and E. J. Ripling, "Fracturing Characterization of Adhesive Joints," Final Report on Contract No. N00019-76-C-0323 for the period January 31, 1976 through January 31, 1977.

4. S. Mostovoy, P. B. Crosley and E. J. Ripling, "Use of Crack-Line-Loaded Specimens for Measuring Plane-Strain Fracture Toughness," Journal of Materials, Vol. 2, No. 3, Sept. 1967, pp. 661-681.

5. J. E. Srawley and Bernard Gross, "Stress Intensity Factor for Crackline Loaded Edge Crack Specimens," Materials Research and Standards, Vol. 7, No. 4, April 1967, pp. 155-162.

6. M. F. Kanninen, "An Augmented Double Cantilever Beam Model for Studying Crack Propagation and Arrest," International Journal of Fracture, Vol. 9, No. 1, March 1973.

7. S. Mostovoy, "Comments on Contoured Double Cantilever Beam Specimens for Fracture Toughness Measurement of Adhesive Joint," Journal of Materials Science, 11 (1976) 570.

8. Wang, Mandell and McGarry, MIT Report R76-1, Feb. 1976.

9. T. Brussat, S. T. Chiu and S. Mostovoy, "Fracture Mechanics for Structural Adhesive Bonds, Phase II," Final Technical Report, Contract No. F33615-75-C-5224, prepared for AFML, Wright-Patterson AFB, OH 45433, August 31, 1978.

10. S. Mostovoy and E. J. Ripling, Final Report, "Fracturing Characteristics of Adhesive Joints," Contract N00019-75-C-0271 for the period January 16, 1975 through January 16, 1976.

11. T. R. Brussat and S. Mostovoy, "Fracture Mechanics for Structural Adhesive Bonds--Second Interim Report," AFML Contract No. F33615-75-C-5224-B for the period 15 September 1975-15 December 1975.

References, Continued

12. T. R. Brussat, and S. Mostovoy, "Fracture Mechanics for Structural Adhesive Bonds--Third Interim Report, " AFML Contract No. F33615-75-C-5224-B for the period 15 December 1975-15 March 1976.

13. T. R. Brussat, S. T. Chiu, and S. Mostovoy, "Fracture Mechanics for Structural Adhesive Bonds--Final Report," AFML-TR-77-163, October, 1977.

14. H. Tada, P. C. Paris and G. R. Irwin, "The Stress Analysis of Cracks Handbook," Del Research Corp., Allentown, PA 1973.

15. E. J. Ripling and Eliezer Falkenstein, Measuring K_R-curves for Thin Sheet," ASTM, STP 480, 1970.

16. T. R. Brussat, S. T. Chiu and S. Mostovoy, "Fracture Mechanics in Structural Adhesive Bonds," Fifth Interim Report, Contract No. F33615-75-C-5224, AFML, AFSC, Wright-Patterson AFB, Ohio, for the period 15 June 1976-15 September 1976.

17. T. R. Brussat, S. T. Chiu, and S. Mostovoy, "Fracture Mechanics for Structural Adhesive Bonds," Final Report, Contract No. F33615-75-C-5224, AFML, AFSC, Wright-Patterson AFB, Ohio, 15 July 1977.

18. Sheldon Mostovoy and E. J. Ripling, Final Report, "Fracturing Characteristics of Adhesive Joints," Contract No. N00019-74-C-0274 for the period January 31, 1974 through January 15, 1975.

Appendix I

Cleaning Procedure for Aluminum Bonding of Specimens Using Film or Liquid Adhesive Systems

1. Solvent Cleaning: Two step procedure.

   (a) Methyl alcohol or equivalent: used primarily to remove the blueing from the machining operation.

   (b) Clean chlorinated solvent or equivalent, e.g., 1, 1, 1, trichloroethane or trichloroethylene: used to remove grease and oil. After cleaning with these solvents, there should be no trace of blueing, grease or oil. The surface to be bonded should be free of obvious machining errors, deep scratches and imperfections that would prevent the specimen adherends to be fitted together to make a satisfactory bond.

2. Alkalene Cleaning.

   Material: Oakite #164 or equivalent. The solution used is 7.5 weight percent and, for the large class jars used for specimen treatment, dissolve 449 grams of Oakite #164 into 6000 ml of deionized water. This solution is suitable for treating at least 5000 $in.^2$ of adherends (about 50 pairs of CDCB's).

   Procedure: Heat solution to 180°F ± 5°F. Immerse specimens for 15 minutes ± 2 minutes and follow with an immediate tap water rinse for five minutes. The time to get from the cleaner to the rinse should not exceed 20 seconds, due to the formation of a difficult to remove film. Proceed from rinse to chromic acid etch.

3. Chromic Acid Etch (e.g., FPL etch).

   Material: The composition of the etch is nominally 30 PPW deionized water, 10 Pbw sulfuric acid (1.84 S.G.) and 1 Pbw sodium dichromate (Na_2CrO_3 powder). For the given glass jars used for etching, the solution was prepared by dissolving 165 grams of sodium dichromate in 4940 ml of water and then adding 895 ml of sulfuric acid.

Procedure: Heat the solution to 150°F ± 5°F. Immerse specimens for 15 minutes ± 5 minutes and follow with an immediate tap water rinse for 3 to 5 minutes. Proceed from rinse to phosphoric acid anodize.

Note: The etch solution begins as a deep blood red solution, however, after 20 sets of adherends (4000 $in.^2$) have been etched, the solution takes on a slightly greenish cast. Work done on bonding to chromic acid etched surfaces has shown that used solution produces more effective bond surfaces than freshly made etch. Nevertheless, in the interest of consistency of treatment prior to the anodize, the etch solution was replaced after about 3000 $in.^2$ of aluminum surface (30 pairs of adherends) had been etched or the solution showed a greenish color.

4. Phosphoric Acid Anodize (Boeing Aircraft specification BAC 5555).

Material: The composition of the anodizing solution is an aqueous 10 volume percent (± 2%) phosphoric acid, H_3PO_4, (85% ortho phosphoric acid: 1.436 S.G.). The solution is prepared for small specimen tanks by adding 600 ml of acid to 5400 ml of deionized water. Covered storage to prevent evaporation will permit use for at least 3000 $in.^2$ of specimen surface over a several month period (30 pairs of adherends) however, it is necessary to discard the solution if there is a color change from clear to green or orange.

Procedure: The solution is used at room temperature, however, the temperature limits are 65 to 85°F. The use of a relatively large volume of solution, e.g., 6000 ml for 200 to 400 $in.^2$ of surface (2 to 4 pairs of adherends) insures that a room temperature solution will not be heated above the limit during anodizing. A stainless steel cathode is connected to the negative pole of a sufficiently large DC power supply and the adherends to be treated connected to the positive pole (anode) of the supply. The voltage is then raised to 10V ± 1V and maintained for 20 to 25 minutes. Within 2 minutes after anodizing the adherends are

immersed in a tap water rinse and washed for 10 to 15 minutes. After this tap water rinse the adherends are suspended such that excess water drains away from the intended bond surface. At this point the adherends are rinsed finally with deionized water and the bond surface blown dry with an air dryer. Once dry, they can be primed, however, from the time they are etched until priming is complete the bond surface cannot be handled at all. This is because the anodize produced oxide is very fragile and requires the primer for stabilation.

The production of a suitable oxide can be determined by viewing the bond surface with polarized light. A uniform light green or light pink color indicates a satisfactory anodize. This color can also be seen by viewing the bond surface at a steep angle.

5. Adhesive Priming Agent (e.g., Bloomingdale's BR 127 or BR 127A).

Material: Adhesive primer is a high solvents content paint that must be stored at 0°F or below. Thus, prior to use it must be warmed to room temperature, then thoroughly mixed and subsequently agitated continually during application. Out-of-date material has proved satisfactory for more than a year if kept cold, however, replacement of out of date material is probably a good idea.

Procedure: Using an acceptable air power paint spray gun and nozzle assembly (several, along with a suitable air pressure range, are recommended by the manufacturer), primer is applied to the bond surface to a dry primer thickness of 0.0001 to 0.0004 in. This is one or two thin coats which can be determined approximately by color comparison of previously painted and calibrated metal coupons. After priming, the parts are air dried for 30 minutes and then oven cured at 250°F for 30 minutes. While handling of the bond surface is to be avoided, should contact occur, the primed areas can be solvent cleaned (e.g., MEK) prior to bonding with no loss in bond properties.

Distribution List

		No. of copies
1.	AIR-5316D Naval Air Systems Command Washington, DC 20360	8
2.	Naval Research Laboratory Washington, DC Code 6170 1 copy Code 8430 1 copy Code 8433 1 copy	3
3.	Naval Surface Weapons Center White Oak, MD 20910 Attn: Code WO-31	1
4.	Naval Ship Engineering Center Washington, DC 20360 Attn: Code 6101E	1
5.	Naval Ship R&D Center Annapolis, MD 21400	1
6.	Naval Ship R&D Center Washington, DC 20007 Attn: Code 725	1
7.	University of Illinois Dept. of Theoretical and Appl. Mech. Champaign, IL 61820 Attn: Prof. H. T. Corten	1
8.	American Cyanamid Co. Bloomingdale Dept. Havre de Grace, MD 21078	1
9.	SEA-035 Naval Sea Systems Command Washington, DC 20360	1

10. Air Force Materials Laboratory — 6
RTD
Wright-Patterson Air Force Base
Dayton, OH 45433

LN	1 copy
LNC	1 copy
LAE	1 copy
LAM	1 copy
LT	1 copy
LTC	1 copy

11. Plastics Technical Evaluation Center — 1
Picatinny Arsenal
Dover, NJ 07801

12. Metals and Ceramics Information Center — 1
Battelle Memorial Institute
505 King Avenue
Columbus, OH 43201

13. Army Materials and Mechanics Research Center — 1
Watertown, MA 02172

14. Directorate of Research and Engineering — 1
Watervliet Arsenal
Watervliet, NY 12189

15. Allegheny Ballistics Laboratory — 1
Cumberland, MD 21502

16. Materials Sciences Corp. — 1
P. O. Box 254
Fort Washington, PA 19034

17. Solar Aircraft Co. — 1
2200 Pacific Highway
San Diego, CA 92112
Attn: Dr. A. G. Metcalfe

18. Professor John Outwater — 1
University of Vermont
Burlington, VT 05401

19. Hughes Aircraft Co. — 1
Aerospace Group, R&D Div.
Culver City, CA 90130

20. A. O. Smith Co. — 1
Milwaukee, WI 53201

21. Air Force Flight Dynamics Laboratory — 1
Wright-Patterson AFB, OH 45433
Attn: FBCB/G. Sendeckyj

22. IIT Research Institute — 1
Technology Center
10 West 35th Street
Chicago, IL 60616

23. PPG Industries — 1
7801 Norfolk Avenue
Room 201
Bethesda, MD 20014

24. Grumman Aerospace Corp. — 1
Bethpage, L. I., NY 11714
Attn: Materials Dept.

25. Vought Aeronautics Division — 1
LTV Aerospace Corp.
P. O. Box 5907
Dallas, TX 75222

26. Union Carbide Plastics Co. — 1
(Mr. A. S. Burhans)
P. O. Box 670
River Road
Bound Brook, NJ 08805

27. Reinforced Plastics Division — 1
Minnesota Mining and Manufacturing Co.
2501 Hudson Road
St. Paul, MN 55119

28. Professor F. McGarry — 1
Massachusetts Institute of Technology
Cambridge, MA 02139

29. Space Sciences Laboratory — 1
General Electric Co.
P. O. Box 8555
Philadelphia, PA 19101

30. Avco Corporation — 1
Lowell Industrial Park
Lowell, MA 01851

31. Arthur D. Little, Inc. 1
Acorn Park
Cambridge, MA 02140
Attn: Stephen L. Kaplan

32. Research Department 1
Dow Corning Corporation
Midland, MI 48640
Attn: Dr. O. K. Johannson

33. Lewis Research Center, NASA 3
21000 Brookpark Road
Cleveland, OH 44135
Attn: Structural Mechanics and Polymers Branch
Chemical Systems Division
Liquid Rocket Technology Branch

34. HITCO 1
1600 W. 135th Street
Gardena, CA 90249

35. Jet Propulsion Laboratory 1
California Institute of Technology
4800 Oak Grove Drive
Pasadena, CA 91103

36. Chief, Materials and Processes 1
Aerospace Group
Space Division
The Boeing Company
P. O. Box 3707
Seattle, WA 98124

37. Union Carbide Corporation 1
Silicones Division
P. O. Box 44
Tonawanda, NY 14152
Attn: Sam Sterman

38. Aero Vehicle Department 2
Naval Air Development Center
Warminster, PA 18974
Attn: Materials Lab. 1 copy
Structures Lab. 1 copy

39. Union Carbide Corporation 1
Carbon Products Division
Parma Research Center
Technical Information Center
P. O. Box 6116
Cleveland, OH 44101

40. Professor L. Broutman — 1
Illinois Institute of Technology
Chicago, IL 60616

41. P. R. Mallory and Co., Inc. — 1
3029 E. Washington Street
Indianapolis, IN 46206

42. Union Carbide Corporation — 1
Materials Systems Division
Technical Library
P. O. Box 24166
Indianapolis, IN 46224

43. Research Center — 1
General Precision, Inc.
1150 McBride Avenue
Little Falls, NJ 07424
Attn: Dr. J. L. Rutherford

44. Plastics and Packaging Laboratory — 1
Feltman Research Laboratory
Picatinny Arsenal
Dover, NJ 07801
Attn: Mr. Bodnar

45. Naval Air Systems Command — 10
Washington, DC 20360
Attn: AIR-950D6

46. Dr. A. Kremheller — 1
Department 72-14
Zone 402
Lockheed-Georgia Company
Marietta, GA 30060

47. TRW Equipment Laboratories — 1
TRW, Inc.
23555 Euclid Avenue
Cleveland, OH 44117

48. Hercules Research Center — 1
Wilmington, DE 19899
Attn: J. T. Paul

49. Bell Telephone Laboratories, Inc. — 1
Murray Hill, NJ 07971
Attn: R. Sabia

50. Professor James L. Lubkin — 1
Department of Civil Engineering
Michigan State University
East Lansing, MI 48823

51. General Dynamics — 1
P. O. Box 748
Fort Worth, TX 76100
Attn: Materials Department

52. McDonnell Douglas Corporation — 1
St. Louis, MO 63166
Attn: Material & Processes Development

53. General Technologies Corporation — 1
1821 Michael Faraday Drive
Reston, VA 22070

54. Advanced Materials R&D — 1
Martin Marietta Corporation
P. O. Box 5837
Orlando, FL 32805

55. Dr. M. I. Jacobson — 1
Manager, Manufacturing Research
Orgn. 47-01, Bldg. 150
Lockheed Missiles and Space Co.
Sunnyvale, CA 94086

56. North American Rockwell Science Center — 1
P. O. Box 1085
Thousand Oaks, CA 91360
Attn: David H. Kaelble

57. Mr. W. D. Sell — 1
A. C. & S. Division
Bldg. 209-1 CW
3M Company
3M Center
St. Paul, MN 55101

58. Mr. Don Croke — 1
Dept. 7451
Box 551, Bldg. 243
Lockheed California Co.
Burbank, CA 91503

59. Mr. Tom B. Frazier — 1
Methods and Materials Research Lab.
Bell Helicopter Co.
P. O. Box 482
Fort Worth, TX 76101

60. Dr. John T. Quinlivan — 1
Boeing Materials Technology
Commercial Airplane Group
Mail Stop 73-43
P. O. Box 3707
Seattle, WA 98124

61. Mr. Carl Weber
B. F. Goodrich Co.
Research Center
Brecksville, OH 44141

62. NASA
George C. Marshall Space Flight Center
Huntsville, AL 35812

63. Mr. R. J. Palmer — 1
Materials & Process Engineering
Flight & Laboratory Development
Douglas Aircraft Company
Mail Code 1-18
3855 Lakewood Blvd.
Long Beach, CA 90801

64. Mr. Dennis Donnelly — 1
Materials Engineer
The Boeing Company
Renton, WA 98055

65. Mr. Herbert S. Schwartz — 1
AFML/MB
Wright-Patterson AFB, OH 45433

66. Mr. Robert L. Kozarek — 1
Alcoa Technical Center
Alcoa Center, PA 15069

67. Mr. Dominick C. Novelli — 1
Lockheed California Co.
Burbank, CA 91503

68. Mr. A. N. Cianciarulo 1
Manager, Development & Service Lab.
Ren Plastics, Inc.
5656 S. Cedar Street
Lansing, MI 48909

69. Dr. Tennyson Smith 1
Rockwell International
1049 Caminos Dos Rios
Thousand Oaks, CA 91360

70. Prof. A. N. Gent 1
Institute of Polymer Science
University of Akron
Akron, OH 44325

71. Dr. Armand Lewis 1
Hughson Chemical
Lord Corporation
2000 West Grandview Blvd.
Erie, PA 16512

72. Dr. Nicholas J. De Lollis 1
Polymer Research & Development
Div. 5813
Sandia Laboratories
Albuquerque, NM 87115

73. Dr. James R. Huntsberger 1
E. I. du Pont de Nemours & Co.
Experimental Station 323/108
Wilmington, DE 19898

74. Mr. Paul Stifel 1
Dept. 247, Bldg. 33
McDonald Aircraft Co.
P. O. Box 516
St. Louis, MO 63166

75. Dr. Richard E. Robertson 1
Ford Motor Co.
Scientific Research Staff
P. O. Box 2053
Dearborn, MI 48121

76. Dr. L. H. Peebles, Jr. 1
Office of Naval Research
Scientific Dept.
495 Summer Street
Boston, MA 02210

77. Dr. James Renton — 1
Vought Corp.
Advanced Technology Center
P. O. Box 6144
Dallas, TX 75222

78. Dr. Louis H. Sharp — 1
Bell Laboratories
Murray Hill, NJ 07974

79. Dr. George C. Sih — 1
Lehigh University
Inst. of Fracture & Solid Mechanics
Bethlehem, PA 18015

80. Dr. Robert H. Gillespie — 1
U. S. Dept. of Agr., Forest Service
Forest Products Laboratory
P. O. Box 5130
Madison, WI 53705

81. Dr. D. A. Yurek — 1
Bldg. 209 - 1 CW
3M Center
St. Paul, MN 55101

82. Dr. R. Levy — 1
McDonnell Douglas Res. Lab.
Dept. 221-22
St. Louis, MO 63166

83. Mr. James E. Hansen — 1
Supervisor, Technical Library Section
Thiokol Corporation
Wasatch Division
Brigham City, UT 84302

84. Dr. H. A. Moreen — 1
Mail Code 6B 93
Auto-Netics Division
Rockwell International
3370 Mira Loma Avenue
Anaheim, CA 92803

85. Mr. J. G. Fasold — 1
D/71, Gp. 522, Bldg. 7
Columbus Aircraft Div.
Rockwell International
4300 E. Fifth Ave.
Columbus, OH 43216

86. Mr. Paul E. Wright 1
Polymers Dept., Res. Labs.
Tech. Center
General Motors Corp.
12 Mile and Mound Road
Warren, MI 48090

Unclassified

SECURITY CLASSIFICATION OF THIS PAGE (When Data Entered)

REPORT DOCUMENTATION PAGE		READ INSTRUCTIONS BEFORE COMPLETING FORM
1. REPORT NUMBER	2. GOVT ACCESSION NO.	3. RECIPIENT'S CATALOG NUMBER
4. TITLE (and Subtitle) FRACTURING CHARACTERISTICS OF ADHESIVE JOINTS		5. TYPE OF REPORT & PERIOD COVERED Final Report 2/1/77 to 9/15/78
		6. PERFORMING ORG. REPORT NUMBER
7. AUTHOR(s) Sheldon Mostovoy and E. J. Ripling		8. CONTRACT OR GRANT NUMBER(s) N00019-77-C-0256
9. PERFORMING ORGANIZATION NAME AND ADDRESS Materials Research Laboratory, Inc. One Science Road Glenwood, IL 60425		10. PROGRAM ELEMENT, PROJECT, TASK AREA & WORK UNIT NUMBERS
11. CONTROLLING OFFICE NAME AND ADDRESS Naval Air Systems Command Washington, DC 20360		12. REPORT DATE May 1979
		13. NUMBER OF PAGES 102
14. MONITORING AGENCY NAME & ADDRESS(if different from Controlling Office)		15. SECURITY CLASS. (of this report) Unclassified
		15a. DECLASSIFICATION/DOWNGRADING SCHEDULE

16. DISTRIBUTION STATEMENT (of this Report)

This document is approved for public release; distribution unlimited.

17. DISTRIBUTION STATEMENT (of the abstract entered in Block 20, if different from Report)

18. SUPPLEMENTARY NOTES

19. KEY WORDS (Continue on reverse side if necessary and identify by block number)

Adhesives
Fracture toughness
Fracture appearance
Opening mode fracturing
Mixed-mode fracturing
Sub-critical crack growth

20. ABSTRACT (Continue on reverse side if necessary and identify by block number)

This report describes the test methods developed by MRL for evaluating the fracture mechanics parameters of adhesive joints. These tests, developed over more than a decade, were designed for measuring crack resistance under Mode I, combined Mode I and II, and combined Mode I and III loading. All of the tests can be applied to monotonically increasing loads, static loads in an environment, i.e., stress corrosion cracking,

DD FORM 1 JAN 73 1473 EDITION OF 1 NOV 65 IS OBSOLETE

Unclassified

SECURITY CLASSIFICATION OF THIS PAGE (When Data Entered)

Block 20, Continued

or to crack growth rate under fatigue loading.

There does not appear to be a general "law" for describing the effect of adding some shear (Mode II or III) onto opening mode loads; rather, the difference between pure and mixed mode loading depends on the load-time profile. Hence, mixed-mode loading must be treated differently for each type of loading (e.g., monotonically increasing vs. fatigue loading).

A section on bond manufacturing and testing details compares the phosphoric acid anodizing (PAA) aluminum adherend treatment to the chromic acid etch (FPL) on the basis of resistance to stress corrosion cracking in the wedge test.

Application of linear elastic fracture mechanics to the prediction of structural life based on the use of finite element as well as an energy analysis are also discussed.